

UNIVERSITY OF OKLAHOMA
GRADUATE COLLEGE

NUMERICAL SIMULATION STUDY ON CO₂ INJECTION FOR ENHANCING
HYDROCARBON RECOVERY AND SEQUESTRATION
IN TIGHT OIL FORMATIONS

A THESIS
SUBMITTED TO THE GRADUATE FACULTY
in partial fulfillment of the requirements for the
Degree of
MASTER OF SCIENCE

By

SUMEER KALRA
Norman, Oklahoma
2014

00
THESIS
KAL
Cop. 2

NUMERICAL SIMULATION STUDY ON CO₂ INJECTION FOR ENHANCING
HYDROCARBON RECOVERY AND SEQUESTRATION
IN TIGHT OIL FORMATIONS

A THESIS APPROVED FOR THE
MEWBOURNE SCHOOL OF PETROLEUM AND GEOLOGICAL ENGINEERING

BY

[Redacted Signature]

Dr. Xingru Wu, Chair

[Redacted Signature]

Dr. Deepak Devegowda

[Redacted Signature]

Dr. Maysam Pournik

Approved by the School of Petroleum and Geological Engineering
Mewbourne School of Petroleum and Geological Engineering

DEDICATION

This work is dedicated to the memory of my father, Mr. S. K. Kalra.

MY DEDICATION

This work is dedicated to the dreams and desires of my father. I hope that this work will help him to achieve his dreams and desires.

I hope that this work will help him to achieve his dreams and desires. I hope that this work will help him to achieve his dreams and desires. I hope that this work will help him to achieve his dreams and desires.

I hope that this work will help him to achieve his dreams and desires. I hope that this work will help him to achieve his dreams and desires. I hope that this work will help him to achieve his dreams and desires.

I hope that this work will help him to achieve his dreams and desires. I hope that this work will help him to achieve his dreams and desires. I hope that this work will help him to achieve his dreams and desires.

I hope that this work will help him to achieve his dreams and desires. I hope that this work will help him to achieve his dreams and desires. I hope that this work will help him to achieve his dreams and desires.

I hope that this work will help him to achieve his dreams and desires. I hope that this work will help him to achieve his dreams and desires. I hope that this work will help him to achieve his dreams and desires.

I hope that this work will help him to achieve his dreams and desires. I hope that this work will help him to achieve his dreams and desires. I hope that this work will help him to achieve his dreams and desires.

ACKNOWLEDGEMENTS

I would like to take this opportunity to thank all those people who have directly and in-directly guided me to complete my thesis and graduate studies.

First and foremost, I humbly thank my advisor and my mentor, Dr. Xingru Wu for his constant support, guidance and patience throughout my research tenure. His acumen for knowledge and strong sight for details has led to my academic and professional growth. I thank him for being such a great Boss.

I thank Dr. Deepak Devegowda for instilling confidence in me by giving an opportunity to pursue my graduate studies in the best petroleum engineering department. I also thank him and Dr. Maysam Pournik for their valuable time to be a member of my thesis defense committee.

I also thank my research group member Wei Tian for his valuable thoughts and discussion throughout the progress of my research projects.

I humbly thank my all dear friends Abhijeet, Aman, Fatema, Kritika, Mounraj, Soham, Yixin for standing with me in my high and low tides. Thank you for being my family.

Most importantly, I owe everything to my parents and my family for constant encouragement and to my fiancé, Risham for being there with me.

TABLE OF CONTENTS

ACKNOWLEDGEMENTS	iv
LIST OF TABLES	ix
LIST OF FIGURES	xi
ABSTRACT	xvi
CHAPTER 1: INTRODUCTION.....	1
1.1 RESEARCH OBJECTIVE.....	1
1.2 LOCATION OF STUDY AREA	2
1.3 RESEARCH CONTRIBUTION	2
1.4 ORGANIZATION OF THESIS	2
CHAPTER 2: LITERATURE REVIEW.....	4
2.1 UNCONVENTIONAL / TIGHT OIL RESERVOIRS.....	4
2.2 PRODUCTION STATUS OF TIGHT OIL RESERVOIRS	6
2.3 CARBON-CAPTURE-STORAGE AND ENHANCED OIL RECOVERY .	9
2.3.1 CO ₂ ENHANCED OIL RECOVERY	10
2.3.2 SUPERCRITICAL STATE OF CO ₂	13
2.3.3 MINIMUM MISCIBILITY PRESSURE	14
2.4 OIL SHALE/TIGHT RESERVOIR CHARACTERISTICS.....	16
2.4.1 SINGLE POROSITY V/S DUAL POROSITY MODELS	17
2.4.2 NATURAL FRACTURE NETWORK	18
2.4.3 ADSORPTION/DESORPTION EFFECT ON OIL PRODUCTION	22
2.4.4 TOTAL ORGANIC CONTENT AND ADSORPTION	27
2.4.5 STRESS DEPENDENT PERMEABILITY (GEOMECHANICS)...	29

2.4.6	DIFFUSION	33
2.6	NEED FOR CO ₂ INJECTION IN TIGHT FORMATIONS	35
CHAPTER 3: MECHANISM STUDY OF CO ₂ INJECTION IN DEPLETED GAS		
	RESERVOIRS.....	38
3.1	INTRODUCTION.....	38
3.2	PHYSICAL PROPERTIES OF CO ₂ AND CH ₄	39
3.3	RESERVOIR DESCRIPTION.....	41
3.4	SENSITIVITY ANALYSIS	44
3.4.1	DEPLETION PRESSURE RATIO	44
3.4.2	LOCATION OF INJECTION WELL	45
3.4.3	ARRANGEMENT OF PERMEABILITY LAYERS AND ANISOTROPY	46
3.5	DIMENSIONLESS NUMBERS ANALYSIS	48
3.6	RESULTS AND DISCUSSIONS	53
CHAPTER 4: MECHANISM STUDY OF CO ₂ INJECTION IN TIGHT OIL		
	RESERVOIRS.....	56
4.1	RESERVOIR SIMULATION TOOL	56
4.1.1	CMG – GEM™ INTRODUCTION	57
4.1.2	INJECTOR – PRODUCER WELL PATTERN.....	57
4.2	BASE RESERVOIR MODEL – ZONE OF STUDY	59
4.3	RESERVOIR DESCRIPTION	61
4.3.1	RESERVOIR FORMATION PROPERTIES.....	61
4.3.2	RESERVOIR FLUID PROPERTIES.....	65

4.3.3	MMP CALCULATIONS	68
4.3.4	ROCK – FLUID PROPERTIES	69
4.3.5	WELL AND RECURRENT DATA.....	71
4.4	MULTIPLE PHYSICS MODEL.....	72
4.4.1	RESERVOIR HETEROGENEITY EFFECT.....	72
4.4.2	NATURAL AND INDUCED FRACTURES EFFECT	76
4.4.3	ADSORPTION / DESORPTION MODEL WITH TOC	82
4.4.4	GEOMECHANICAL COUPLING WITH RESERVOIR SIMULATOR.....	87
CHAPTER 5: SIMULATION RESULTS – RESERVOIR MODEL		90
5.1	INJECTOR – PRODUCER PATTERN.....	90
5.2	ANALYSIS OF RESERVOIR CHARACTERISTICS.....	92
5.2.1	HOMOGENEOUS V/S HETEROGENEOUS MODEL.....	93
5.2.2	EFFECT OF SIMULATED NATURAL FRACTURES	94
5.2.3	EFFECT OF ADSORPTION / DESORPTION	99
5.2.4	EFFECT OF STRESS DEPENDENT PERMEABILITY.....	102
5.3	ANALYSIS OF PRODUCER BOTTOMHOLE PRESSURE.....	105
CHAPTER 6: SENSITIVITY ANALYSIS.....		108
6.1	SENSITIVITY PARAMETERS	108
6.2	ONE-PARAMETER-AT-A-TIME (OPAAT) STUDY	111
6.2.1	OPAAT WITH NATURAL FRACTURE MODEL	111
6.2.2	NO NATURAL FRACTURE MODEL – OPAAT ANALYSIS	115
6.3	RESPONSE SURFACE MODELING APPROACH	119

6.3.1	DESIGN OF EXPERIMENT (DOE)	119
6.3.2	RSM WORKFLOW	121
6.3.3	RSM PROXY MODEL VALIDATION	124
6.3.4	OIL RECOVERY – RSM.....	128
6.3.5	HCPV CO ₂ INJECTED – RSM.....	133
CHAPTER 7: CASE STUDY- CO ₂ INJECTION -PARSHALL FIELD		139
7.1	BAKKEN PETROLEUM SYSTEM.....	139
7.2	PARSHALL FIELD	141
7.3	FIELD SCALE RESERVOIR MODEL.....	142
7.4	HISTORY MATCHING APPROACH.....	146
7.5	CO ₂ -EOR PROSPECTS IN PARSHALL FIELD.....	150
CHAPTER 8: CONCLUSIONS AND RECOMMENDATIONS		155
8.1	CONCLUSIONS	155
8.2	RECOMMENDATIONS FOR FUTURE RESEARCH	158
REFERENCES		160
APPENDIX A: BASE MODEL RESERVOIR DESCRIPTION.....		168
APPENDIX B: PERMEABILITY ESTIMATION FOR EACH GRID BLOCK FROM DYKSTRA-PARSONS COEFFICIENT		171
APPENDIX C: PRODUCTION RATE HISTORY FOR BARTELSON 1-3H		173
APPENDIX D: STATISTICAL ANALYSIS FOR PROXY EQUATION BY RESPONSE SURFACE MODEL.....		175

LIST OF TABLES

Table 2.1:	Constant parameters of different components for Langmuir Isotherm (data: Ambrose et al. (2011)).....	26
Table 3.1:	Properties of CO ₂ and CH ₄ at reservoir depth of 10,000 ft and 200 °F..	39
Table 3.2:	Grid and formation properties for gas reservoir model	42
Table 3.3:	Input parameters for dimensionless analysis	50
Table 4.1:	Range and average reservoir properties for the base model	63
Table 4.2:	Grid dimensions and volume calculations for the base model	64
Table 4.3:	Hydraulic fracture properties in the reservoir model	65
Table 4.4:	Compositional fluid data and binary Interaction parameters for reservoir fluid (Nojabaei et al. 2013).....	67
Table 4.5:	MMP calculations from WINPROP	69
Table 4.6:	Tabulated MMP calculations from Adekunle (2014).....	69
Table 4.7:	Relative Permeability curves for matrix blocks	70
Table 4.8:	Relative Permeability curves for fracture blocks	70
Table 4.9:	Well Properties in the model	72
Table 4.10:	Permeability variation with different litho-facies.....	74
Table 4.11:	Heterogeneous thickness layer in reservoir model	74
Table 4.12:	Effective permeability for the Matrix-Fracture interactions	80
Table 4.13:	Langmuir’s Isotherm parameters (data: Ambrose et al. (2011))	83
Table 4.14:	Adsorption parameters input to GEM	84
Table 4.15:	Adsorption Parameter calculations.....	86
Table 4.16:	Stress parameters for Middle Bakken (Zeng and Jiang 2009)	87

Table 4.17:	Stress dependent permeability multiplier input to CMG-GEM	89
Table 5.1:	CO ₂ mole fraction profile in the perforation plane affected by natural fractures	95
Table 5.2:	Reservoir pressure profile in the Injector – Producer perforation plane	96
Table 6.1:	Parameters for sensitivity analysis	109
Table 6.2:	Sample summary of fit table.....	125
Table 6.3:	Uncertainty parameters for RSM approach.....	127
Table 6.4:	Parameters for % oil recovery proxy model.....	130
Table 6.5:	Validation 1: Oil recovery proxy model.....	131
Table 6.6:	Parameters for HCPV CO ₂ Injection (%) proxy model.....	134
Table 6.7:	Validation 1: HCPV CO ₂ Injection proxy model	136
Table 7.1:	Screening Criteria for CO ₂ - EOR operations	141
Table 7.2:	Reservoir properties of Parshall field	142
Table 7.3:	Formation properties for Parshall field model.....	143
Table 7.4:	Grid definition for the dual porosity field model	145
Table 7.5:	History match parameters for field study	147
Table 7.6:	Optimum parameters from history match.....	149

LIST OF FIGURES

Figure 2.1:	Distinguishing parameters between 'conventional' and 'unconventional' reservoirs (Baker 2013)	5
Figure 2.2:	Production profile of an unconventional oil/gas reservoir	6
Figure 2.3:	Major Tight/Shale Formations of USA (Sieminski 2014)	7
Figure 2.4:	Rig count and oil production for US oil shale reservoirs; black curve is the rig count	7
Figure 2.5:	Shale gas production across North America (EIA 2013)	8
Figure 2.6:	Tight oil production across North America (EIA 2013)	9
Figure 2.7:	CO ₂ emission statistics from energy industry (EIA 2014)	10
Figure 2.8:	Conceptual CO ₂ EOR in tight/shale formations (Sorensen et al. 2013b).....	12
Figure 2.9:	CO ₂ injection project cycle.....	13
Figure 2.10:	Volume-Depth type curve for CO ₂	14
Figure 2.11:	Pseudo-Ternary phase diagram for Miscibility	16
Figure 2.12:	Ultraviolet Fluorescence (UVF) analysis of micro fractures in Middle Bakken (Sorensen et al. 2013a)	18
Figure 2.13:	(a) Red color represents a non-planar fracture (b) representative path through the fracture cells in the model	20
Figure 2.14:	Dissection of a fracture cell to account for matrix-fracture interaction .	21
Figure 2.15:	Langmuir's Isotherm Curve	23
Figure 2.16:	Langmuir Adsorption Isotherm for five shale gas reservoirs across North America (Yu and Sepehrnoori 2014)	25

Figure 2.17:	Laboratory measurements for Extended Langmuir Isotherm for different hydrocarbon components (data: Ambrose et al. (2011))	27
Figure 2.18:	Stress dependent porosity and permeability for Bakken well	31
Figure 2.19:	Changes in matrix and fracture permeability in a core with effective stress (Wang et al. 2009)	32
Figure 2.20:	Closure stress effect on propped fracture conductivity	33
Figure 3.1:	Density comparison with increasing formation depth	40
Figure 3.2:	Viscosity comparison with increasing formation depth	40
Figure 3.3:	2D reservoir model	43
Figure 3.4:	Relative permeability curves for the reservoir model	43
Figure 3.5:	Impact of CO ₂ injection on gas recovery	44
Figure 3.6:	Depletion pressure impact on natural gas recovery and CO ₂ storage	45
Figure 3.7:	Injection well location effect on the natural gas recovery	46
Figure 3.8:	Arrangement of permeability layers for simulation study	47
Figure 3.9:	Permeability arrangement impact on natural gas recovery	47
Figure 3.10:	Effect on natural gas recovery with buoyancy number, N_G at varying effective aspect ratio, R_L (dimensionless analysis)	51
Figure 3.11:	Effect on natural gas recovery with effective aspect ratio, R_L varying dip angle group N_θ (dimensionless analysis)	52
Figure 3.12:	Sensitivity study of affecting parameters on natural gas recovery	54
Figure 3.13:	Sensitivity study of affecting parameters on CO ₂ storage volume	54
Figure 4.1:	Injector - Producer well pattern in Bakken formation	58
Figure 4.2:	X-Y cross section plane of the wells highlighting the Zone of Study	59

Figure 4.3:	Base reservoir model built using CMG-GEM.....	60
Figure 4.4:	X-Y cross section of permeability in the perforation plane	64
Figure 4.5:	3-D view of injection hydraulic fracture	65
Figure 4.6:	Pressure-Temperature diagram displaying 2 phase envelope for the representative fluid (WINPROP™)	68
Figure 4.7:	Litho-facies of the Middle Bakken formation (LeFever 2011)	73
Figure 4.8:	Heterogeneous model for three layers in the model.....	75
Figure 4.9:	3-D heterogeneous reservoir model.....	76
Figure 4.10:	Natural and induced fracture network simulated in the reservoir	77
Figure 4.11:	Perforation plane with natural and induced fractures.....	81
Figure 4.12:	Permeability variation on log scale	82
Figure 4.13:	Extended Langmuir's Isotherm simulated in reservoir model	83
Figure 4.14:	Methane adsorption isotherm curve with varying TOC wt%.....	86
Figure 4.15:	Permeability as a function of confining stress.....	88
Figure 4.16:	Extrapolated Stress dependent permeability curve.....	89
Figure 5.1:	Oil Recovery comparison with and without CO ₂ injection	91
Figure 5.2:	Reservoir profile in XY-direction with injector-producer perforation...	92
Figure 5.3:	CO ₂ flow profile for homogeneous and heterogeneous reservoir model	93
Figure 5.4:	Simulation results for various reservoir models after 30 years	97
Figure 5.5:	CO ₂ mole fraction in the producer well for various reservoir models ...	99
Figure 5.6:	Oil recovery with adsorption effects with respect to TOC wt%	101
Figure 5.7:	Variation in CO ₂ production due to adsorption effects	101
Figure 5.8:	Permeability multiplier for different rock types	102

Figure 5.9:	CO ₂ mole fraction profile for Soft and Stiff rock type geomechanical model with time progression	104
Figure 5.10:	Effects on oil recovery and CO ₂ injected with different rock types	105
Figure 5.11:	Simulation results of producer bottomhole pressure analysis	106
Figure 5.12:	Reservoir pressure profile for producer bottomhole pressure analysis	107
Figure 6.1:	Study workflow for sensitivity analysis (CMG-CMOST 2013)	110
Figure 6.2:	Oil recovery -Tornado Chart (OPAAT with NF)	112
Figure 6.3:	HCPV CO ₂ Injected -Tornado Chart (OPAAT with NF).....	113
Figure 6.4:	HCPV CO ₂ Injected and Oil recovery for OPAAT with NF cases	115
Figure 6.5:	Oil recovery -Tornado Chart (OPAAT- No NF)	116
Figure 6.6:	HCPV CO ₂ Injected -Tornado Chart (OPAAT- No NF).....	117
Figure 6.7:	HCPV CO ₂ injected and oil recovery for OPAAT without NF cases. .	119
Figure 6.8:	Snapshot of RSM Model accuracy input parameters	123
Figure 6.9:	Sample response surface verification plot.....	125
Figure 6.10:	Effect estimate of uncertainty parameters on oil recovery (%).....	129
Figure 6.11:	Validation 2: Oil recovery proxy model verification plot	132
Figure 6.12:	Effect estimate of uncertainty parameters on HCPV of CO ₂ injected..	133
Figure 6.13:	Validation 2: HCPV CO ₂ injection proxy model verification plot.....	136
Figure 6.14:	Histogram and simulation results of RSM engine.....	137
Figure 6.15:	Cross plot of objective functions	138
Figure 7.1:	Regional Structural Map of the Williston Basin, Bakken Formation ..	140
Figure 7.2:	Oil production status from Bakken formation (EIA-DPR 2014)	140



Figure 7.3: Aerial view of selected zone in the Parshall field, with red zone simulated as a two well Inj-Prod system 144

Figure 7.4: X-Y cross section perforation plane of field reservoir model 144

Figure 7.5: Simulation production rate and the rate history match..... 146

Figure 7.6: History match results for oil recovery and oil production rate..... 148

Figure 7.7: Comparison of production rate and oil recovery for Optimum and Base case solution 149

Figure 7.8: Parshall field CO₂-EOR simulation results with primary recovery..... 150

Figure 7.9: CO₂ injected volume and mole fraction of CO₂ in producer well 151

Figure 7.10: Pressure profile for field model: NO Injection & CO₂ Injection..... 153

Figure 7.11: CO₂ mole fraction profile with time progression in the field model.... 154






ABSTRACT

Hydrocarbon resources from unconventional reservoirs, especially tight/shale plays, are changing the North America's energy prospect. Single digit percentage of oil shale recovery with current best practices, leaves a large room for recovery improvement. While aqueous phase injection into tight formation is extremely challenging, other recovery techniques need to be evaluated and pilot tested for secondary recovery in oil shale reservoirs. Injecting Carbon Dioxide (CO₂) into oil shale formations can potentially improve oil recovery. Furthermore, the large surface area in the organic rich shale could permanently store CO₂ volume without jeopardizing the formation integrity.

This work is a study on evaluating the effectiveness of CO₂ enhanced oil shale recovery and shale formation CO₂ sequestration capacity. The work identified the most favorable reservoir properties and operating envelop for field application of CO₂-EOR in tight formations. A compositional reservoir simulator is used to model CO₂ injection in a tight / oil shale reservoir. Formation and petrophysical properties, and reservoir fluid composition of the Middle Bakken formation is used to set up the base model for simulation. For investigating the technical feasibility of increasing oil production by CO₂ injection, a sector of Parshall field from Bakken formation is modeled with two active wells. The reservoir model considered petrophysical characteristics of tight formation that affects CO₂ flow migration such as (1) reservoir heterogeneity (2) in-situ stress change (geomechanical) impact on permeability of natural fracture networks and hydraulic fractures during simultaneous injection and production, (3) impact of adsorption and diffusion on carbon storage in organic rich shale, (4) presence of natural



fractures, secondary fracture geometry and connectivity, fracture density and orientation effect.

The results are based on sensitivity analysis of the characteristic tight formation petrophysical, geomechanical properties and displacement mechanisms. Sensitivity analysis also focused on injection schemes and completion practices for most economic field applications. Sensitivity analysis is implemented by two methods. First method analyzed each uncertain parameter individually and reproduced the results in terms of a tornado chart, defining the critical parameters. Second method analyzed all uncertain parameters together using the Design of Experiment (DoE) and Response Surface Modeling (RSM) approach to counter the interaction between parameters and influential parameters into generating a proxy model for optimizing oil recovery and CO₂ injection into the formation.


The results show that facilitating oil recovery from shale reservoirs by CO₂ injection is much higher than primary depletion depending on fracture network connectivity. This research outlines the capabilities of CO₂ injection for improving oil production from unconventional reservoirs. Also, significant CO₂ storage capacity, if applicable in shale formations, could be a major step towards advances in CO₂ sequestration in widely spread shale reservoirs.

CHAPTER 1: INTRODUCTION

The technological advances in the process of horizontal drilling and multi-stage hydraulic fracturing led to the economic gas production from unconventional shale/tight gas reservoirs. With gaining technical expertise, in the past decade, the industry diverted their attention to achieve economic oil production by developing unconventional tight reservoirs. Single digit percentage of oil shale recovery with current best practices, still leaves a large room for recovery improvements. On the other end, there has been strong emphasis on the critical role of carbon capture and storage projects to tackle the ever increasing problem of global warming. As a byproduct of fossil fuel utilization, the rise of Carbon Dioxide (CO_2) content within the atmosphere, has caused concerns over temperature increase. Injecting Carbon Dioxide (CO_2) into oil shale formation can potentially improve oil recovery with many field practices. Furthermore, the large surface area in the organic rich shale can permanently store CO_2 volume without jeopardizing the formation integrity. CO_2 storage capacity of shale formation is still unknown; CO_2 -EOR for unconventional reservoirs is still not field tested and very limited research is pursued on these issues.

1.1 RESEARCH OBJECTIVE

The research objective of this thesis is to determine the technical feasibility of Enhanced Oil Recovery (EOR) by CO_2 injection from oil shale/tight reservoirs and analyzing these formations for potential CO_2 sequestration. The project scope includes examining the reservoir characteristics of tight/shale formations, building a base reservoir simulation model representing oil shale/tight formation and field scale reservoir simulation for investigating the technical capabilities of improving oil



recovery by injecting CO₂ into tight formations. Also, the thesis has incorporated a chapter on mechanism study of CO₂ injection for enhancing gas recovery from depleted conventional gas reservoirs.

1.2 LOCATION OF STUDY AREA

To better characterize the low permeability tight formation properties and to cater to reservoir simulation needs, Bakken Petroleum System in the Williston Basin has been considered for this study. Formation and petrophysical properties, and reservoir fluid composition of the Middle Bakken reservoir were used to set up the base model for simulation. For investigating of the technical feasibility of field operations of increasing oil production by CO₂ injection, a sector of Parshall field, Mountrail County from Bakken formation is modeled with two active wells.

1.3 RESEARCH CONTRIBUTION

An important contribution of this research is in defining the importance of presence of micro-natural and induced fractures for considering CO₂-EOR opportunities for tight/oil shale reservoirs. Instead of matrix permeability, natural fractures network is the main pathway for CO₂ to flow through the reservoir. Through sensitivity analysis, importance of in-fill drilling injector wells is observed. Proxy models were developed using the technique of Response Surface Modeling to calculate oil recovery and amount of CO₂ injected in the reservoir. These proxy models could be used to analyze the effect of completion parameters without running simulations each time.

1.4 ORGANIZATION OF THESIS

The research study conducted has been divided into seven chapters.

Chapter 1 covers the introduction and research needs to study this topic.

Chapter 2 covers the background and literature review for the study including the extensive review of critical reservoir and petrophysical properties required to model an oil shale reservoir.

Chapter 3 focuses on the mechanism study of CO₂ injection for enhancing gas recovery from depleted conventional gas reservoirs. This work developed the research base to further look into the current thesis topic. The chapter covers the mechanism and findings of the study. This study is limited to this chapter and not discussed in further chapters.

Chapter 4 focuses on the mechanism study of CO₂ injection into a tight oil reservoir. A compositional reservoir simulator was used to build up a base reservoir model for this research and to access potential EOR schemes.

Chapter 5 covers the findings and simulation results for the base reservoir model. The simulation results focus on emphasizing the effect of shale formation characteristics properties on oil recovery and the amount of hydrocarbon pore volume of CO₂ injected into the formation.

Chapter 6 covers the study of sensitivity analysis of completion parameters utilizing OPAAT analysis and Response Surface Modeling approach. The chapter also focuses on the physical interpretation and explanations for the simulated results.

Chapter 7 covers the field application of the base reservoir model, by developing a two well reservoir model from a sector in Parshall field, Mountrail County, North Dakota and analyzing the technical feasibility of CO₂-EOR operations.

Chapter 8 summarizes the major conclusions of the study and recommends potential future studies in this research area.

CHAPTER 2: LITERATURE REVIEW

The chapter provides the fundamental understanding of unconventional/tight oil reservoirs, integrating carbon capture and storage with CO₂ - Enhanced Oil Recovery. Furthermore, this chapter also provides an insight to the current production trends in North American unconventional resources with a focus on Bakken Petroleum System. The chapter covers Bakken formation and Shale/Tight formation characteristics properties. Finally, the chapter will justify the need of CO₂-EOR in tight formations and analyzing these formations for potential carbon sequestration.

2.1 UNCONVENTIONAL / TIGHT OIL RESERVOIRS

Unconventional reservoir is a term to describe a hydrocarbon resource that could not be technically or economically recoverable without stimulation and distinguishes itself from conventional reservoirs by their special characteristic properties. **Figure 2.1** provides an abstract understanding of distinguishing parameters between ‘conventional’ and ‘unconventional’ reservoirs based on formation permeability scale. Tight reservoirs are defined with permeability less than 0.1 mD with shale reservoirs having characteristic permeability much less than 0.001 mD. Reservoir quality of tight formations is categorized in terms of porosity and permeability as very poor because the ultra-low permeability restricts fluid movement within the reservoir. This leads to single digit oil recovery factors and costly development activities. Tight formations are usually rich in light crude oil in the petroleum bearing formations which are often characterized as oil shale formations or tight sandstone (Mills 2008). Tight oil formations are also characterized with low porosity within the rock, usually less than 10%. The technological advances including horizontal drilling and multiple stage hydraulic

fracturing have led to the development of unconventional oil and gas reservoirs. These techniques enable larger exposure of surface area to a single well and increased flow area for reservoir fluid to flow towards the wellbore (IHS 2012). Commercial development of low permeability, ultra-tight formations by these techniques has led to the production of significant amount of hydrocarbons.

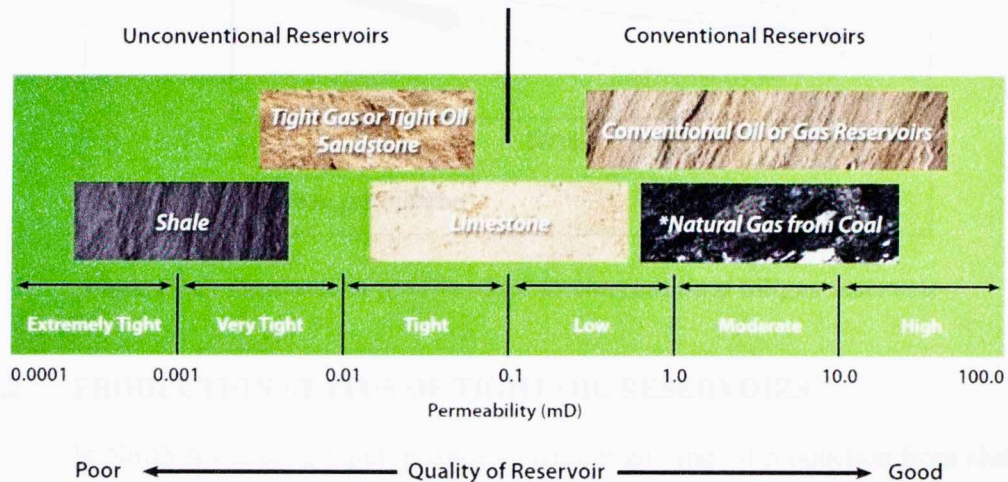


Figure 2.1: Distinguishing parameters between 'conventional' and 'unconventional' reservoirs (Baker 2013)

A typical production profile of an unconventional tight oil formation is illustrated in **Figure 2.2**. The high initial production rates are usually due to hydraulic fractures with a high pressure drawdown. Oil rate declines once the oil near the fractured zone is produced, leading to a steep fall in production rate. Beyond this rate, the flow is mainly controlled by inter-porosity mass transfer between the matrix and fracture network. In literature, there is not much research being done in the areas of improving recovery from tight oil reservoirs.

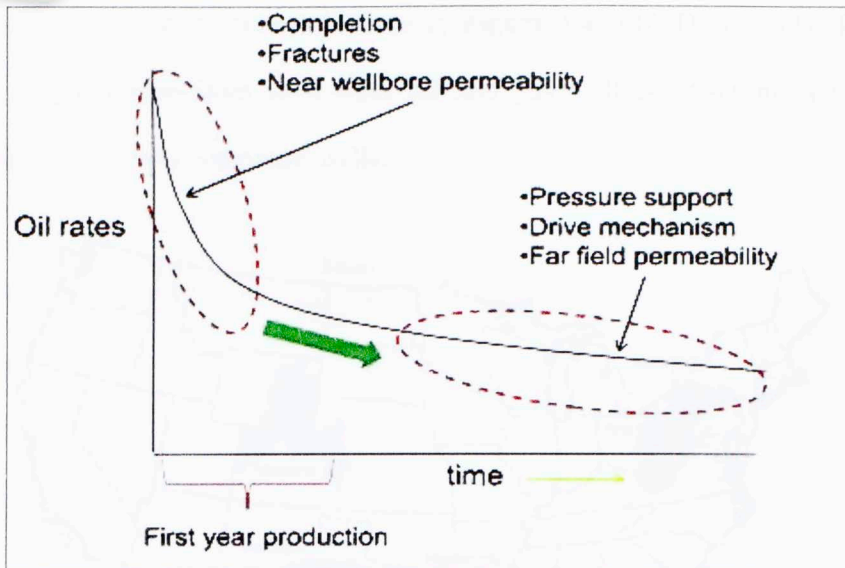


Figure 2.2: Production profile of an unconventional oil/gas reservoir

2.2 PRODUCTION STATUS OF TIGHT OIL RESERVOIRS

In North America, a rapid increase in natural gas and oil production from shale and tight formations has been experienced. Shale Basins of USA are estimated with technically recoverable resources of 24 billion barrels of tight oil production and 862 TCF of shale gas production (Baker 2013). **Figure 2.3** maps the major shale and tight formations of the USA. These six tight oil and shale gas formations have accounted for a total of 90% domestic oil production growth and 100% of domestic natural gas production in the fiscal years 2011-2013 (EIA 2013). From production statistics of February 2014, Bakken formation in North Dakota and Montana and Eagle Ford in South Texas formation accounted for 63% of the total US tight oil production growth and the Marcellus shale accounted for 75% of the natural gas production growth (EIA 2014). Recent improvements in drilling efficiencies and optimization of multi-stage hydraulic fracturing techniques are responsible for the recent production growth instead

of increase in the rig count, as observed in **Figure 2.4** (EIA-DPR 2014). The steep decline in production from each tight oil and gas well is offset by the growing production from newly completed wells.

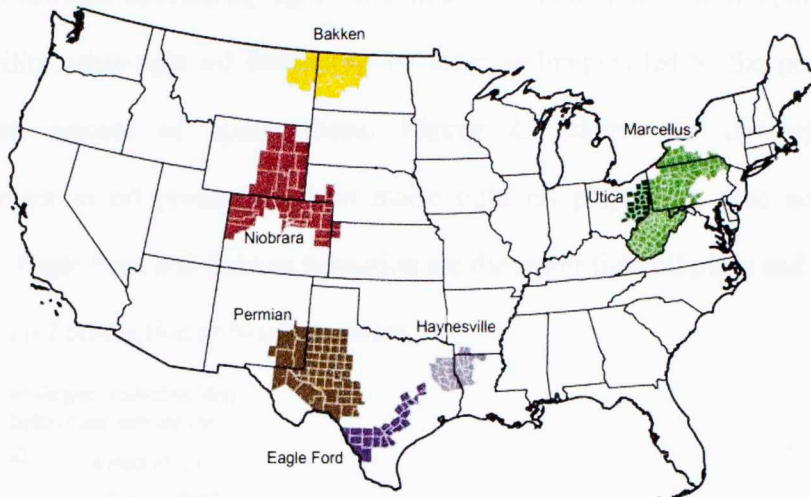


Figure 2.3: Major Tight/Shale Formations of USA (Sieminski 2014)

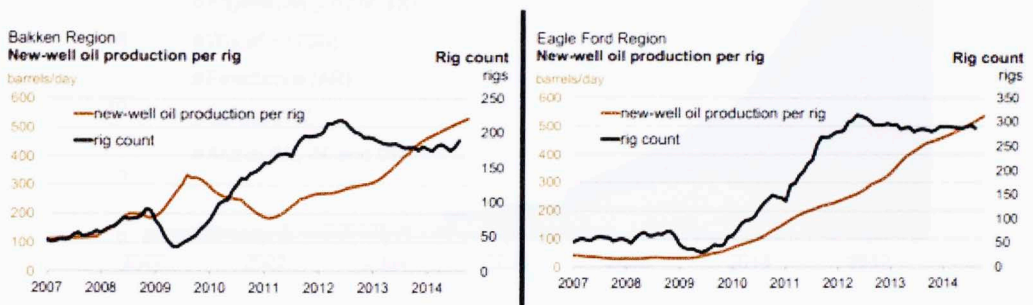


Figure 2.4: Rig count and oil production for US oil shale reservoirs; black curve is the rig count

Activities to develop tight formations were very meager until early 2005. With the advances in technology, Mitchell Energy led to the first shale play development of Barnett Shale (Wang and Krupnick 2013). Shale gas production achieved new measures in Barnett because of advances in multi-stage hydraulic fracture technology and this

technology transfer led to the development of other shale gas reservoirs across USA as observed in **Figure 2.5**. With gaining expertise in development of tight formations by shale gas and also dipping natural gas prices, in early 2010 companies shifted their attention towards developing tight oil formations. Commercial development of low permeability, ultra-tight oil formations by these techniques led to the production of significant amount of hydrocarbons. **Figure 2.6** shows the development and improvement in oil production from major tight oil plays with time across North America. Eagle Ford and Bakken formation are the major tight oil plays and contributes to a major oil production in North America.

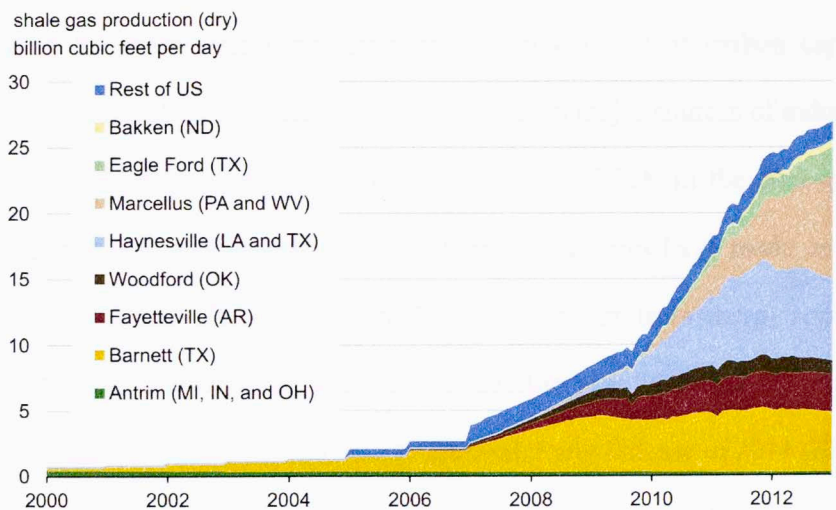


Figure 2.5: Shale gas production across North America (EIA 2013)

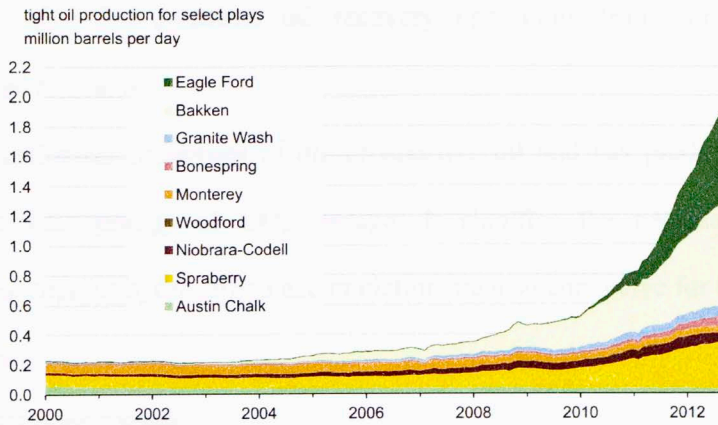


Figure 2.6: Tight oil production across North America (EIA 2013)

2.3 CARBON-CAPTURE-STORAGE AND ENHANCED OIL RECOVERY

There has been strong emphasis on the critical role of carbon capture and storage projects to tackle significant CO₂ emission from major sources of industries. As a byproduct of fossil fuel utilization, the rising trend of CO₂ in the atmosphere has caused concerns over temperature increase. Energy industries have made an effort to reduce CO₂ emission as shown in **Figure 2.7**. CO₂ emission from energy sources have actually reduced by 9% in recent years as compared to year 2005 and are projected to remain low as per the recent Annual Energy Outlook Early Release of 2014 (EIA 2014). But, emission from other CO₂ byproduct sources, such as electricity and heat generation, transportation, industrial and residential etc. is a cause of concern for increasing global warming. Power plants are responsible for one-third of CO₂ emissions in US. Carbon Capture and Storage (CCS) in geological formations deep beneath the water level is an important and productive mechanism to reduce anthropogenic CO₂ emissions present in the atmosphere (Sorensen et al. 2009). Geological formations with proven formation integrity like depleted oil and gas reservoirs, deep saline formations,

and CO₂ flooding for enhanced oil recovery operations from conventional and unconventional formations.

The geological properties of the prospective oil and gas producing fields are analogous to the geology of CO₂ storage. It signifies the necessary geological conditions that support hydrocarbon accumulation are also conducive for CO₂ storage in the formation.

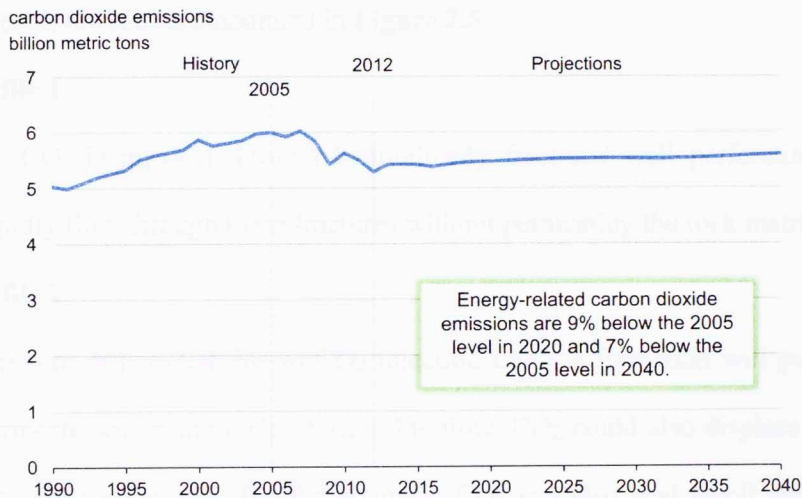



Figure 2.7: CO₂ emission statistics from energy industry (EIA 2014)

2.3.1 CO₂ ENHANCED OIL RECOVERY

CO₂ Enhanced Oil Recovery is a process of injecting CO₂ into the formation to displace hydrocarbons in a miscible or pseudo-miscible manner. Onshore CO₂ flooding is a mature technology and has been used widely. For example, Occidental Petroleum operates 74% of their EOR operations by CO₂ flooding, leading to an incremental oil recovery of 110% since 2010 in Permian Basin (Occidental Petroleum Corporation 2014). Furthermore, CO₂ reinjection in a closed loop will allow CO₂ to be permanently trapped and stored into the formation.



Compared with a conventional reservoir EOR, CO₂ injection and displacement process would be significantly different in tight/shale formations. In tight formations, flow through natural and hydraulic fractures will dominate CO₂ displacement within the formation, eliminating the conventional displacement mechanism of sweeping hydrocarbons from matrix.

The conceptual understanding of CO₂ flow in tight formations as explained by Sorensen et al. (2013b) is elaborated in **Figure 2.8**.

Flow Profile 1:

As CO₂ is injected through hydraulically fractured well perforations, it will rapidly flow through these fractures without permeating the rock matrix.

Flow Profile 2:

Pressure differential due to CO₂ injection into the formation will push CO₂ to permeate within the rock. During this flow, CO₂ could also displace oil deeper into the rock matrix. On the contrary, CO₂ can also lead to oil swelling, and hence displacing more oil out of the rock matrix.

Flow Profile 3:

As CO₂ continues to permeate within the rock matrix, oil will be displaced to migrate out of the rock surface and towards the fractures based on lower viscosity and oil swelling generated by CO₂.

Flow Profile 4:

As pressure is equalized throughout the low permeability matrix, oil and CO₂ miscible phase will improve oil mobilization. Beyond this point, concentration

gradient driven diffusion will displace oil out of rock matrix towards the fractures.

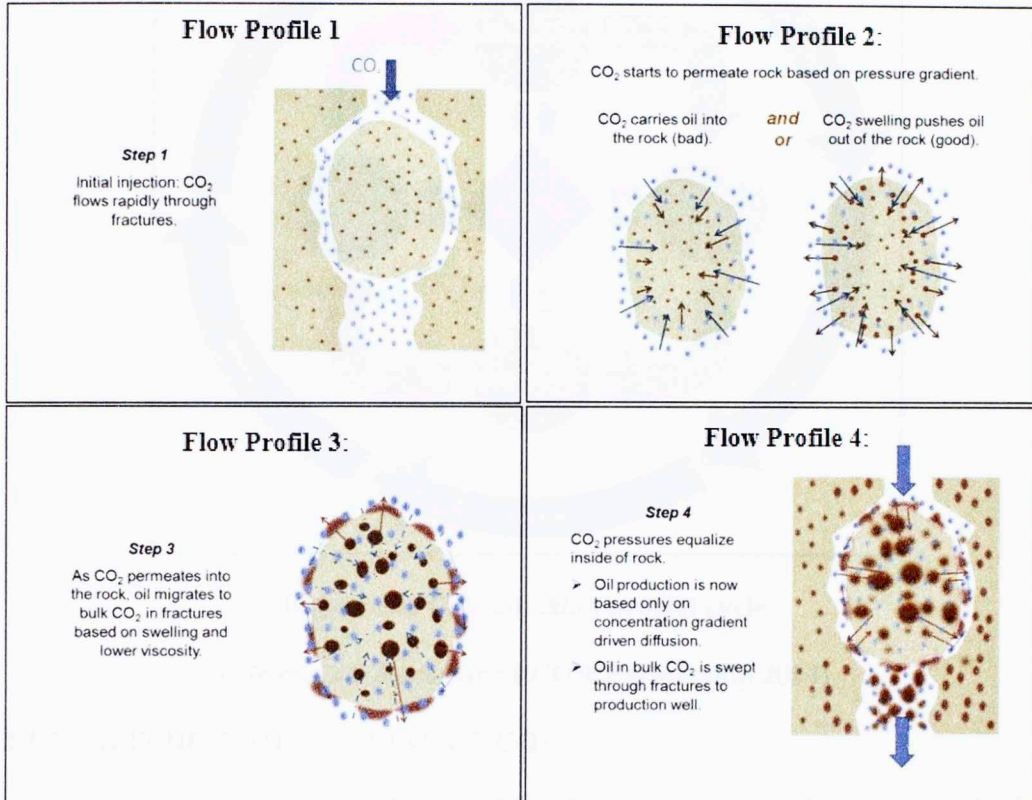


Figure 2.8: Conceptual CO₂ EOR in tight/shale formations (Sorensen et al. 2013b)

Plains CO₂ Reduction PCOR Partnership (2014) presented an integrated approach for practical application of CO₂ sequestration and EOR projects in North America as illustrated by **Figure 2.9**. The focus of this study is only towards modeling and simulation of CO₂ EOR and CO₂ Sequestration. This research focuses on evaluating the reservoir characteristics that are critical to CO₂ injection, evaluating injection scenarios, and in order to understand the displacement mechanism of CO₂ into a tight oil formation.

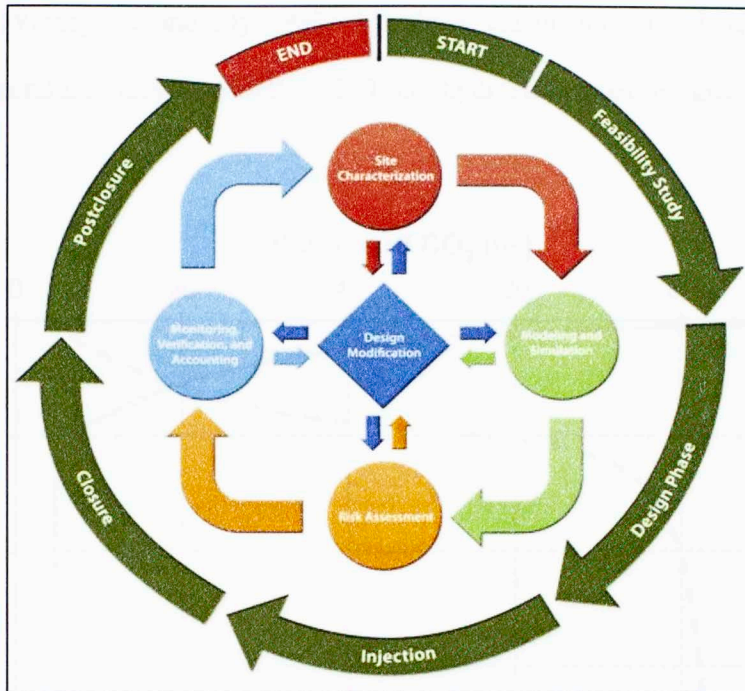


Figure 2.9: CO₂ injection project cycle

(Plains CO₂ Reduction PCOR Partnership 2014)

2.3.2 SUPERCRITICAL STATE OF CO₂

A supercritical state of CO₂ is achieved when pressure and temperature in the reservoir is above 83° F and 1070 psia, respectively. CO₂ at deep reservoir conditions behave as a super critical fluid which has viscosity of a gas and density of a liquid. The super critical state of CO₂ allows greater volume of CO₂ to be efficiently stored in the reservoir, as any given mass of CO₂ will occupy less space 10,000 ft below the surface.

Figure 2.10 shows the volume changes of CO₂ with respect to depth. A volume of 100 *ft*³ of CO₂ at surface conditions will reduce to 4.4 *ft*³ at reservoir depth of 11,000 ft. Volume is inversely proportional to density and CO₂ density increases with depth. That is the reason for the supercritical behavior of CO₂ i.e. density of a liquid and

viscosity of a gas. CO₂ density is estimated by an equation developed by Chapela and Rowlinson (Younglove and Ely 1987) All above calculations are done considering normal temperature gradient of 0.015 °F/ft and hydrostatic pressure gradient of 0.433 psia/ft.

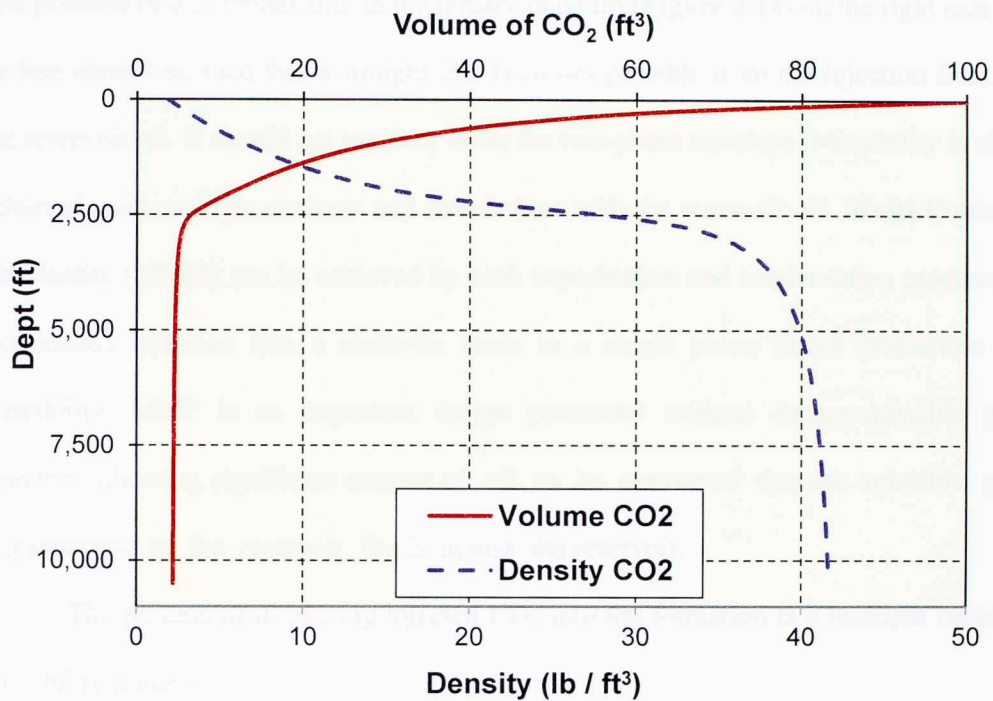



Figure 2.10: Volume-Depth type curve for CO₂

2.3.3 MINIMUM MISCIBILITY PRESSURE

CO₂ flooding can be a miscible displacement process in the reservoir condition if the reservoir pressure is above the Minimum Miscible Pressure (MMP). Miscibility between injection gas and hydrocarbon component will eliminate the interfacial tension so that high displacement efficiency could be achieved in an ideal system. There are two types of miscibility; 1) first contact miscibility and 2) multi contact miscibility.



First Contact Miscibility (FCM) is achieved when the injected gas instantaneously becomes miscible with the reservoir fluid. It indicates that there is no composition exchange, a single phase is present all the time. First contact signifies that at any composition of two components, they will always remain in state of miscibility. The position of oil composition in the ternary diagram (**Figure 2.11**) on the right side of tie line should be such that a straight line becomes possible from the injection fluid to the reservoir oil. It should not touch or cross the two-phase envelope. Miscibility is also achieved with multiple contacts and interactions with the reservoir oil. **Multi Contact Miscibility (MCM)** can be achieved by both vaporization and condensation processes. Continuous injection into a reservoir leads to a single phase liquid production at miscibility. MMP is an important design parameter utilized during miscible gas injection, allowing significant amount of oil to be recovered through miscible gas displacement of the reservoir fluids across the reservoir.

The process of displacing injected CO₂ into the formation is a multiple contact miscibility process.

The most crucial parameter in an EOR process by miscible gas injection is to attain the Minimum Miscibility Pressure (MMP). At a constant temperature and a given composition, MMP is the lowest pressure at which a first or multiple contact miscibility could be achieved (Mihcakan 1994). The reservoir pressure must always be higher than the first contact miscibility of the injection fluid. Miscibility can be achieved by either first contact or multiple contact.

At MMP, the interfacial tension is zero and no interface exists between the fluids. A ternary phase diagram in **Figure 2.11** shows the concept of miscibility in a three pseudo-component system at reservoir pressure and temperature.

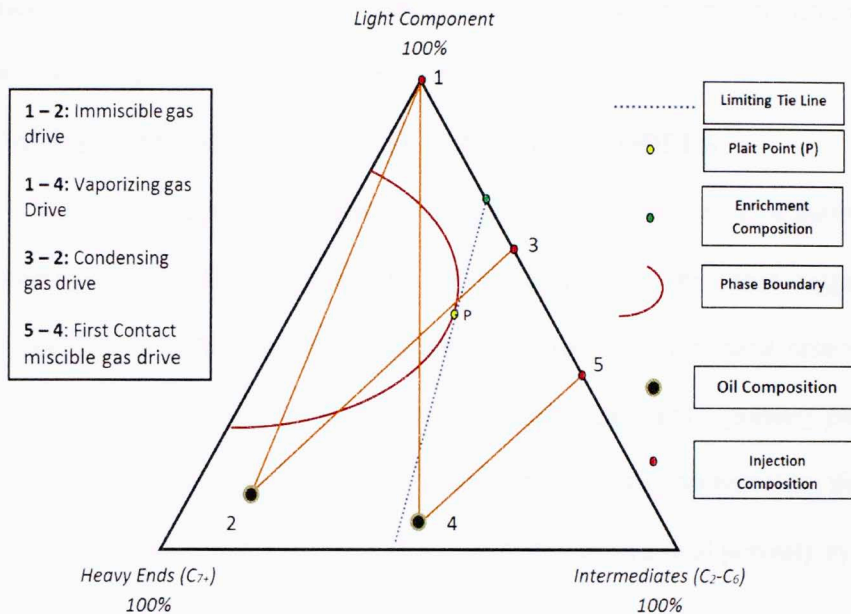


Figure 2.11: Pseudo-Ternary phase diagram for Miscibility; red curve represents two-phase region, black dot represents the oil composition.

Light components usually represents the injected gas (100% CO₂, CH₄). The other two corner points represent the intermediate components (C₂-C₆) and heavier components (C₇+). The concentration of the injection component and the location of oil composition determine the form in which miscibility would take place. The different orange lines are representative of the various possible gas drive possible.

2.4 OIL SHALE/TIGHT RESERVOIR CHARACTERISTICS

To model a tight formation with ultra-low permeability, complex fracture networks are a crucial part of model. This includes primary hydraulic fractures, induced secondary fractures usually perpendicular to primary fractures, and natural fractures. In

the study model, hydraulic fractures and natural fractures in a single porosity system are explicitly modeled for simulation.

Wu et al. (2014) presented a mathematical model to simulate tight formation gas production considering physical processes like adsorption/desorption, geomechanics effect, Klinkenberg effect and Non-Darcy flow across fractures.

2.4.1 SINGLE POROSITY V/S DUAL POROSITY MODELS

A naturally fractured reservoir is a complex system consisting of matrix blocks surrounded by irregular fracture networks. Warren and Root (1963) first suggested that a single porosity system could not characterize the naturally fractured reservoirs and proposed a dual porosity system. Dual porosity system considers a primary porosity of inter granular pore spaces combined with a secondary porosity representing the natural fractures. Shape factor defines matrix-fracture interactions in a dual porosity system and are based on pseudo steady state assumption.

Kucuk and Sawyer (1980) adopted the Warren and Root model to model a shale gas reservoir and also incorporated physical characteristics like gas desorption from organic content, Knudsen flow in pores and fully transient model for matrix.

Wu et al. (2014) analyzed the reservoir simulation of unconventional shale gas reservoir using both single and dual porosity models. Shape factor plays a critical role to model the matrix-fracture interaction which significantly affects production from tight formations. Difference in gas production was approximately 15% after 20 years of production and this could be attributed to the effect of matrix-fracture interactions.

The Middle Bakken layer is a tight dolomitic siltstone formation. Pitman et al. (2001) reported that the majority of oil resides within the natural fracture pores and

matrix contribution is very minimal in Middle Bakken. For a dual porosity media, these natural micro-fractures will represent the matrix porosity. Fracture porosity is a measure of hydraulic fracture and natural fractures in the dual porosity media.

CO₂ storage in the New Albany Shale was studied using dual porosity and dual permeability models (Liu et al. 2013). This study reported the feasibility of CO₂ sequestration in shale formations, but improvement in natural gas recovery was very minimal around 1%. This could be attributed to the unstimulated tight formation between the injector and producer well.

2.4.2 NATURAL FRACTURE NETWORK

For the Bakken formation, presence of natural fractures is a known fact. Pitman et al. (2001) reported that the microscopic and macroscopic natural fractures are present all around the Middle Bakken, with majority to be inclined horizontal, open and aperture widths greater than 30 microns. It is also observed that these discontinuous fractures form dense networks if the host rock consists of high residual oil saturation.

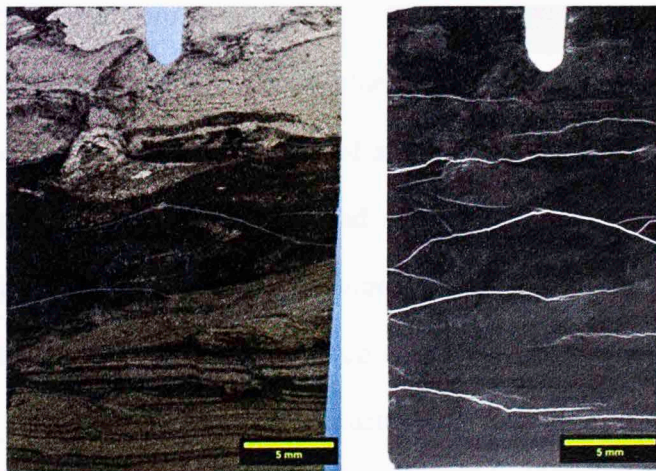


Figure 2.12: Ultraviolet Fluorescence (UVF) analysis of micro fractures in Middle Bakken (Sorensen et al. 2013a)




Figure 2.12 shows the comparison between a thin section from a Middle Bakken core in plane-polarized light and Ultraviolet Fluorescence (UVF) (Sorensen et al. 2013a). Induced fractures from hydraulic fracturing and natural fractures play a critical role in production from tight and shale formations. In order to better understand and visualize the effects of non-planar induced and natural fractures on transport properties, Sakhaee-Pour and Wheeler (2013) proposed a fractured cell approach to model flow behavior from densely fractured tight formations. The fracture cell model accounted for matrix-fracture and fracture-fracture interactions along with matrix-matrix interactions in the reservoir to calculate the effective anisotropic permeability for each grid blocks containing these three forms of interactions. For CO₂ injection, natural fractures in tight formation play a critical role for flow migration. Discrete modeling of natural fractures in the reservoir model would evaluate the flow mechanism of CO₂ to sweep reservoir matrix. With this consideration, the fracture cell model was implemented into the reservoir model to account for the presence of natural fractures, instead of relying on dual porosity models.

The main advantage of using the fracture cell model was that it does not require local grid refinement to model these natural and induced fractures into the reservoir model. The paper defined the approach and methodology to calculate the effective permeability for grid blocks containing fractures. For each grid with fractures present, effective permeability in X - and Y - direction can be calculated based on the resulting matrix-fracture and/or fracture-fracture interactions. A fracture cell in a reservoir grid system is a grid block that contains atleast one fracture inside it. The transport properties of this grid block can be modified in a reservoir simulator by changing the

permeability and porosity. This effective permeability depends on the possible interaction of this grid block with the adjacent grid blocks like matrix-matrix, matrix-fracture and fracture-fracture interactions. **Figure 2.13** shows the cells consisting of fractures and modeling approach.

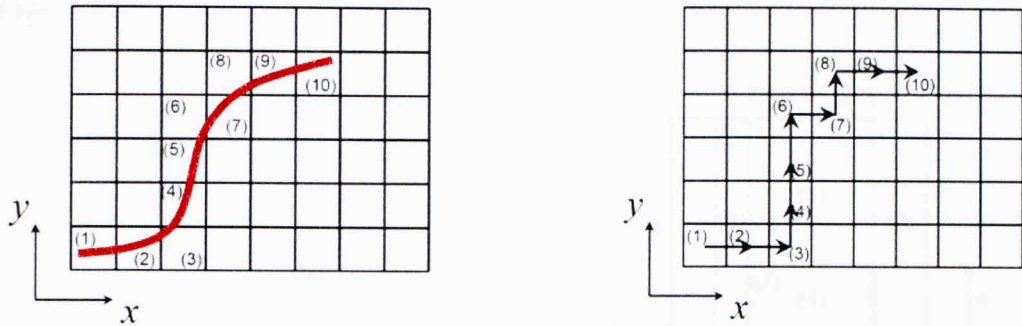


Figure 2.13: (a) Red color represents a non-planar fracture (b) representative path through the fracture cells in the model (Sakhaee-Pour and Wheeler 2013)

The cells defining the representative path in the reservoir model are the fracture cells. The authors proposed a hypothesis to calculate the fracture-fracture permeability and the matrix fracture permeability for each fracture cell. For fracture cells connecting through a fracture, the effective permeability due to fracture-fracture interactions was calculated by:

$$k_{ff} = \left(\frac{l_c}{l_f}\right) \frac{w^3}{12h} \dots\dots\dots (2.1)$$

Where, k_{ff} = effective permeability of fracture cells,

l_c = length of representative path, ft

l_f = length of curved fracture between two points, ft

w = aperture size of fracture, ft

h = cell size, ft

For the fracture cells not connected to the adjacent cells by a fracture, the effective permeability depends on the matrix-fracture interactions. To calculate these interactions, the fracture cell were divided into two zones, one accounting for region containing discrete fracture parts and the other surrounding matrix zone as displayed in **Figure 2.14**.

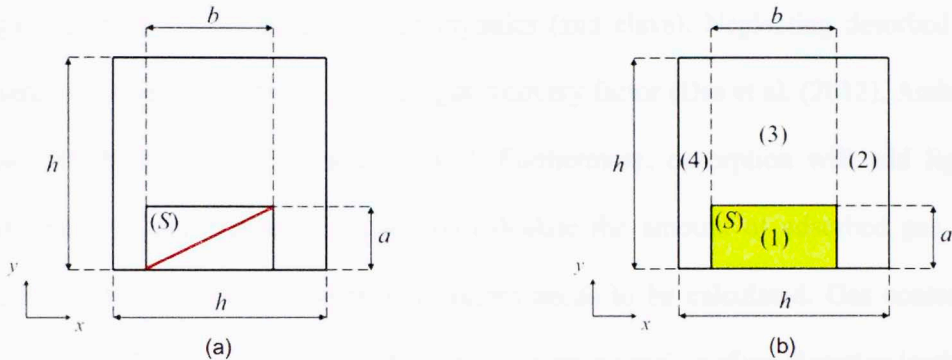


Figure 2.14: Dissection of a fracture cell to account for matrix-fracture interaction
(Sakhaee-Pour and Wheeler 2013)

The yellow zone in the **Figure 2.14(b)**, represents a zone of enhanced permeability due to presence of a disconnected natural fracture. This will account for the flow taking place through the grid block due to a dominating permeability.

$$k_{MF-x} = \frac{1}{\frac{1-\frac{b}{h} + \frac{w}{h}k_f \cos^2 \theta_x + (1-\frac{a}{h})k_m}{\frac{b}{h}}} \dots\dots\dots (2.2)$$

Where, k_{MF-x} = effective matrix-fracture interaction permeability, ft²

k_m = matrix permeability, ft²

$\frac{b}{h}$ = geometry parameter in X- direction

$\frac{a}{h}$ = geometry parameter in Y- direction

w = fracture aperture size, ft

θ_x = angle between fracture curve and boundary, °

The effective permeability of each fracture cell in the representative path was calculated from the dominating mechanism between k_{MF-x} and k_{FF} .

2.4.3 ADSORPTION/DESORPTION EFFECT ON OIL PRODUCTION

In shale formations, in addition to free gas, shales can hold significant quantities of gas adsorbed on the surface of the organics (and clays). Neglecting desorbed gas volume will underestimate the ultimate gas recovery factor (Das et al. (2012), Ambrose et al. (2010), Bumb and McKee (1988)). Furthermore, desorption will add lighter components in the produced stream. To calculate the amount of adsorbed gas, gas content V_g (SCF/ton) and adsorption isotherm needs to be calculated. Gas content is defined as total amount of gas adsorbed on the reservoir rock surface. Sorption isotherm is the reservoir rock capacity to stick the adsorbed gas with respect to pressure at constant temperature (Mengal and Wattenbarger 2011). Sorption and desorption onto organic carbon in shale formations can be empirically modeled using the Langmuir's Isotherm (Langmuir 1916) concept as applied in coal bed methane reservoirs (**Figure 2.15**). The sorption isotherm is defined as:

$$v_{sg} = (1 - \phi^m - \phi^f) \epsilon_{sc} \rho_r V_s \dots\dots\dots (2.3)$$

Where, V_g = Adsorbed gas volume at standard conditions per unit solid mass

ρ_r = solid rock density

ϵ_{sc} = gas mole density at standard condition

A Langmuir isotherm is established to measure the adsorption isotherm for the prospective area of the basin using available data on TOC and on thermal maturity to

establish the Langmuir volume (V_L) and the Langmuir pressure (P_L). The volume of adsorbed gas at constant temperature depends on pressure in the following way:

$$V_s = \frac{V_L P}{P_L + P} \dots\dots\dots (2.4)$$

Where, V_s = Gas content, SCF/Ton

V_L = Langmuir Volume, the maximum adsorption capacity, SCF/Ton

P_L = Langmuir Pressure, the pressure at a point when 50% of the gas is desorbed, psia

P = reservoir pressure, psia

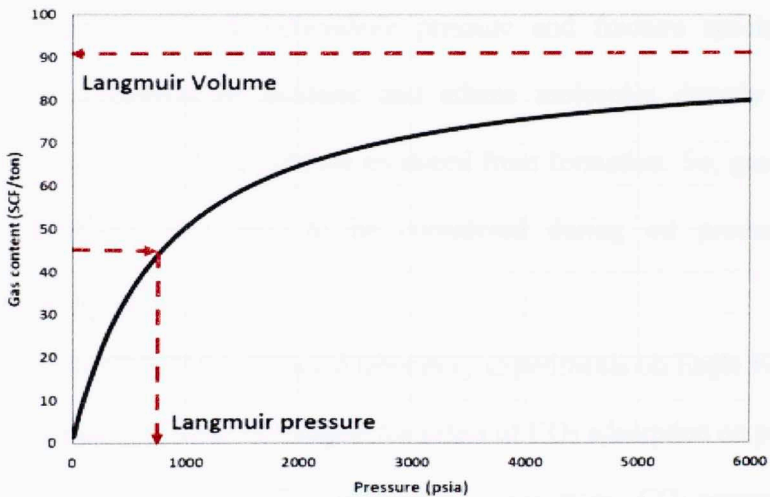



Figure 2.15: Langmuir's Isotherm Curve

Different studies have been conducted in various literatures to account for the effect of gas desorption on oil and gas production from tight reservoirs. Thompson et al. (2011) indicated that the adsorption mechanism is activated when there is a significant drop in reservoir pressure due to production and accounted for a 17% increase due to gas desorption in EUR after 30 years of production from a horizontal well in Marcellus shale gas reservoir.



Small pore diameters in tight/shale reservoirs in range of nanometers results in extremely low formation permeability. Small pore diameter results in large surface area being exposed in the porous media with large volume of gas adsorbing on the pore surface. The smaller pore size will increase CO₂ adsorption, leading to desorption of hydrocarbon components. With decreasing pore size, the ratio of free gas to adsorbed gas storage capacity decreases (Beliveau 1993).

In a recent study to simulate gas desorption effects in production from shale gas reservoirs, Wu et al. (2014) concluded that gas desorption plays a critical role in tight formations at a significant pressure drawdown. Also, gas desorption effects are inversely proportional to well bottomhole pressure and fracture spacings. In oil production, gas desorption of methane and ethane molecules directly affect the hydrocarbon composition of the light oil produced from formation. So, gas desorption effects are significant and need to be considered during oil production from tight/unconventional reservoirs.

Al Ismail et al. (2014) conducted laboratory experiments on Eagle Ford vertical and horizontal shale samples to investigate the effect of CO₂ adsorption on permeability anisotropy. CO₂ adsorption also affect permeability anisotropy. CO₂ permeability was reduced by a magnitude order in a vertical sample and only reduced 10% in a horizontal sample. The study suggested that the negative effect of CO₂ adsorption on the vertical permeability will be helpful in providing a vertical seal for geological migration of CO₂ when it is considered as a potential injection gas to improve oil recovery and also for CO₂ sequestration projects.

Yu and Sepehrnoori (2014) reported an increase in Estimated Ultimate Recovery (EUR) by 20% from New Albany and Marcellus Shale gas reservoirs. Gas desorption accounted for less than 10% incremental EUR for Haynesville after 30 years of production. **Figure 2.16** shows the Langmuir Isotherm curves used in the study by Yu and Sepehrnoori (2014). The study considered the desorption effect in the entire reservoir. The model was a highly fractured reservoir and pressure dropped down to 500 psia in SRV after 30 years of production. Due to high pressure drop, it is evident to observe significant amount of gas desorption during production.

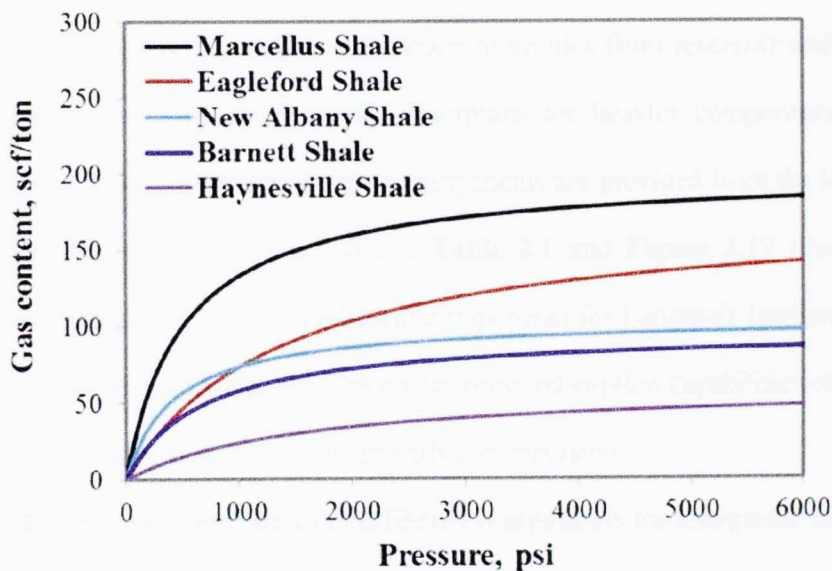


Figure 2.16: Langmuir Adsorption Isotherm for five shale gas reservoirs across North America (Yu and Sepehrnoori 2014)

For a fluid mixture of different hydrocarbon components, a multi-component adsorption considers the effect of gas phase composition at partial pressure of each composition. The model used in literature to account for multi-component adsorption is Extended Langmuir Model (Hall et al. (1994), Ambrose et al. (2010)).

$$V_{s,i} = \frac{V_{L,i} \left(\frac{P_L}{P_{L,i}} \right)}{1 + \sum \left(\frac{P_L}{P_{L,i}} \right)} \dots\dots\dots (2.5)$$

Where, V_s = Adsorbed gas volume per rock weight, SCF/Ton,

$V_{L,i}$ = Maximum Langmuir Volume for component i ,

$P_{L,i}$ = Partial pressure of component i

P_L = Langmuir pressure, psia,

In this study, Extended Langmuir Isotherm model is employed to account for adsorption of CO₂ and desorption of hydrocarbon components in reservoir simulation. Considering desorption of methane and ethane molecules from reservoir and ignoring other higher components by assuming desorption for heavier components is very minimal. Adsorption parameters for these components are provided from the laboratory experiments from Ambrose et al. (2011). **Table 2.1** and **Figure 2.17** illustrate the constant adsorption parameters of different components for Langmuir Isotherm model. **Figure 2.17** shows that at higher reservoir pressure, adsorption capabilities of CO₂ are significantly higher as compared to hydrocarbon components.

Table 2.1: Constant parameters of different components for Langmuir Isotherm

(data: Ambrose et al. (2011))

Component	$V_L \left(\frac{SCF}{Ton} \right)$	$P_L(psia)$
Methane, C1	56	1,562
Ethane, C2	91	811
Carbon Dioxide, CO ₂	145	836

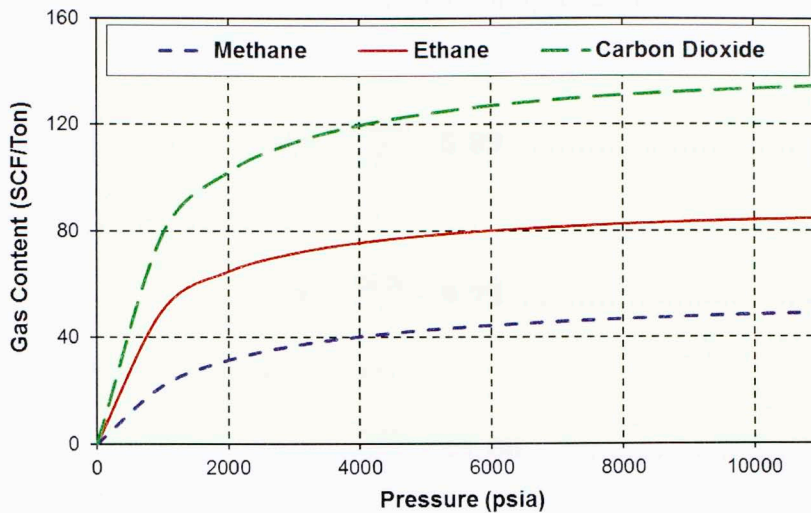


Figure 2.17: Laboratory measurements for Extended Langmuir Isotherm for different hydrocarbon components (data: Ambrose et al. (2011))

2.4.4 TOTAL ORGANIC CONTENT AND ADSORPTION

The adsorption capacity of a porous media is directly proportional to active surface area of the shale matrix content. The presence of organic matter in shale lowers the density, increase the porosity, impart anisotropy, provide the source of gas, and ultimately facilitate adsorption capabilities (Sondergeld et al. 2010, Ambrose et al. 2010). Langmuir's Isotherm can be mathematically also defined as:

$$V_P = V_{max} \frac{KP}{1+KP} \dots\dots\dots (2.6)$$

Where, K = Langmuir constant, 1/psi

Kerogen type and the TOC wt% content both affect the adsorption capacity in a formation. Zhang et al. (2012) developed an empirical model to account for gas adsorption affected by organic matter type and thermal maturity for methane by conducting adsorption isotherm experiments in temperature range of 35 °C and 65 °C. Based on adsorption isotherms, empirical correlations were developed stating relation

between the Langmuir's constant and kerogen type as defined in the following equations:

$$\text{Type I Kerogen} \quad \ln K = \frac{1241}{T} - 5.89 \dots\dots\dots (2.7)$$

Type II Kerogen with $R_o < 1.4\%$

$$\ln K = \frac{2628}{T} - 9.75 \dots\dots\dots (2.8)$$

Type II Kerogen with $R_o > 1.4\%$

$$\ln K = \frac{3366}{T} - 11.06 \dots\dots\dots (2.9)$$

Where, T = Temperature, Kelvin

K = Langmuir Constant, 1/MPa

R_o = Vitrinite reflectance

Simenson (2010) reported kerogen of Type I and Type with $R_o < 1$ for the Middle Bakken formation, so **Equation 2.7** is used in further study to calculate the Langmuir constant.

Zhang et al. (2012) developed a correlation using linear regression between TOC wt % and maximum adsorption capacity, V_{max}

$$V_{max} = 724 [0.0134 * TOC + 0.0148] \dots\dots\dots (2.10)$$

Where, V_{max} = Maximum adsorption capacity, SCF/Ton

TOC = Total Organic Content, wt %

The above correlation is valid in temperature range of 35 °C and 65 °C. Lewis et al. (2004) developed empirical correlations that extrapolate the above study and evaluate the adsorption components at Bakken reservoir temperature of 240 °F (115 °C). These correlations were originally developed for Coal Bed Methane reservoirs but can be applied to this study.

$$V_{LT} = 10^{(-c3.T+c4)} \dots\dots\dots (2.11)$$

$$P_{LT} = 10^{(-c7.T+c8)} \dots\dots\dots (2.12)$$

$$c4 = \log V_L + (c3.T_i) \dots\dots\dots (2.13)$$

$$c8 = \log P_L + (c7.T_i) \dots\dots\dots (2.14)$$

Where, T_i = Isotherm temperature (65 °C)

V_L = Adsorption capacity at T_i , from **Equation 2.6**

P_L = Langmuir’s constant at T_i , from **Equation 2.6**

T = Reservoir temperature (115 °C)

V_{LT} = Adsorption capacity at reservoir temperature

P_{LT} = Langmuir’s constant at reservoir temperature

$c3$ = 0.0027

$c7$ = 0.005

This study estimated the adsorption parameters, V_{max} and K with respect to organic content at 65 °C using correlations developed by Zhang et al. (2012). The correlations developed by Lewis et al. (2004) were then utilized to extrapolate the adsorption parameters at Middle Bakken reservoir temperature of 240 °F.

2.4.5 STRESS DEPENDENT PERMEABILITY (GEOMECHANICS)

Geomechanics plays a very critical role in oil and gas production from tight or unconventional reservoirs. Production from these reservoirs is strongly dependent on the flow through hydraulic fractures and natural fracture networks. The critical properties of these fractures are very sensitive to stress changes in the formation. In low permeability formations, well bottomhole pressure is reduced to the minimum pressure possible to achieve desirable gas production rate. This results in significant pressure

change leading to major changes in stress field of the formation. With production, induced stresses will alter the aperture and permeability of micro fractures and hydraulic fractures. The induced stresses will close the fracture openings, decreasing the permeability and could significantly block the fluid flow from fracture to matrix and ultimately to the well perforation. During injection, it will try to keep the fractures open. So neglecting the effect of stress induced permeability, significantly over estimates the oil recovery which will not be observed during real time production. Bustin et al. (2008) reported that the effect on permeability due to stress changes is significantly higher in shale formations than that in sandstone formations.

For reservoir simulation, geomechanics will quantify the stress changes in a formation impacting the porosity and permeability and the relationship is defined in terms of mean effective stress. Injection rate critically depends on the stress distribution near the wellbore and is defined by the Terzaghi Law (Terzaghi 1943). The law relates the mean effective stress with the formation pore pressure by the following equation:

$$\sigma_{eff} = \sigma - \alpha P_p \dots\dots\dots (2.15)$$

Where, σ_{eff} = mean effective stress

σ = total stress

α = Biot's factor.

Biot's factor is defined in terms of stress changes as:

$$\alpha = 1 - \frac{K_{bulk}}{K_{grain}} \dots\dots\dots (2.16)$$

Where, K_{bulk} and K_{grain} are bulk and grain modulus.

Stress/Pressure dependent permeability and porosity in the Bakken formation is validated a number of times by laboratory core experiments and buildup tests in a

particular well at different time and pressure levels (Breit et al. 1992). DST results indicated a highly stress sensitive permeability for the Bakken. The results as shown in **Figure 2.18** quantify the relationship between the permeability/porosity and the reservoir pressure. It suggests that during high drawdown conditions, fractures close near the wellbore and as fluid pressure increases, these fractures open again.

Wang et al. (2009) reported a study on effective CO₂ flooding in low permeability formations with focus on the effect of effective stress on displacement efficiency in both matrix and fracture. The study concluded that CO₂ displacement efficiency would improve with increasing effective stress because the fractional reduction in fracture permeability is significantly higher as compared to changes in matrix permeability (**Figure 2.19**).

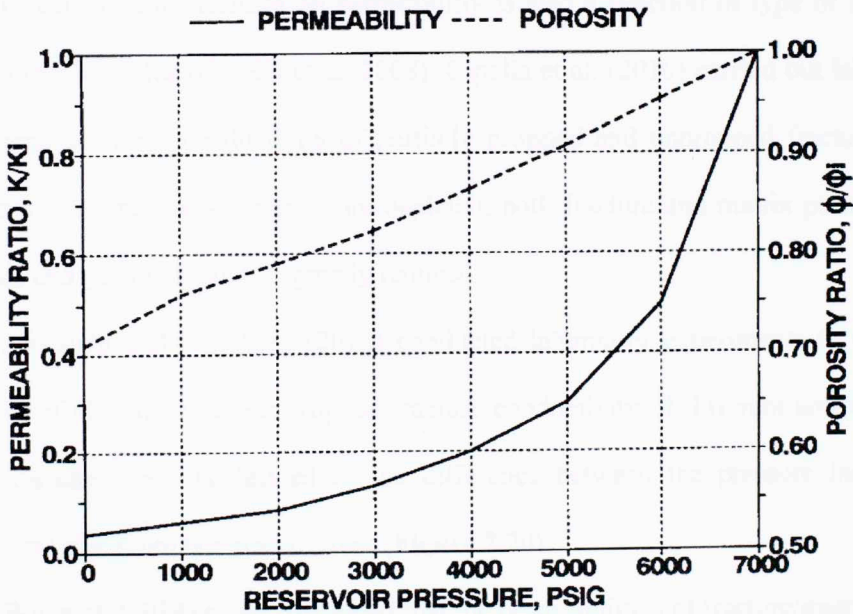


Figure 2.18: Stress dependent porosity and permeability for Bakken well

(Breit et al. 1992)

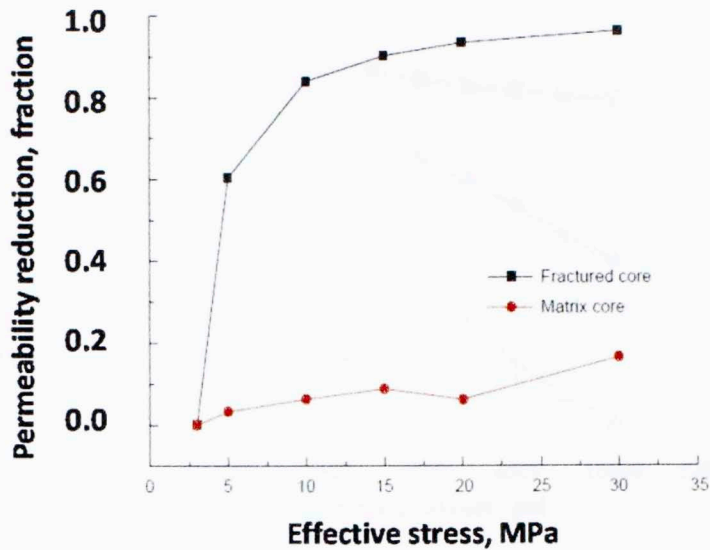


Figure 2.19: Changes in matrix and fracture permeability in a core with effective stress (Wang et al. 2009)

Effect of geomechanics on permeability is also a function of type of fractures and Young's Modulus (Cipolla et al. 2008). Cipolla et al. (2010) carried out laboratory experiments to relate conductivity of partially propped and unpropped fractures as a function of closure stress. As pressure depleted, both fracture and matrix permeability decreases and gas production is greatly reduced.

Alramahi and Sundberg (2012) conducted laboratory experiments to evaluate the effect of closure stress on propped fracture conductivity of different soft and stiff shales. Closure stress is defined as the difference between the pressure inside the fracture and minimum horizontal stress (**Figure 2.20**).

Wu et al. (2014) study concluded that the permeabilities of fracture/matrix could be reduced by 1 to 2 orders of magnitude. In highly stress sensitive formations, the gas production was reduced in range of 36% to 47% depending upon the fracture spacing.

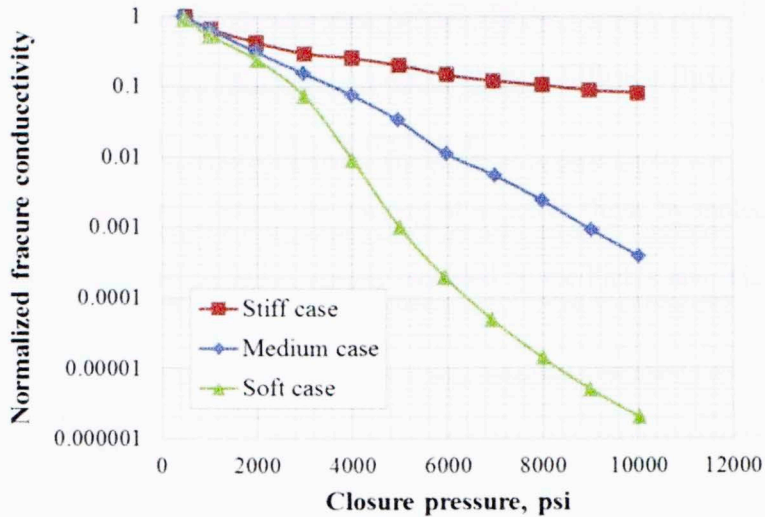


Figure 2.20: Closure stress effect on propped fracture conductivity

2.4.6 DIFFUSION

Reservoir parameters such as permeability heterogeneity and phase behavior of fluids in reservoir condition usually define the dominating production mechanism, while gravity drainage mechanism is not the dominating flow mechanisms in reservoirs with low matrix permeability, insignificant density difference between oil and injected gas. In these reservoirs, matrix block size affects the characteristic length of diffusion and fracture intensity determines the specific gas-oil contact surfaces. Therefore, molecular diffusion with strong dependence on fracture intensity, matrix block size, and the magnitude of diffusion coefficient, will control the mass cross-flow rates between fractures and matrix.

Diffusion refers to the net transport of material within a single phase in the absence of mixing (by mechanical means or by convection). Diffusion can be due to pressure gradient, temperature gradient (thermal diffusion), external force fluids (forced diffusion) and concentration gradients. The last type, concentration gradient means that

the diffusion is an isothermal and isobaric system and no external force field gradients apply (Poling et al. 2001). The proportionality between diffusion fluxes and diffusion potential is called diffusion coefficient or diffusivity.

Molecular diffusion defines the mixing of miscible fluids by molecular transfer due to concentration gradient and is usually modeled by the Fick's law. The law defines diffusion flux as:

$$J = -D \frac{\partial C}{\partial x} \dots\dots\dots (2.16)$$

Where, J = diffusion flux

D = molecular diffusion coefficient

C = concentration

x = position

Diffusion coefficient depends on tortuosity of formation, and porosity. The tortuous nature of pores, cross sectional area and pore size affects the diffusion in natural porous media. Diffusion of CO₂ into oil will lead to mass transfer of oil from matrix to fracture. The rate of CO₂ diffusion depends on diffusion coefficient. Diffusion could be a main recovery mechanism in tight fractured formations (Lie 2013)

There are three methods to model diffusion in reservoir simulation: 1) Classical Fick's law, 2) Maxwell-Stephan (MS) Model, 3) Generalized Fick's law. Multi-component diffusion by Fick's law considers only main diffusion terms and neglects the cross diffusion terms, making it a simplified approach. It means that the diffusion flux of each component is independent and the driving force of diffusion of each component is proportional to self-concentration gradient.


With this approach, the diffusion coefficient is considered independent of composition and PVT conditions and remains constant during simulation. CMG and various simulators use the classical Fick's law to model diffusion. Chawathe et al. (2014) studied flow mechanisms to model a shale gas simulator. Shale systems include organic matter, inorganic matter and natural fractures. They considered a multi-mechanism (desorption, convection and diffusion) and multi-porosity (organic, inorganic and fractured). It takes into account gas transport due to pressure driven convection, and concentration driven diffusion, desorption of multi-component gas from the organic surface, multi-mechanistic organic-inorganic material mass transfer.

For pore size larger than μm , effect of pore size can be neglected on flow behavior. The flow mechanism accounted for are convection (pressure gradient) and molecular diffusion (concentration gradient). Mass transport of fluid occurs in same phase during molecular diffusion.

2.6 NEED FOR CO₂ INJECTION IN TIGHT FORMATIONS

Present completion methods of hydraulic fracturing and horizontal drilling in the Bakken and other tight formations still leaves approximately 85 - 90% of hydrocarbons in the reservoir. High volumes of oil remaining in place or very low recovery factors are the strong motivation to investigate the applications of enhanced oil recovery techniques involving CO₂ injection.

There is a need to understand the controlling mechanisms for CO₂ injection. Even 1% increase in oil recovery will add approximately 2-9 billion barrels of cumulative oil. Based on US-DOE, methodology to estimate CO₂-EOR and storage capacity of Bakken, EERC suggested injection of 37-58 TCF CO₂ yielding 4-7 Billion




barrels of incremental oil. This is based on the utilization factor of 8 MCF of CO₂ per barrel of incremental oil.

Elm Coulee field was the first field to be developed in the Middle Bakken formation. Shoaib and Hoffman (2009) evaluated the capabilities of CO₂ injection for improving oil recovery in the Elm Coulee field. They carried out different scenarios of miscible CO₂ injection to define the optimum CO₂ injection pattern for Middle Bakken. Simulation results of their study reported an incremental oil recovery of 20% by CO₂ injection. Hoffman (2012) looked into the aspects of immiscible and miscible hydrocarbon gas injection into Middle Bakken and reported simulated incremental oil recovery of 13% and 21% respectively.

Zhou et al. (2008) carried out studies to evaluate the geomechanical stability of Williston Basin for potential CO₂ storage sites. They reported that since CO₂ is less dense than water, formation for CO₂ injection should be overlain by low permeability formation with an ability to stop the upward buoyancy – driven forces of the CO₂ injected. Zeng and Jiang (2009) evaluated the stress field present in Bakken formation. The study objective was to optimize the well alignments in the Bakken formation with futuristic applications for enhanced oil recovery by CO₂ flooding.

Xu (2013) carried out simulation models to evaluate the effective hydraulic fracture orientation in Elm Coulee field, Middle Bakken for miscible CO₂ injection. They reported an incremental oil recovery of 24% and also stated that transverse fractures will provide better reservoir connectivity and injection efficiency. Wan et al. (2013) used numerical simulation approach to analyze EOR potential by cyclic CO₂



injection in a fractured oil shale reservoir. The study reported the importance of stimulated fracture network connectivity improving the macroscopic sweep efficiency.

Sorensen et al. (2013b) carried out laboratory experiments on samples from Middle Bakken formation to propose the CO₂ EOR mechanisms in tight oil formations. They exposed the rock to CO₂ under Bakken reservoir pressure and temperature (230° F and 5000 psia) and the mobilized hydrocarbons were collected for analysis. They reported that 95% of hydrocarbon recovery was possible from Middle Bakken cores but required a longer exposure time when compared with conventional formation cores.

From these literature reviews, it is evident the CO₂ injection can boost oil production from tight formations. Further reservoir simulation and field scale pilot application are very critical to developed CO₂ EOR opportunities.

CHAPTER 3: MECHANISM STUDY OF CO₂ INJECTION IN DEPLETED GAS RESERVOIRS

In case of depleted gas reservoirs, some reservoirs are abandoned at high pressure because of variety of reasons such as formation subsidence, water invasion, and non-economic production rates. In gas reservoir development, high pressure at abandonment indicates that there is still a large quantity of natural gas available for further development by pushing the subsurface and technical limits. A technique to repressurize the reservoir is to inject CO₂ to displace the remaining gas present in the formation. As pressure builds up, cumulative production could be increased. In addition to this, the depleted reservoir could also act as an ideal carbon sink for long-term storage. In summary, injecting CO₂ in depleted gas reservoir would not only potentially rejuvenate the gas production by pressure buildup but will also store the greenhouse gas in a proven subsurface formation.

3.1 INTRODUCTION

There are four primary reasons why a depleted gas reservoir can be an ideal candidate for CO₂ storage. First of all, a gas reservoir is a container with proven integrity. One big concern of CO₂ subsurface storage is that it could potentially leak out to aquifer and surface (Klusman 2003, Maldal and Tappel 2004, Michael et al. 2010). For a depleted gas reservoir, its integrity has been tested by the original natural gas in geological time scale. Secondly, CO₂ can efficiently displace the remaining natural gas because of gravity segregation. Therefore, natural gas can be produced from an upper part of the reservoir and CO₂ injected at bottom part of the formation for better sweep efficiency and avoiding gas mixing to a great extent. Thirdly, the cost of sequestration

and storage of CO₂ could be offset by income from additional gas production; vice versa, the gas production cost will be mitigated via taxes of using CO₂. Fourthly, industry could capitalize on existing wells (previous producer or injector) rather than drilling new wells, which potentially makes the project more economically viable. Therefore, depleted gas reservoirs could be the potential targets for CO₂ storage as well as enhancing gas production.

3.2 PHYSICAL PROPERTIES OF CO₂ AND CH₄

Knowledge of thermodynamic properties of CO₂ and CH₄ is important as these properties are responsible to optimize compression, monitor transportation and model mobility of gas in the reservoir conditions. Critical parameters of CO₂ and CH₄ at reservoir depth of 10,000 are listed in **Table 3.1**.

Table 3.1: Properties of CO₂ and CH₄ at reservoir depth of 10,000 ft and 200 °F

PHYSICAL PROPERTIES OF CO ₂ AND CH ₄				
Parameter	CH ₄	CO ₂	Unit	References
Critical Temperature	116.6	88.0	°F	(Chase 1998)
Critical Pressure	667	1,075	psia	(Chase 1998)
Density	16.4	57.1	$\frac{lb}{ft^3}$	(Younglove and Ely 1987)
Viscosity	0.022	0.256	cP	
Solubility (Salinity: 1 mol/kg)	24.4	182	SCF/STB	(Chang et al. 1998) (Duan and Mao 2006)

Figure 3.1 describes the density comparison of CH₄ and CO₂ changes with depth. Methane density is calculated using Jacobsen and Stewart equation (Angus et al. 1976) and CO₂ density is estimated by an equation developed by Chapela and

Rowlinson (Younglove and Ely 1987). The figure clearly signifies that CO₂ is highly denser than CH₄ throughout the reservoir pressure range.

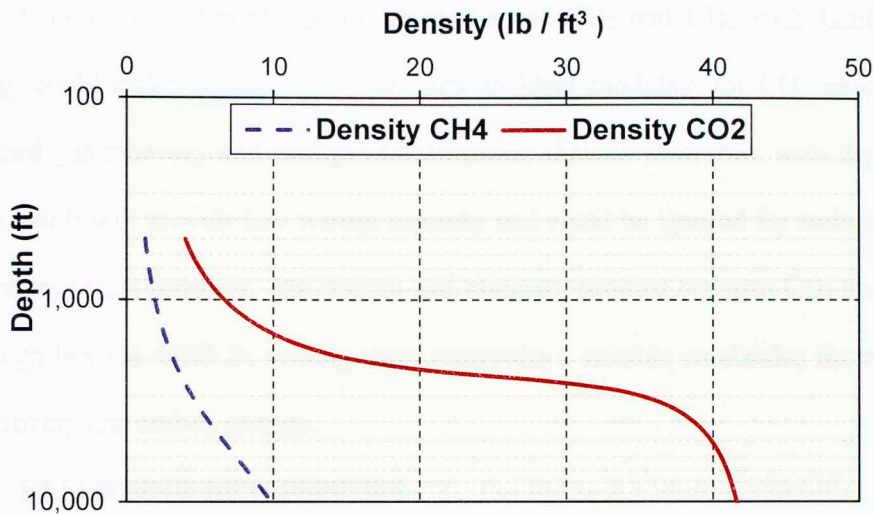


Figure 3.1: Density comparison with increasing formation depth

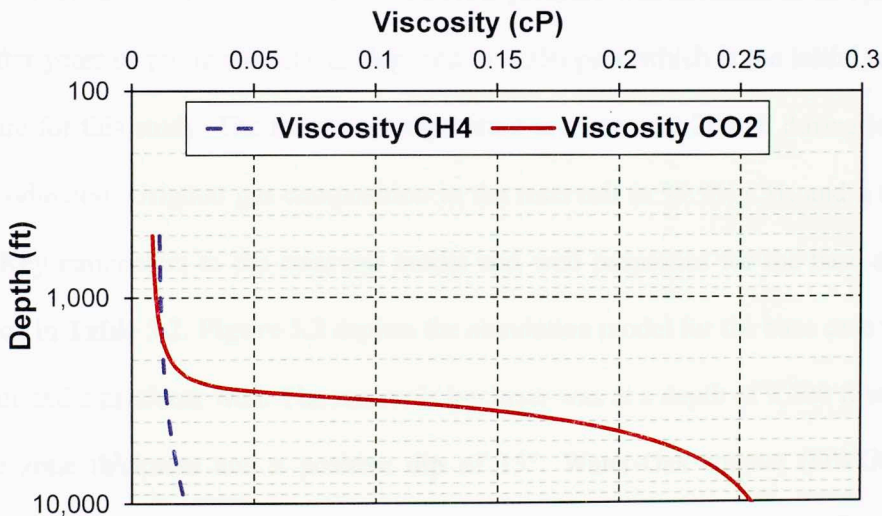


Figure 3.2: Viscosity comparison with increasing formation depth

Figure 3.2 shows the viscosity comparison of CO₂ and CH₄ with respect to formation depth. The mobility ratio of CH₄ displacement by CO₂ will be highly favorable rendered by highly viscous property of CO₂. All above calculations are done

considering normal temperature gradient of 0.015 °F/ft and hydrostatic pressure gradient of 0.433 psi/ft.

It could be inferred that the properties of CO₂ and CH₄ with limited inter mixing, could make depleted gas reservoirs an ideal candidate for CO₂ injection for enhanced gas recovery and storage. Furthermore, shallow reservoirs with depths less than 4,000 ft will provide less storage capacity and could be ignored for carbon storage and enhanced gas recovery. The density and viscosity contrast between CO₂ and CH₄ is very high beyond 4,000 ft; making these reservoirs a suitable candidates for enhanced gas recovery and carbon storage.

3.3 RESERVOIR DESCRIPTION

A depleted gas reservoir was modeled for this study using a commercial simulator CMG-GEMTM. The original reservoir pressure was assumed to be 7,000 psia and after years of production it was depleted to 4,350 psia, which is the initial reservoir pressure for this study. The reservoir temperature is a constant 200 °F during injection and production. Original gas composition in the reservoir is 99.9% CH₄ and a trace of CO₂. Key parameters in the reservoir model and well properties for the base case are outlined in **Table 3.2**. **Figure 3.3** depicts the simulation model for the base case with an injector and a producer well. The reservoir top layer was at a depth of 9,700 ft with 300 ft pay zone thickness and a positive dip of 15°. Water-Gas contact (DWGC) was defined at 9,700 ft signifying the presence of aquifer zone ($S_w=1.0$). **Figure 3.4** illustrate the relative permeability curve used in the simulation study.

Table 3.2: Grid and formation properties for gas reservoir model

RESERVOIR PROPERTIES		
Length	7,500	ft
Width	75	ft
Thickness	300	ft
Reservoir Grid	(NX, NY, NZ)	(100, 1, 10)
Dip	15°	degree
Initial Pressure	4,350	psia
Reference depth	10,000	Ft.
Initial Temperature	200	°F
k_v/k_h	1	
Reservoir Permeability	100	mD
Reservoir Porosity	20	%
Initial Water Saturation	0.1	
WELL PROPERTIES		
Injection Rate	4.5	MMSCF/Day
Maximum Injection Bottomhole Pressure Limitation	7,000	psia
Production Rate	3.0	MMSCF/Day
Minimum Production Bottomhole Pressure Limitation	1,000	psia
Simulation Time	10	years

Initially, the reservoir is saturated with natural gas and 10% residual water saturation. Injector well perforations are in the lower most grid block and producer well perforations are in the top layer because of the density contrast to delay CO₂ breakthrough during natural gas production. For all simulation models, natural gas production is stopped at a time when mole fraction of CO₂ in the producing stream

reaches a set value of 50%. For the base case, the reservoir had a uniform permeability of 100 mD.

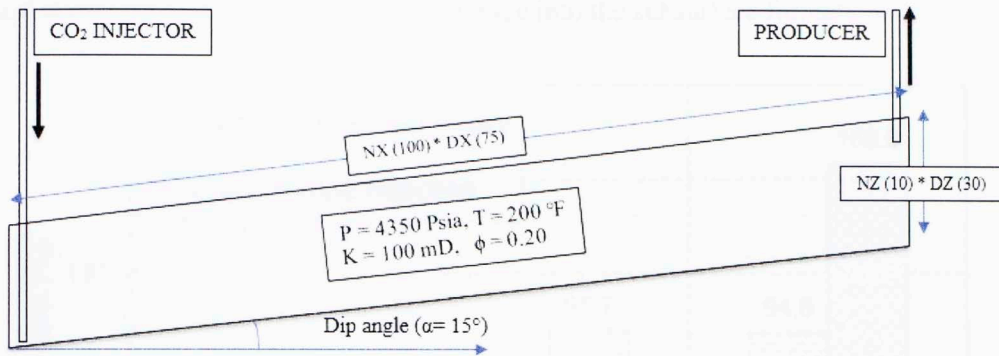


Figure 3.3: 2D reservoir model

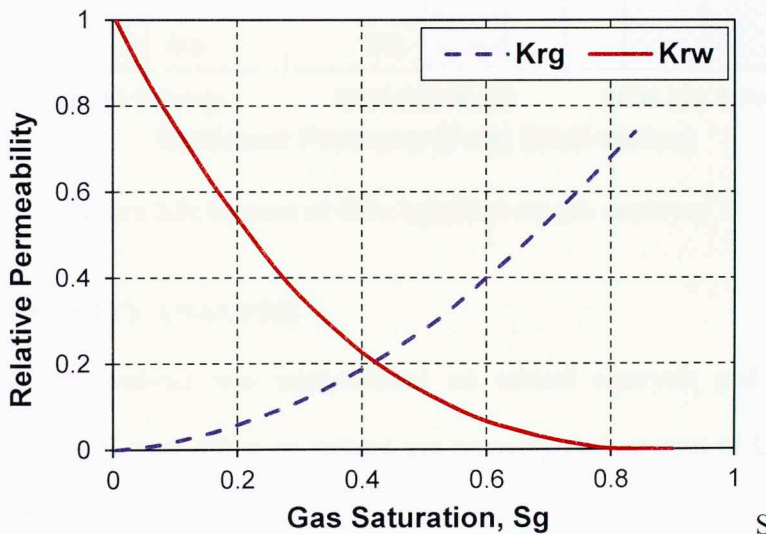


Figure 3.4: Relative permeability curves for the reservoir model

Figure 3.5 demonstrates the importance of CO₂ injection in a depleted gas reservoir. Three scenarios are simulated: No injection (reservoir blowdown till the reservoir pressure reaches 2000 psia); No Production case, and using CO₂ injection simultaneously with natural gas production. It showed that natural gas recovery factor increased from 46.3% to 94.8% and also the percent hydrocarbon pore volume

(%HCPV) of CO₂ injected increased from 95.8% to 166.6%. The simulation results justifies the importance of CO₂ injection to potentially rejuvenate the gas production and also allow higher quantity of CO₂ storage into the subsurface formation.

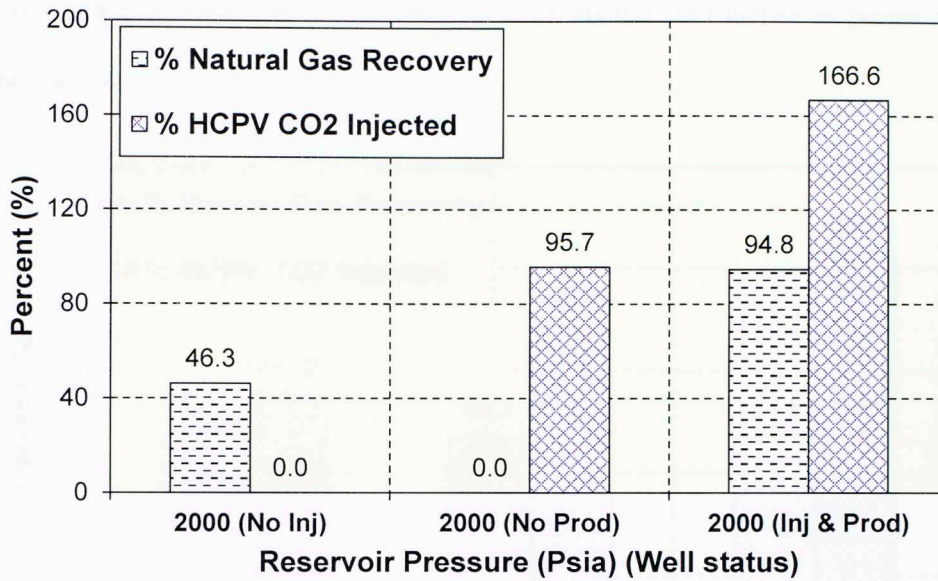


Figure 3.5: Impact of CO₂ injection on gas recovery

3.4 SENSITIVITY ANALYSIS

Sensitivity analysis was implemented on critical reservoir and completion properties to analyze their effect on natural gas recovery and amount of CO₂ injected into the formation.

3.4.1 DEPLETION PRESSURE RATIO

Depletion pressure ratio is defined as the ratio of initial reservoir pressure when EGR starts to the original reservoir pressure. Depletion pressure provided broader understanding of the present reservoir conditions instead of analyzing results considering only current reservoir pressure. It could serve in the decision making for the time frame in a reservoir development to be considered for CO₂ injection and allow

production through secondary recovery period. Three cases with initial reservoir pressures of 4,500, 3,000 and 2,000 psia were considered for the study. These pressures results into corresponding depletion pressure ratios of 0.65, 0.43 and 0.30. The results shown in **Figure 3.6** indicate that CO₂ injection should start as late as possible if no other detrimental factors are involved.

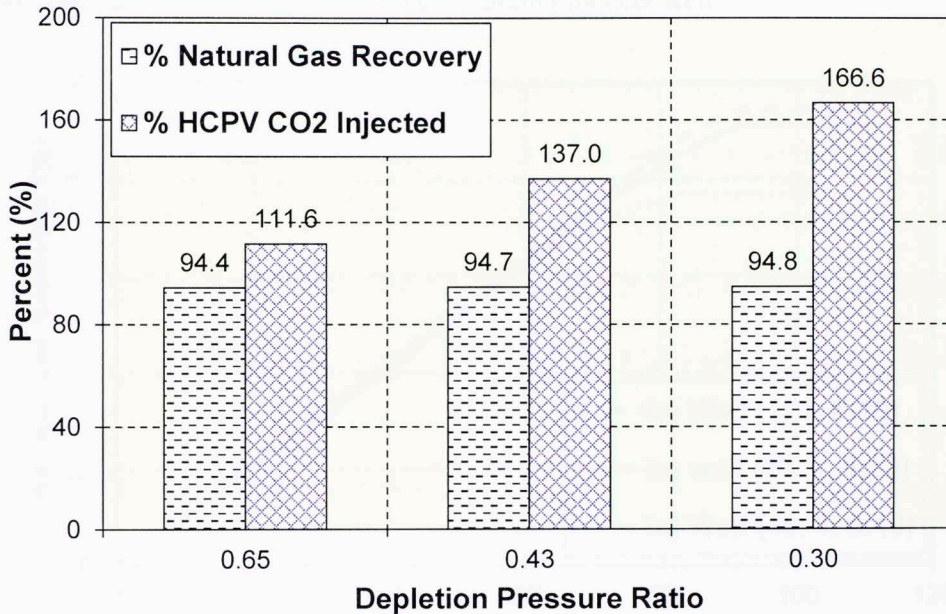


Figure 3.6: Depletion pressure impact on natural gas recovery and CO₂ storage

3.4.2 LOCATION OF INJECTION WELL

Existing wells (previous producer or injector) are usually considered for CO₂ injection rather than drilling new wells. Therefore, location of injection well is an important parameter in planning for CO₂ injection in a field. A case study is run by changing the location of injection well and relocating it towards the producer well in the reservoir. Three injection well locations are simulated in the cells 1, 20, and 40 in the x-direction. **Figure 3.7** shows the recovery factor of natural gas and amount of CO₂

injected. The result shows that perforating an injection well closer to the producer will lead to significantly less natural gas recovery and CO₂ storage. With early producer well shut-in, the reservoir pressure will build up at a higher rate as compared to an injector well at a farther location and less amount of CO₂ will be sequestered in the reservoir. So, considering all candidate injection wells in a reservoir, decision could be made to select the well which is very far from the current producer well.

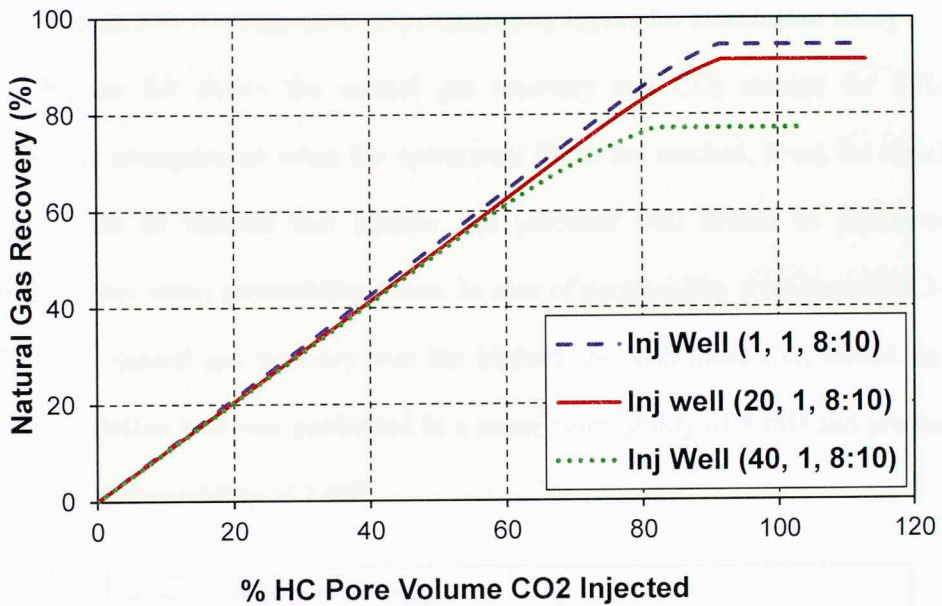


Figure 3.7: Injection well location effect on the natural gas recovery

3.4.3 ARRANGEMENT OF PERMEABILITY LAYERS AND ANISOTROPY

In order to incorporate heterogeneity in the reservoir, a 5 layers permeability model is built through the pay zone thickness of 300 ft. The reservoir grid block is modified to (100, 1, 5) (NX, NY, NZ) with each layer in the vertical direction had a different mean permeability and permeability of each grid block in that layer is calculated using Dykstra-Parsons Coefficient of 0.5. The schematic of different permeability arrangements used for the simulation study are drawn in **Figure 3.8**.

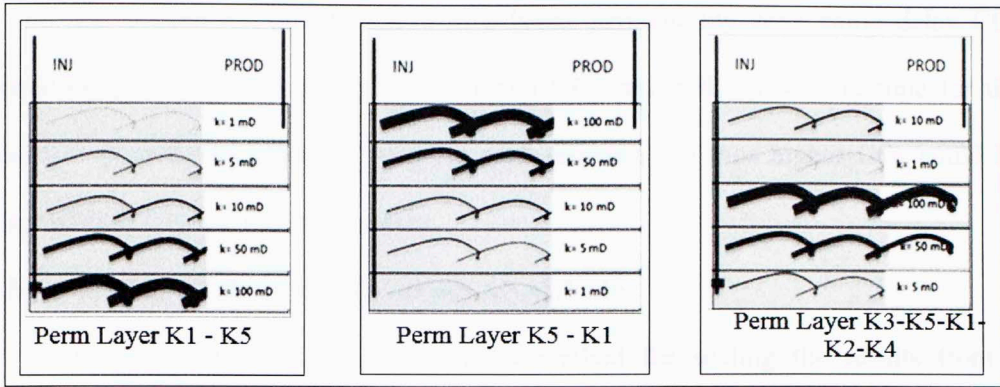


Figure 3.8: Arrangement of permeability layers for simulation study

Figure 3.9 shows the natural gas recovery and CO₂ storage for different permeability arrangements when the operational limits are reached. From the simulated results, it can be inferred that injector and producer well should be perforated in relatively lower mean permeability zones. In case of permeability arrangement (K3-K5-K1-K2-K4), natural gas recovery was the highest and also more CO₂ stored. In this case, the injection well was perforated in a mean permeability of 5 mD and production well in mean permeability of 1 mD.

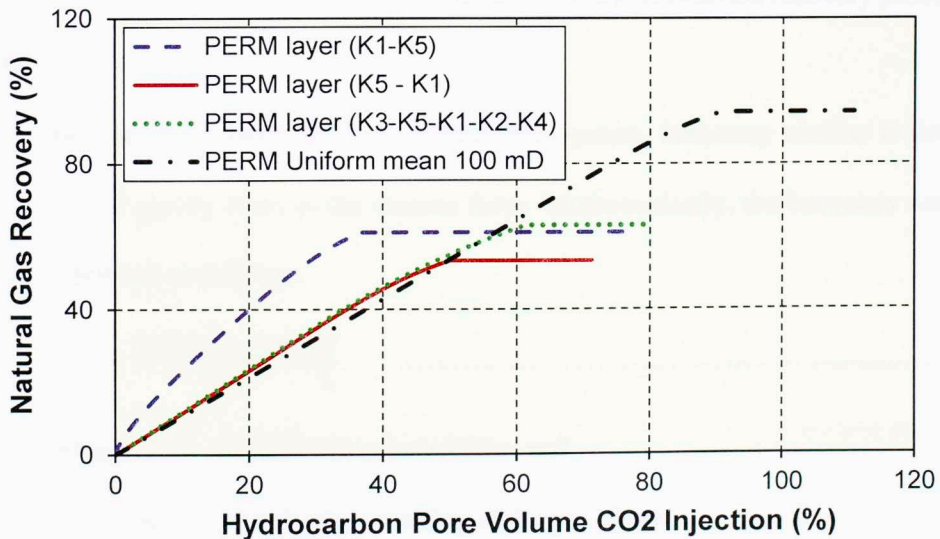


Figure 3.9: Permeability arrangement impact on natural gas recovery

Perforating the producer well in a lower permeability zone could delay CO₂ breakthrough into the producer well to reach 50% and will allow more time for the reservoir pressure to reach the injection well pressure and thus higher CO₂ could be injected into the subsurface formation.

3.5 DIMENSIONLESS NUMBERS ANALYSIS

Dimensionless analysis is a critical method for scaling the results from a reservoir to quantify other reservoirs. Utilization of dimensionless variables will reduce the number of varying parameters in the study and avoid unit conversions. Dimensionless analysis for the governing equations of fluid flow in a reservoir can provide insight into the relative importance of driving forces such as viscous force, gravity force, and capillary force on the displacement mechanisms. Independent dimensionless groups that control immiscible flow in porous media were derived by Shook, Li and Lake (Shook et al. 1992) using inspectional analysis of the governing equations and boundary and initial conditions. These dimensionless groups provided the guidelines for selecting the variables that influence the hydrocarbon recovery process in EGR by CO₂ injection.

Buoyancy Number (N_g°): In a fluid flow system, buoyancy number is defined as the ratio of gravity force to the viscous force. Mathematically, the buoyancy number can be expressed as follows:

$$N_g^\circ = \frac{k \lambda_r^\circ \Delta \rho g \cos \theta H}{u_T L} \dots\dots\dots (3.1)$$

Where, k = reservoir permeability, mD

λ_r° = end-point mobility of the gas phase

$\Delta\rho$ = density difference between the displacing fluids and displaced fluid, $\frac{lb}{ft^3}$

g = gravitational acceleration, $9.81\ m/sec^2$

u_T = total flux velocity, m/sec

H = reservoir thickness, ft

L = reservoir length in the flow direction, m

θ = reservoir dip angle, degree

Buoyancy number typically ranges from 0.01 to 10. In the higher value range of N_g° , the flow is mainly controlled by gravitational forces. This indicates that the flow rate is low and will allow CO₂ to settle to the bottom of reservoir. At lower value range, the flow is controlled by viscous forces indicating a higher rate and providing less time for CO₂ to segregate to the bottom of reservoir.

Effective Aspect Ratio (R_L): The effective aspect ratio R_L is defined as a characteristic ratio of time for fluid to cross the reservoir in the horizontal direction to that in the vertical direction. The effective aspect ratio is defined as follow.

$$R_L = \frac{L}{H} \sqrt{\frac{k_v}{k_h}} \dots\dots\dots (3.2)$$

Where, L = reservoir length in the flow direction, m

H = reservoir thickness, ft

k_h = horizontal permeability, mD

k_v = vertical permeability, mD

If R_L is large, saturation or pressure variations in the vertical direction are much less than that in the horizontal direction. The effective aspect ratio is mainly used to

identify the validity of the assumption of vertical equilibrium (VE) for a particular reservoir is valid or not.

Dip Angle Group (N_θ): Dip angle group accounts for the geometry of a reservoir.

$$N_\theta = \frac{L}{H} \tan \theta \quad \dots\dots\dots (3.3)$$

Simulation studies are carried out to quantify natural gas recovery using above dimensionless variables. The input parameters for the simulation model are summarized in **Table 3.3**. Dimensionless variables are analyzed so that the above simulation results of sensitivity analysis can be scaled up to apply for several types of reservoir.

Table 3.3: Input parameters for dimensionless analysis

RESERVOIR PARAMETERS			
Parameter		Field Units	SI values
Horizontal Permeability	k_x	100 mD	9.87 E-14 m ²
Vertical Permeability	k_y	100 mD	9.87 E-14 m ²
Reservoir Thickness	H	300 ft	91.5 m
Lateral Well Spacing	L	7,500 ft	2,286 m
CO ₂ Density	ρ_{CO_2}	57.1	914 kg/m ³
CH ₄ Density	ρ_{CH_4}	16.4	263 kg/m ³
CO ₂ Viscosity	μ_{CO_2}	0.26 cP	2.56 E-04 Pa.s
CH ₄ Viscosity	μ_{CH_4}	0.02 cP	2.17 E-05 Pa.s
End point-Gas relative permeability	k_r	0.74	

Natural gas recovery was calculated with respect to buoyancy number (N_G) with varying effective aspect ratio (R_L) as shown in **Figure 3.10**. It was observed that with

decrease in R_L , natural gas recovery also decreases, as the fluid movement along vertical direction is more stringent with decrease in effective aspect ratio. A significantly less variation is observed in the buoyancy number, which, is a function of reservoir dip angle with other parameters kept constant. Buoyancy number decreases with increase in dip angle. Therefore, it could be stated that Buoyancy number is insensitive to changes in the reservoir parameters. With higher buoyancy number, natural gas recovery is diminishing, which is attributed to the increasing gravity effects. This replicates the understanding of buoyancy number that it is inversely proportional to the flux velocity (relative to production rate).

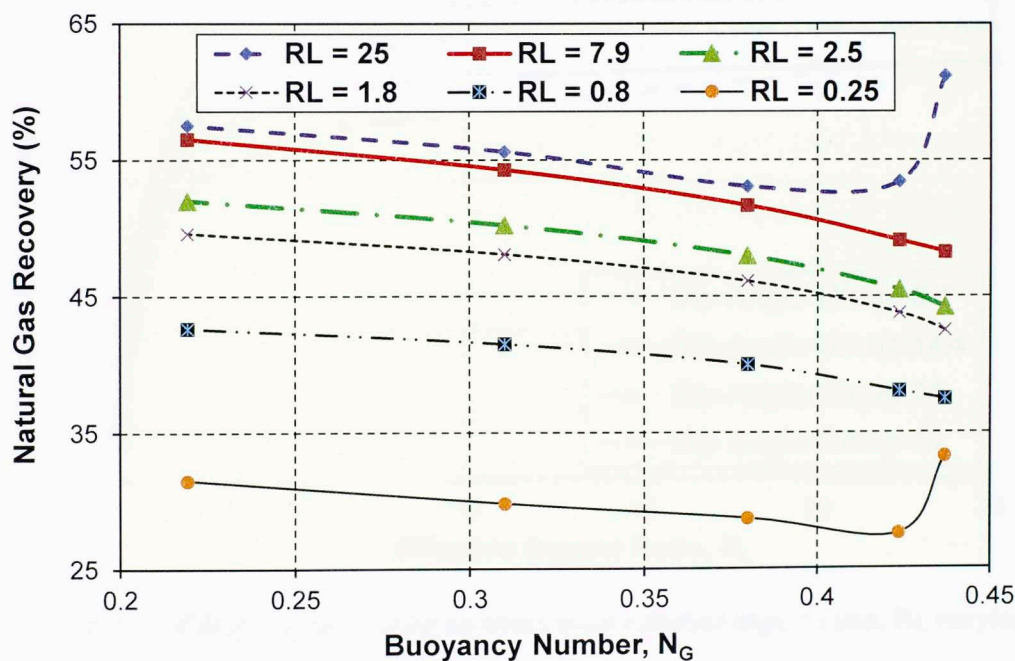


Figure 3.10: Effect on natural gas recovery with buoyancy number, N_G at varying effective aspect ratio, R_L (dimensionless analysis)

Very low values of buoyancy number indicates viscous dominated flow regimes, therefore gas displacement is critically dependent upon residual phase saturation and

relative permeability (Shook et al. 1992). The results of natural gas recovery with respect to effective aspect ratio (R_L) with varying dip angle group (N_θ) are shown in **Figure 3.11**. Natural gas recovery increases with an increase in effective aspect ratio. Natural gas recovery increases very rapidly with changes in effective aspect ratio ($R_L < 10$). With higher R_L , fluid movement becomes less restrictive along vertical direction and no effect on natural gas recovery can be observed. Natural gas recovery further increase by higher dip angle group which is directly proportional to the reservoir dip angle.

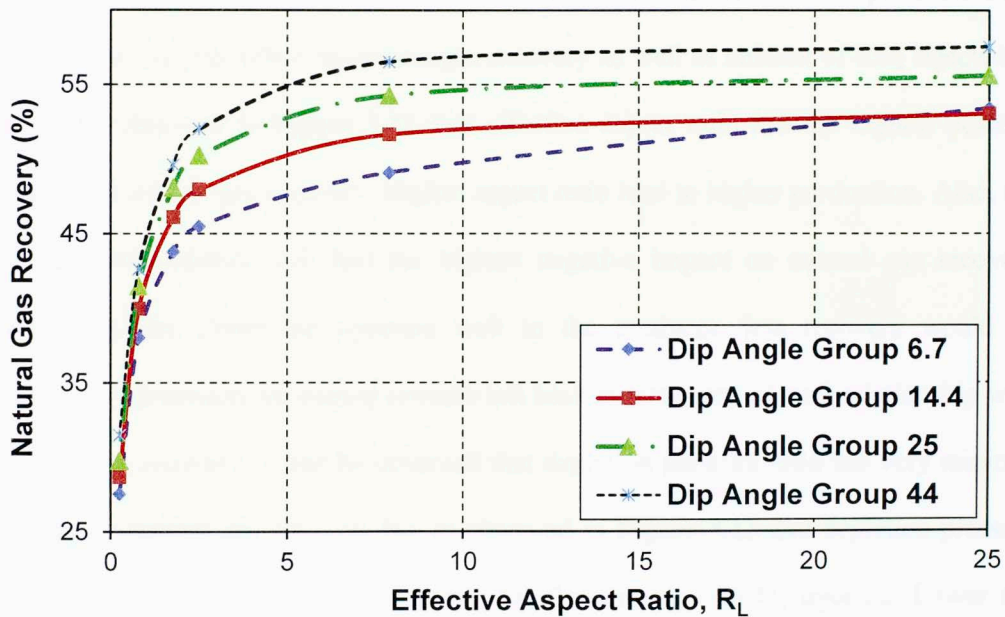


Figure 3.11: Effect on natural gas recovery with effective aspect ratio, R_L varying dip angle group N_θ (dimensionless analysis)

Dip angle group analysis is very critical before considering vertical equilibrium (VE). In reservoirs with consideration of vertical equilibrium, effective aspect ratio (R_L) is neglected. This implies that natural gas recovery, saturation profiles and mixing

zones are independent of the changes in effective aspect ratio. This assumption could lead to major errors in the study and production profile can vary significantly than as expected. With higher effective aspect ratio, natural gas recovery increases but it stabilizes after a certain range, indicating the establishment of vertical equilibrium.

3.6 RESULTS AND DISCUSSIONS

Critical reservoir parameters and well characteristics are analyzed during the sensitivity analysis. Tornado study is applied on the results to have an understanding of most important parameters while planning CO₂ injection for enhanced gas recovery and sequestering large volumes of CO₂ into the reservoir. Impact of all the parameters are analyzed to see the effect on natural gas recovery as well as amount of CO₂ injected. It could be observed in **Figure 3.12** that effective aspect ratio has the highest positive impact on natural gas recovery. Higher aspect ratio lead to higher production. Also, the location of injection well had the highest negative impact on natural gas recovery indicating that closer the injection well to the producer, less recovery would be achieved. Parameters increasing towards left have inverse proportional relationship with natural gas recovery. It can be observed that depletion pressure ratio has very minimal impact on natural gas recovery but as observed in **Figure 3.13** that depletion pressure ratio is the most dominating parameter for the amount of CO₂ injected. Lower the depletion pressure ratio, higher volume of CO₂ can be sequestered in the reservoir. This study provides clear understanding of the important parameters to be considered while designing CO₂ injection for enhanced gas recovery in depleted gas reservoirs.

Natural Gas Recovery

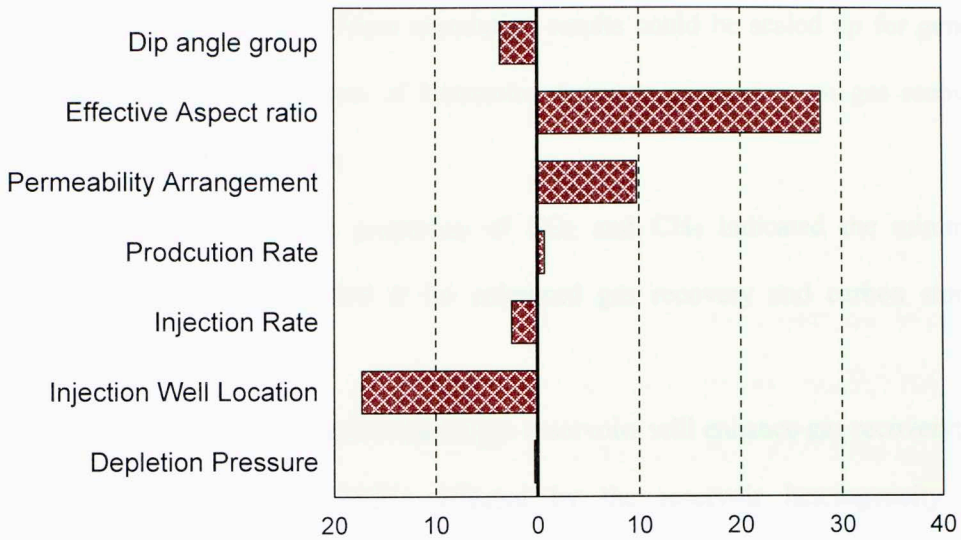


Figure 3.12: Sensitivity study of affecting parameters on natural gas recovery

Hydrocarbon Pore Volume of CO₂ Injected

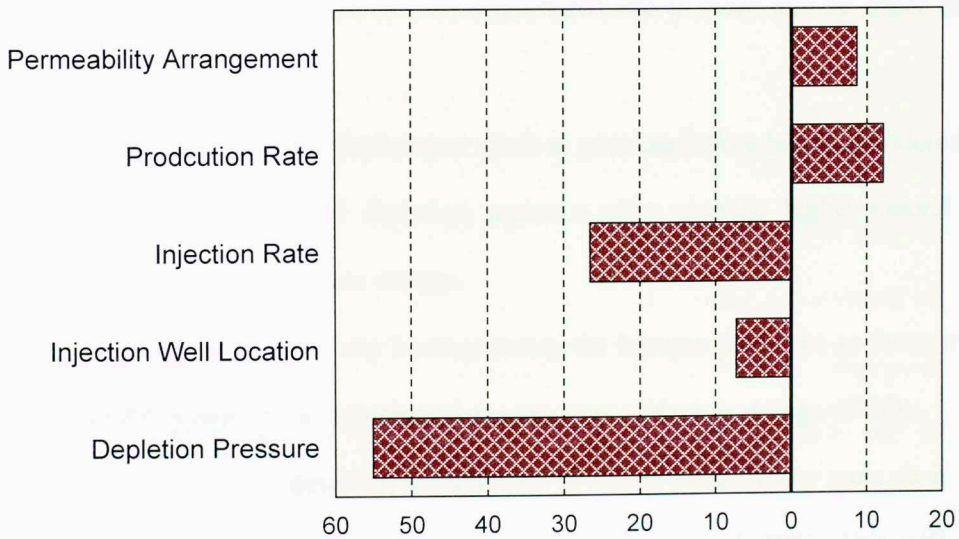


Figure 3.13: Sensitivity study of affecting parameters on CO₂ storage volume

Based on above analysis, the following conclusions could be drawn:

1. The results in the study are represented with dimensionless groups governing the displacement of fluid. These simulation results could be scaled up for generic reservoirs and the effects of interaction between parameters on gas recovery could be better analyzed.
2. The study of physical properties of CO₂ and CH₄ indicated the minimum formation depth of 4,000 ft for enhanced gas recovery and carbon storage projects.
3. Injecting CO₂ into depleted natural gas reservoirs will enhance gas recovery; the recovery factors are highly affected by the reservoir heterogeneity and anisotropy. In absence of a thief zone, an additional 60% or more of gas in the depleted reservoir can be recovered. However, highly heterogeneous reservoir can also lead to lower natural gas recovery and reduction in the percentage hydrocarbon pore volume of CO₂ sequestered due to more mixing zones in the formation.
4. Gas reservoirs must be depleted as much as possible before being considered for CO₂ injection as lower depletion pressure ratios provide higher natural gas recovery and more carbon storage.
5. If the reservoir is relatively homogeneous, the injector should be as far as away from the producer for high natural gas recovery and more storage of CO₂.
6. Perforations of producer well should be in lower permeability zone as it will delay CO₂ breakthrough into the producer well to reach 50%. This will also allow more time for reservoir pressure to reach injection well pressure and higher CO₂ can be injected into the subsurface formation.

CHAPTER 4: MECHANISM STUDY OF CO₂ INJECTION IN TIGHT OIL RESERVOIRS

The chapter provides detailed reservoir description for the base simulation model of the Bakken formation. The simulation model will cater to the need of investigating the effects of CO₂ injection in a tight oil formation and CO₂ storage possibilities. This chapter elaborates the methodology to implement the important shale/tight formation characteristic properties into the reservoir model. This will provide significant understanding of how these properties affect CO₂ flow migration into the reservoir and also oil production. The properties were discussed in detail in Chapter 2. The objective of this research is to understand the mechanism of flow in tight formations and to understand the physics of shale/tight formation properties affecting flow migration of CO₂ into the reservoir while displacing the oil out of the reservoir and up to the surface.

4.1 RESERVOIR SIMULATION TOOL

This research utilizes a reservoir simulator to model CO₂ injection in a simulated tight oil formation. The simulators should account for CO₂ migration in a reservoir, the incremental oil and gas recovery and the amount of CO₂ being sequestered into the formation. The present simulators have the ability and flexibility to incorporate the physical processes discussed in Chapter 2. The physical processes are built-in mechanism in the simulator and are activated through mathematical formulations and keywords. The main deliverables of this research come from running sensitivity study on the critical shale/tight properties and this requires a fast and robust iterative calculations tool. A compositional reservoir simulation tool was required to model the

formation and fluid properties of the Bakken and other tight formations, which led to the use of CMG – GEM™.

4.1.1 CMG – GEM™ INTRODUCTION

CMG- GEM™ is an advanced general equation-of-state (EOS) compositional simulator to model reservoir fluid flow during primary and enhanced oil recovery processes. GEM can incorporate various EOS, dual porosity – dual permeability models, CO₂-miscible and hydrocarbon injection, volatile oil, gas condensates, and complex phase behavior (CMG-GEM 2013). GEM provides mathematical formulation and coupling of various flow mechanisms with the finite grid model to simulate the reservoir heterogeneity and flow dynamics.

4.1.2 INJECTOR – PRODUCER WELL PATTERN

With the advancement in horizontal drilling and hydraulic fracturing, wells in tight formations are completed with long horizontal laterals and multiple hydraulic fracturing stages. An Injector-Producer well pattern consists of parallel long horizontal lateral wells with multiple fracturing stages. Center well is used as an injector well with each fracture perforation utilized to inject gas/water into the formation to enhance productivity of the nearby wells. Gas injection for EOR has not been field tested for tight formations and various operators are planning to introduce CO₂ or natural gas injection into tight formation to improve productivity of the nearby wells. One of the proposed project is to evaluate 1,320 ft spacing between injector and producer wells into the Middle Bakken as displayed in **Figure 4.1**. Horizontal wells in tight formations are completed with 5,000 - 6,000 ft laterals and 10 - 20 fracture stages.

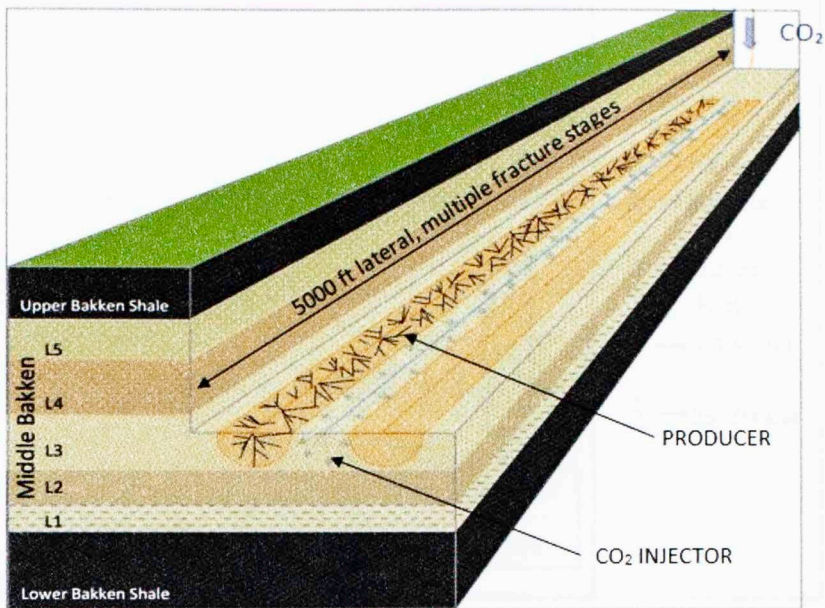


Figure 4.1: Injector - Producer well pattern in Bakken formation

(Sorensen et al. 2013a)

To focus on the flow mechanism of CO₂ into the reservoir, only the **Zone of Study (ZoS)**, as marked in green in **Figure 4.2** is simulated using CMG-GEM. With the injector and producer well in the formation, the zone between the injector fracture and the producer fracture is modeled using reservoir simulator. The critical requirement is to understand the flow mechanism of CO₂ as it is injected into a tight formation and the sweep efficiency it can create to displace oil towards the producer well.

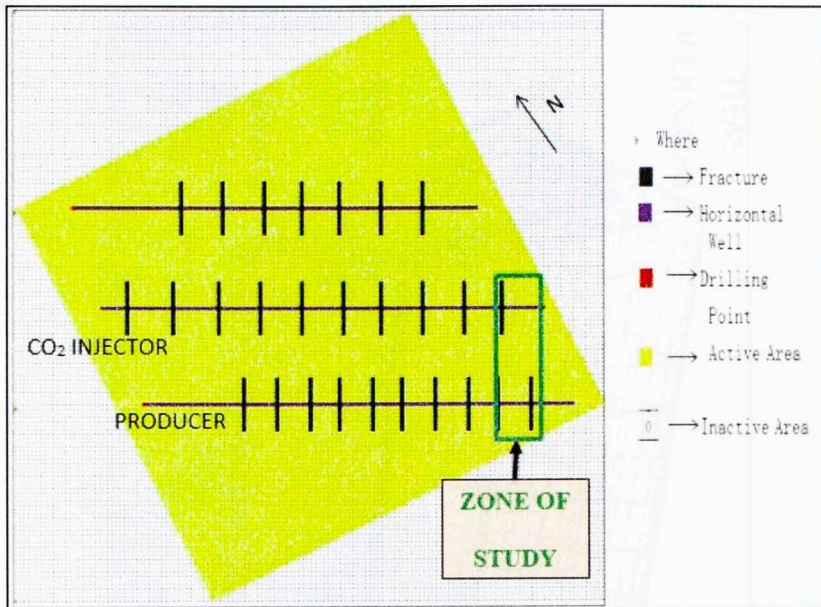


Figure 4.2: X-Y cross section plane of the wells highlighting the Zone of Study

4.2 BASE RESERVOIR MODEL – ZONE OF STUDY

With the aim of understanding the flow behavior in the Zone of Study (ZOS), a reservoir model was created with an injector and a producer well, each well with 1 open perforated hydraulic fracture. The reservoir model is a representation of Bakken Petroleum System in the Williston Basin. Formation and petrophysical properties, and reservoir fluid composition of the Middle Bakken reservoir is used to set up the base model for simulation. The Zone of Study (ZoS) is shown in **Figure 4.3**.

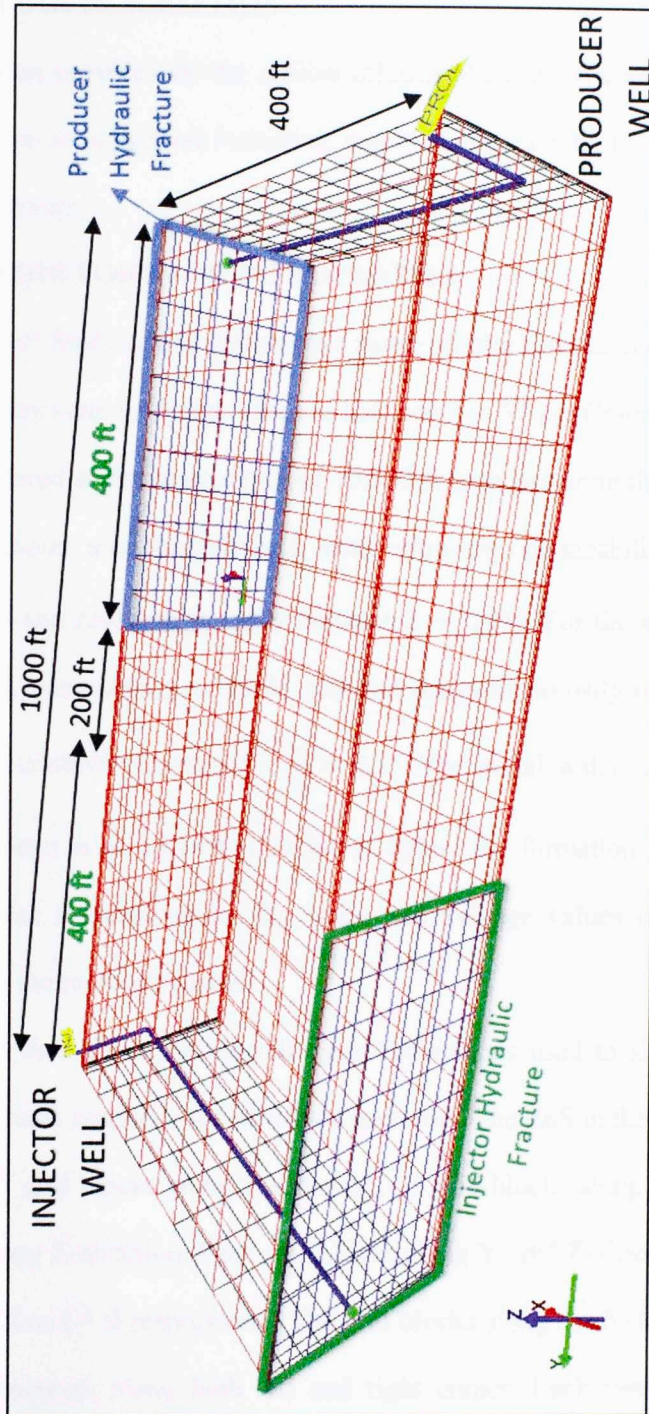


Figure 4.3: Base reservoir model built using CMG-GEM

4.3 RESERVOIR DESCRIPTION

This section provides all the critical information and parameters necessary to develop a prototype for a tight oil formation, and to incorporate the flow mechanisms in the simulated reservoir.

4.3.1 RESERVOIR FORMATION PROPERTIES

The Zone of Study (**ZoS**) represents a reservoir at a formation depths of 10,000 – 11,000 ft. The pay zone thickness varies in between 5 – 57 *ft* (Cramer 1986). For the model, we considered a formation depth of 10,500 ft with pay zone thickness of 40 ft. Tight oil formations are characterized with ultra-low permeability in range of 0.001 – 0.01 *mD* and reservoir porosity between 2 – 10%. For the simulated model, an average matrix permeability of 0.005 *mD* and reservoir porosity of 5.0 % is used. The permeability contrast considered is $\frac{k_v}{k_h} = 0.1$. The initial water saturation is 0.30 and water-oil contact is at 10,540 *ft* which is below the formation pay zone depth. **Table 4.1** provides information on the range and average values of the formation properties used in the reservoir model.

Table 4.2 lists down the reservoir grid dimensions used to simulate the base model and the volume estimates for simulated reservoir. The **ZoS** in the reservoir model is divided into 28 grid blocks along X-direction, 25 grid blocks along Y-direction and 10 grid blocks along Z-direction. Each grid blocks along Y- and Z- direction have equal dimension of 40 ft and 4 ft respectively. The grid blocks along the X-direction consists of local grid refinement along both left and right corner. Each corner represents a hydraulic fracture with a grid dimension of 0.0292 *ft*, with logarithmically increasing

grid size towards the center to avoid convergence issues. The structural top for all the grid blocks is defined at the formation depth of 10,500 *ft* in GEM.

As observed in **Figure 4.3**, the reservoir model is built in a way to account for the flow between the injector fracture and the producer fracture i.e. only half fractures are used for both injector and producer. **Figure 4.4** shows the X-Y cross section of the permeability in X- direction of the perforation plane. **Figure 4.4** also displays the local grid refinement in X- direction for both the injector and the producer fracture. Grid block 1 in X-direction has the injector hydraulic fracture of width 0.0292 *ft* and fracture half-length of 400 *ft* in Y-direction. The fracture height is assumed to be across the Middle Bakken formation i.e. 40 *ft*, shown in **Figure 4.5**. The grid blocks in red denote the hydraulic fracture with an increased permeability of 230 *mD*. There exists a hydraulic fracture corresponding to the producer at the other end with same fracture width and fracture height as that of the one corresponding to injector well but a different fracture permeability of 70 *mD*. The hydraulic fractures properties defined in the reservoir model are summarized in **Table 4.3**. Matrix grid blocks in blue denote the reservoir area with permeability of 0.005 *mD*. The dense black grid lines near the fractures acknowledge the local grid refinement generated across the fracture to tackle convergence issues during simulation (Cipolla et al. 2010).

In summary, the reservoir model has a homogenous permeability of 0.005 *mD* and porosity of 5%. Further improvements in model are discussed in later parts of the chapter.

Table 4.1: Range and average reservoir properties for the base model

RESERVOIR PROPERTIES OF MIDDLE BAKKEN					
Parameter	Range		Average	Unit	References
	Min.	Max.			
Reference Depth	9,500	11,500	10,500	<i>ft</i>	Wang et al. (2010)
Initial Reservoir Pressure	4,060	7,325	6,000	<i>psia</i>	Cramer (1986)
Pay Zone Thickness	25	75	40	<i>ft</i>	Cramer (1986)
Total Compressibility	2.0 E-06	8.5 E-06	6.4 E-06	$\frac{1}{psia}$	Dechongkit and Prasad (2011)
Reservoir Temperature	175	260	240	$^{\circ}F$	LeFever (2005)
Oil API Gravity	39	45	42	$^{\circ}API$	Clark (2009), Breit et al. (1992)
Reservoir Permeability	0.0001	0.02	0.005	<i>mD</i>	Sarg (2012), Simenson (2010)
k_v/k_h	0.001	1	0.1		Pitman et al. (2001)
Reservoir Porosity	2.0	10.0	5.0	%	Sonnenberg (2011)
Initial Water Saturation	0.25	0.45	0.30		Simenson (2010)

The matrix and fracture compressibility are assumed to be equal with total compressibility of $6.4 E - 06 \frac{1}{psia}$. The reference pressure for the assigned compressibility is 6000 *psia*.

Table 4.2: Grid dimensions and volume calculations for the base model

GRID PROPERTIES AND RESERVOIR VOLUME		
Length, L	400	<i>ft</i>
Breadth, B	1,000	<i>ft</i>
Thickness, h	40	<i>ft</i>
Number of Grid Blocks	NX, NY, NZ	28, 25, 10
Grid Dimensions	LX, LY, LZ	(...), 40, 4 X-direction has variable length (local grid refinement)
Bulk Reservoir Volume	1.6 E+07	<i>RES FT³</i>
Total Pore Volume	8.0 E+05	<i>RES FT³</i>
Hydrocarbon Pore Volume	5.6 E+05	<i>RES FT³</i>
Original Oil in Place (OOIP)	6.6 E+04	<i>STB</i>
Original Gas in Place (OGIP)	9.1 E+07	<i>SCF</i>

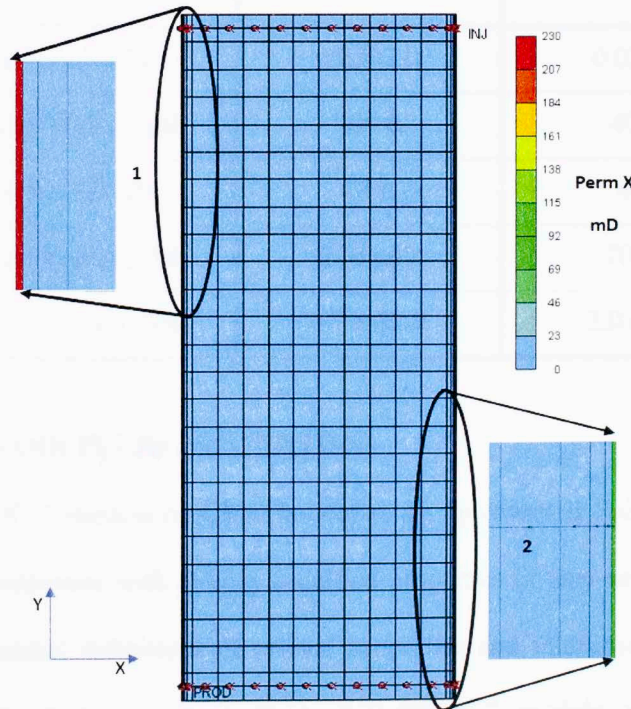


Figure 4.4: X-Y cross section of permeability in the perforation plane

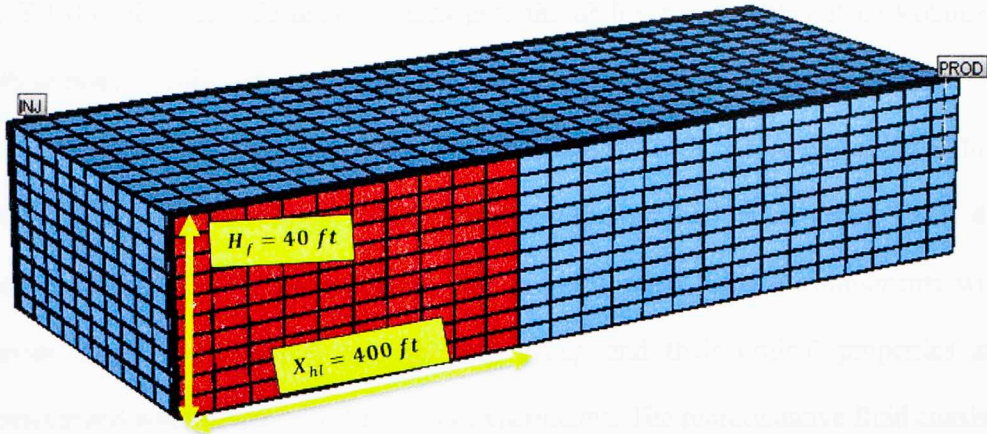


Figure 4.5: 3-D view of injection hydraulic fracture

Table 4.3: Hydraulic fracture properties in the reservoir model

HYDRAULIC FRACTURE PROPERTIES		
Parameter	Injector Fracture	Producer Fracture
Fracture Width	0.0292 ft	0.0292 ft
Fracture Half length	400 ft	400 ft
Fracture Height	40 ft	40 ft
Fracture Permeability	230 mD	70 mD
Fracture Conductivity	6.7 mD-ft	2.0 mD-ft

4.3.2 RESERVOIR FLUID PROPERTIES

WINPROPTM module by CMG is used to set up reservoir fluid model either by using in-built component with already specified properties or user defined components which allows manual definitions of critical properties and interaction parameters for each component of the reservoir fluid. WINPROPTM module will generate the component properties to be used in CMG compositional simulator GEM. Additionally,

the WINPROP™ module also provides user the ability to use either Peng-Robinson EOS or Soave-Redlich-Kwong EOS to model fluid properties of oil and gas phases.

The representative fluid composition for this research is modeled using a fluid composition that replicates the Middle Bakken reservoir fluid as shown in **Table 4.4** (Nojabaei et al. 2013). The reservoir fluid is categorized using 8 components with heavier components lumped together into group and their critical properties are characterized with reference to laboratory experiments. The representative fluid consists of 36.7 % Methane, 14.9 % Ethane, 9.3 % Propane, 5.8 % n-Butane and rest 33.3 % of heavier components ranging from C5 to C80. The ninth component added in the fluid model is CO₂ which is the injected component. **Table 4.4** summarizes the characteristic fluid properties with Peng-Robinson Equation of State used for the GEM model. The average oil gravity of the Bakken formation is 42° API, indicating a light crude oil with lower viscosity. Modified Pederson correlation was implemented to estimate the viscosity of the reservoir fluid.

Using WINPROP™, the Pressure – Temperature diagram displaying the two phase envelope for the representative fluid is generated (**Figure 4.6**). At reservoir temperature of 240 °F and pressure of 6000 psia, the reservoir fluid is a single phase liquid as the above mentioned conditions exist above the bubble point curve. The isothermal production (decline in pressure) will cross through the bubble point curve at 2800 psia after which the fluid starts exhibiting two phase behavior

Table 4.4: Compositional fluid data and binary Interaction parameters for reservoir fluid (Nojabaei et al. 2013)

COMPOSITIONAL RESERVOIR FLUID DATA							
Component	Molar Fraction	Critical Pressure	Critical Temperature	Acentric Factor	Molar Weight	Critical Volume	Parachor Coefficient
		<i>Atm</i>	<i>K</i>		$\frac{lbm}{lbm\ mol}$	$\frac{LT}{lbm\ mol}$	
C02	0.0	72.8	304.2	0.225	44.01	0.094	78
C1	0.36736	44.57	186.31	0.0102	16.54	44.74086	74.8
C2	0.14885	49.13	305.54	0.1028	30.43	66.26178	107.7
C3	0.09334	41.9	369.98	0.152	44.1	92.03025	151.9
C4	0.05751	37.18	421.78	0.1894	58.12	116.38287	189.6
C5-C6	0.06406	31.39	486.38	0.2684	78.3	152.62863	250.2
C7-C12	0.15854	24.72	585.14	0.4291	120.56	249.47277	350.2
C13-C21	0.0733	16.98	740.05	0.7203	220.72	430.13523	590
C22-C80	0.03704	12.94	1024.72	1.0159	443.52	1019.412	1216.8

BINARTY INTERACTION PARAMETERS FOR COMPONENTS										
Component	C02	C1	C2	C3	C4	C5-C6	C7-C12	C13-C21	C22-C80	
C02	zero	0.103	0.13	0.135	0	0	0	0	0	
C1	0.103	zero	0.005	0.0035	0.0035	0.0037	0.003	0.0033	0.0033	
C2	0.13	0.005	zero	0.0031	0.0031	0.0031	0.003	0.0026	0.0026	
C3	0.135	0.0035	0.0031	zero	0	0	0	0	0	
C4	0	0.0035	0.0031	0	zero	0	0	0	0	
C5-C6	0	0.0037	0.0031	0	0	zero	0	0	0	
C7-C12	0	0.0033	0.0026	0	0	0	zero	0	0	
C13-C21	0	0.0033	0.0026	0	0	0	0	zero	0	
C22-C80	0	0.0033	0.0026	0	0	0	0	0	zero	



Figure 4.6: Pressure-Temperature diagram displaying 2 phase envelope for the representative fluid (WINPROP™)

4.3.3 MMP CALCULATIONS

Using WINPROP™, the Minimum Miscibility Pressure (MMP) and the First Contact Miscibility (FCM) can be evaluated for a given oil composition at a particular reservoir temperature. WINPROP™ offers two ways to calculate MMP. 1) Cell-to-Cell simulation method and 2) Semi-Analytical Tie Line method (CMG-WINPROP 2013).

Table 4.5 displays the MMP calculated using WINPROP™.

The Minimum Miscibility Pressure calculated using WINPROP™ for the defined reservoir fluid and CO₂ as injection gas, matches very closely with the MMP results from the Rising Bubble Apparatus experiments carried out at Colorado School of Mines (Adekunle 2014), displayed in **Table 4.6**. A low MMP for CO₂ and reservoir fluid resulted the injection pressure was always being above the MMP, leading to

complete miscibility in the reservoir. The injection pressure is 10,000 psia for this study.

Table 4.5: MMP calculations from WINPROP

Calculation Method	MMP	
	First Contact Miscibility	Multiple Contact Miscibility
Cell to Cell Simulation	4235 psia	3470 psia
Semi Analytical Tie Line Model	4235 psia	2120 psia

Table 4.6: Tabulated MMP calculations from Adekunle (2014)

Experimental Model and Empirical Correlations	MMP
Rising Bubble Apparatus at 215 °F	2340 psia
Adjusted Rising Bubble Apparatus at 237 °F	2670 psia
WINPROP @ 237 °F	2632 psia
Cronquist Model	2992 psia
Alston Model	3391 psia

4.3.4 ROCK – FLUID PROPERTIES

Two separate sets of relative permeability curves were used in this study, one defining matrix and other hydraulic fractures flow media. **Table 4.7** and **Table 4.8** display the relative permeability curves for the matrix and fracture grid blocks respectively. The initial water saturation is 0.30.

Table 4.7: Relative Permeability curves for matrix blocks

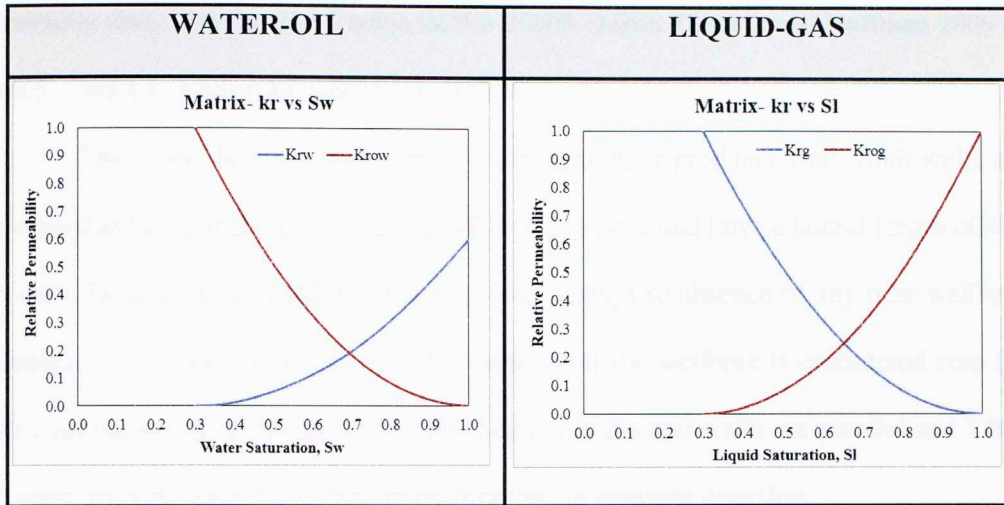
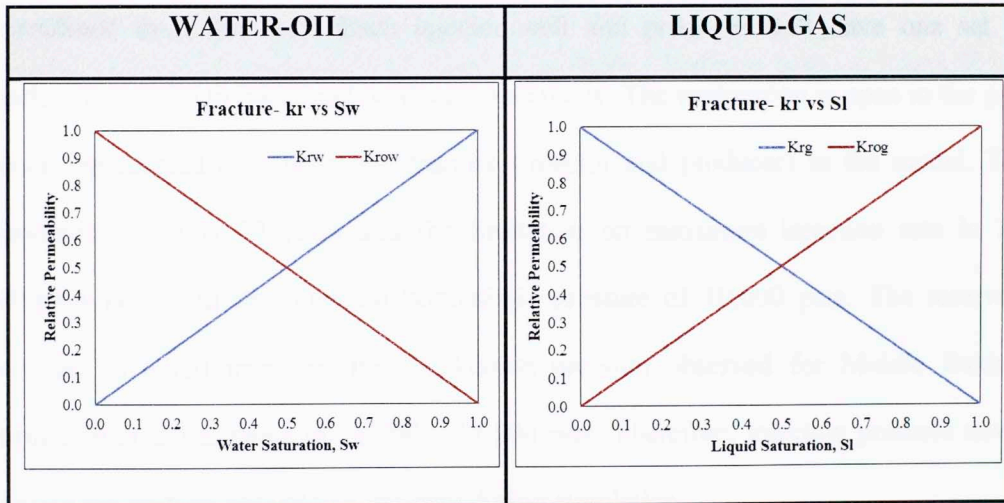


Table 4.8: Relative Permeability curves for fracture blocks



In GEM, two ROCKTYPES can be used to define two sets of relative permeability curves. For example in this study, RPT 1 corresponds to Matrix relative permeability curves and RPT 2 corresponds to Fracture relative permeability curves. Here RPT is a syntax for the in-built function ROCKTYPE in GEM. Relative

permeability curves used in the study closely match the curves obtained by history matching data from the Elm Coulee field in North Dakota (Shoaib and Hoffman 2009).

4.3.5 WELL AND RECURRENT DATA

The model has two wells, one injector and other producer well. Both wells are modeled as horizontal wells within the 40 ft of pay zone and have a lateral length of 400 ft each, located in the middle of the pay zone. Complete absence of any near wellbore damage is assumed and hence, the skin factor near the wellbore is considered zero for the injector as well as the producer. The laterals of the two wells are parallel and 1,000 ft apart, to each other, with fracture perforations in opposite direction.

The injector well is modeled to inject 100% CO₂ and no production is considered from this well. Each injector well and producer well have one set of perforations open to inject and produce respectively. The perforation is open in the grid block represented as a hydraulic fracture (injector and producer) in the model. The simulation time is 30 years and the limitation on maximum injection rate is 1.0 MMSCF/Day with the injection bottomhole pressure of 10,000 psia. The reservoir pressure is 6,000 psia and the breakdown pressure observed for Middle Bakken formation is in the range of 11,000 – 11,500 psia. Therefore, injection pressure never crosses the fracture breakdown pressure during simulation.

The producer well has a maximum production rate limitation of 300 STB/day. The producer bottomhole pressure was constrained to a minimum of 500 psia. Also, the producer bottomhole pressure was maintained constant at 500 psia during the simulation time of 30 years. The injection and production constraints are summarized in

Table 4.9.

Table 4.9: Well Properties in the model

WELL PROPERTIES			
Injector Well	Maximum Rate	1.0	<i>MMSCF/Day</i>
	Injection Bottomhole Pressure	10,000	<i>psia</i>
Producer Well	Maximum Rate	300	<i>STB/day</i>
	Production Bottomhole Pressure	500	<i>psia</i>
Simulation Time		30	<i>years</i>

The operating schedule for the wells is a simultaneous injection and production. The injection well continuously injects CO₂ from year 2010 until year 2040 and oil and gas productions are recovered from the producer well in the same working schedule.

4.4 MULTIPLE PHYSICS MODEL

The reservoir model described before this section is very important and is necessary to model any type of a reservoir, be it sandstone or shale. The reservoir characteristics discussed in this section are very crucial in order to model an oil shale or tight formation. These properties set these reservoirs apart from conventional reservoirs.

4.4.1 RESERVOIR HETEROGENEITY EFFECT

Reservoir heterogeneity is an important parameter to be considered for numerical simulation studies because reservoir permeability defines the flow path of the reservoir fluid. Reservoir heterogeneity depends on lithology of formation, depositional environment, formation of sweet spots and fracture development due to stress changes.

Figure 4.7 represents the stratigraphy of the Middle Bakken reservoir consisting of five

types of lithology. The formation is highly heterogeneous in the pay zone thickness of 40 ft. Simenson (2010) studied the lithology and depositional environment of the Parshall field in North Dakota and summarized the Middle Bakken formation into eight different litho-facies along depth, as observed in various studies (LeFever 2011, Simenson 2010).

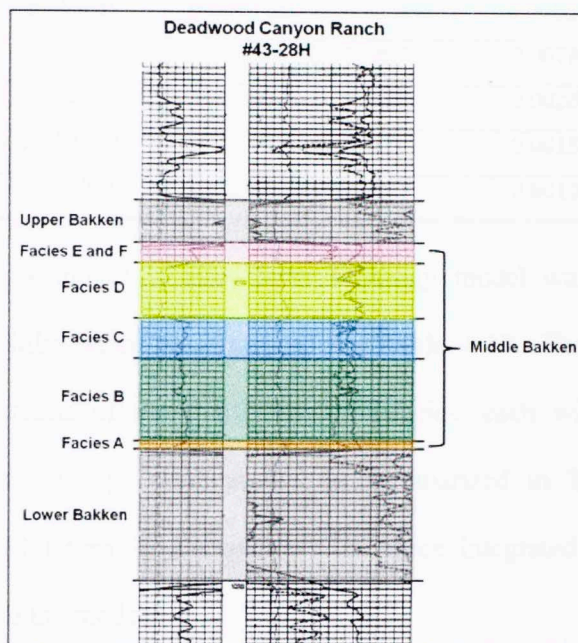


Figure 4.7: Litho-facies of the Middle Bakken formation (LeFever 2011)

Table 4.10 summarizes the range of permeability and formation thickness for eight different litho-facies as observed in Middle Bakken.

Table 4.10: Permeability variation with different litho-facies

FACIES	THICKNESS RANGE	PERMEABILITY RANGE	AVERAGE PERMEABILITY
F	0.2 – 3.0 ft	0.0005- 0.075 mD	0.00482 mD
E1	5.0 - 11.0 ft	0.0001-0.083	0.002 mD
D2	0.0 -22.0 ft	0.0001 – 0.055 mD	0.0042 mD
D1	2.0 - 5.0 ft	0.0003 mD- 0.0012 mD	0.0008 mD
C2	3.0 ft	0.0005 – 0.027 mD	0.0079 mD
C1	2.0 – 14.0 ft	0.0001 – 0.01 mD	0.0026 mD
B	3.0 – 34.0 ft	0.0001 – 0.03 mD	0.0015 mD
A	1.0 – 5.0 ft	0.0001-0.0057 mD	0.0012 mD

For the reservoir model, a three layer lithology model was considered by integrating the eight litho-facies as discussed in **Table 4.10**. The formation pay thickness of 40 ft consists of three different litho-facies, each with characteristic permeability range and average permeability, as summarized in **Table 4.11**. The reservoir model has 10 layers in Z-direction. The three integrated litho-facies are divided into 10 layers of the model.

Table 4.11: Heterogeneous thickness layer in reservoir model

LAYER	FACIES	PAY ZONE	GENERATED PERMEABILITY RANGE	AVERAGE PERMEABILITY
1-2	E1, F, D2	8 ft	0.0002 - 0.0065 mD	0.002 mD
3-6	C1, C2, D1	16 ft	0.00086 – 0.0234 mD	0.009 mD
7-10	A, B	16 ft	0.0002 – 0.0094 mD	0.004 mD

Dykstra-Parsons Coefficient (DPC) is used to quantify reservoir heterogeneity in the model. Dykstra-Parsons Coefficient relates standard deviation of permeability

profile to the median permeability. Using average permeability for layer 1, 2 and 3, a heterogeneous permeability range is generated using standard deviation of 0.5.

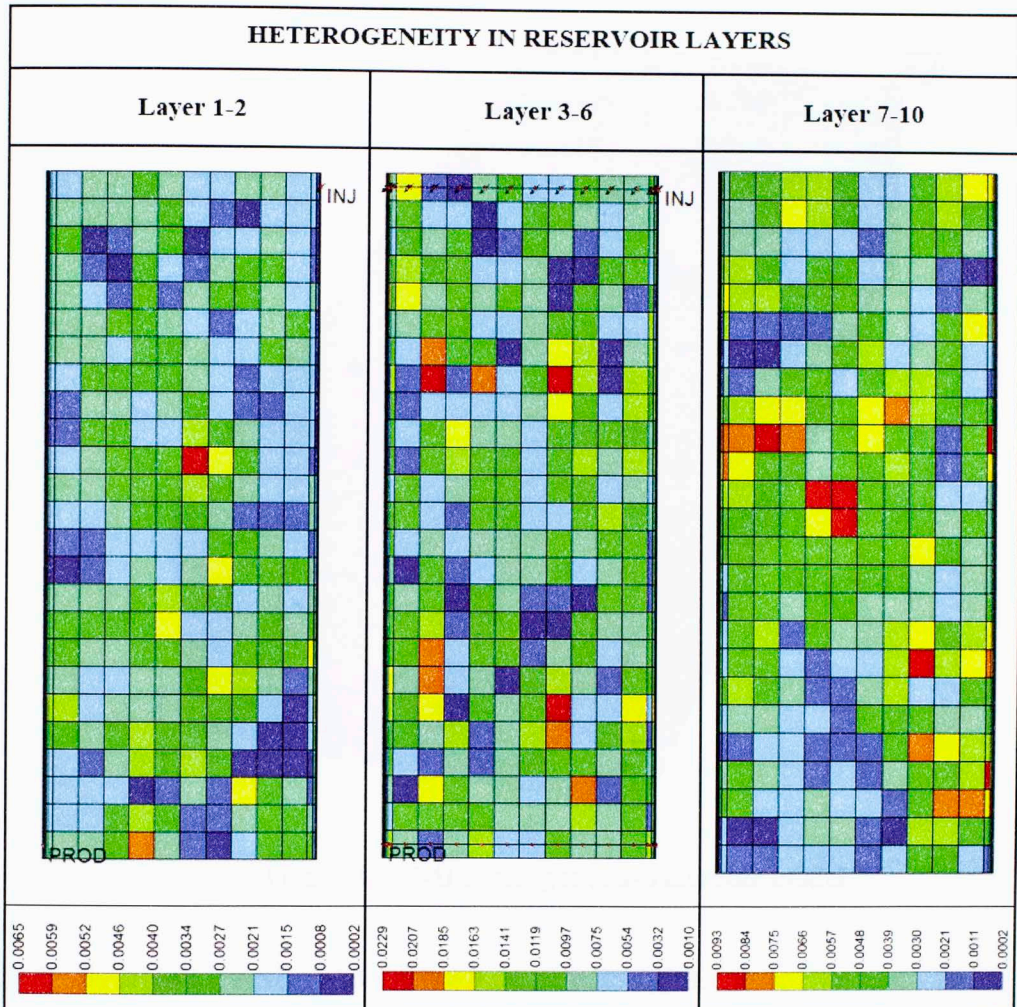


Figure 4.8: Heterogeneous model for three layers in the model

Figure 4.8 shows the variation in permeability for each layer defining a heterogeneous reservoir. Layer 1 and 2 have one set of heterogeneity, layer 3-6 have second set of heterogeneity and layer 7-10 have third set of heterogeneity. For each set, average permeability, as defined in **Table 4.11** was used to generate heterogeneous permeability for each grid blocks in the given permeability range. The layers 1-10 are

stacked together and the three dimensional reservoir model is displayed in **Figure 4.9**. Dykstra-Parsons Coefficient (DPC) is further explained in **APPENDIX B**.

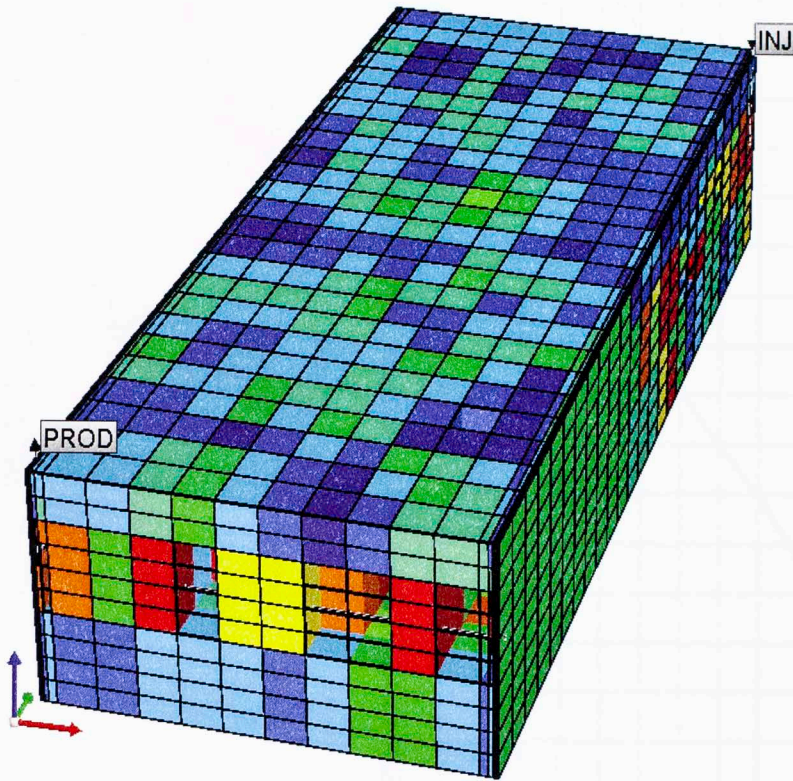


Figure 4.9: 3-D heterogeneous reservoir model

4.4.2 NATURAL AND INDUCED FRACTURES EFFECT

Natural and induced fractures are modeled using the fracture cell model (Sakhaee-Pour and Wheeler 2013) as discussed in chapter 2. **Figure 4.10** displays the perforation plane of the reservoir model containing natural and induced fracture networks. The rectangles in yellow signify the hydraulic fracture length and location in the model (invisible due to local grid refinement).

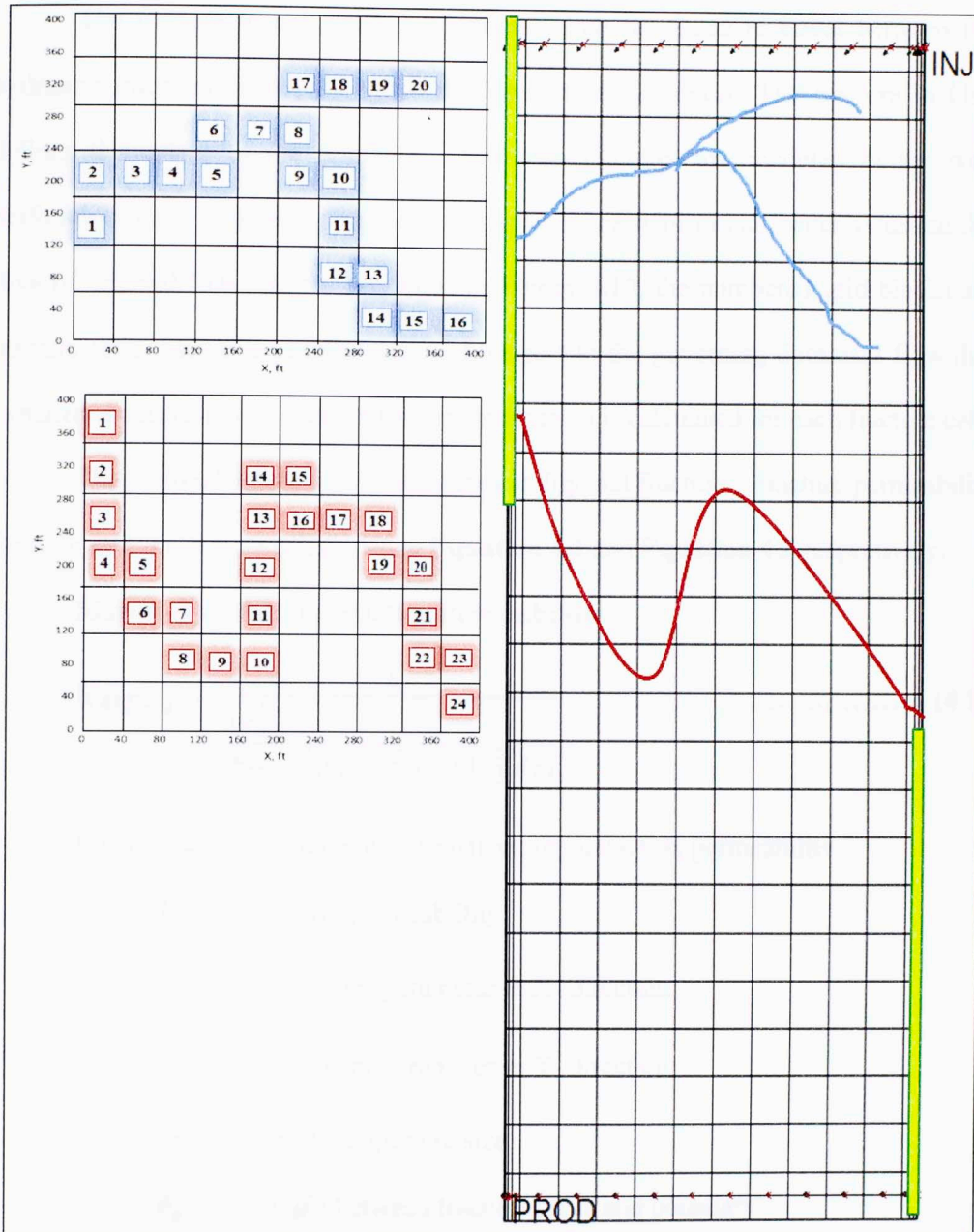


Figure 4.10: Natural and induced fracture network simulated in the reservoir

Red color fracture signifies the network of induced and natural fractures. Blue color fracture is to define the extent of natural fractures in the reservoir. The right side are the numbered grid block containing natural fractures.

The fracture in red forms a connective path for fluids to travel between the hydraulic fractures corresponding to the injector and producer. The fracture in blue defines the extent of the reservoir. These two fractures are modeled in the well perforation plane to account for the flow transport mechanism and better visualize the flow of injected CO₂ into the reservoir. In **Figure 4.10**, the numbered grid blocks are fracture cells. Effective permeability with respect to the governing dominant flow due to matrix-fracture and/or fracture-fracture interaction is calculated for each fracture cell.

The matrix-fracture interaction permeability and fracture – fracture permeability for each grid block is calculated using **Equation 4.1** and **Equation 4.3** respectively.

Matrix –Fracture Interaction Permeability:

$$k_{MF-x} = \frac{1}{\frac{1-\frac{b}{h}}{k_m} + \frac{\frac{b}{h}}{\frac{w}{h}k_f \cos^2 \theta_x + (1-\frac{a}{h})k_m}} \dots\dots\dots (4.1)$$

Where, k_{MF-x} = effective matrix-fracture interaction permeability

k_m = matrix permeability

$\frac{b}{h}$ = geometry parameter in X- direction

$\frac{a}{h}$ = geometry parameter in Y- direction

w = fracture aperture size

θ_x = angle between fracture curve and boundary

It can be noticed in **Equation 4.1** that the second term in denominator has a fracture permeability term in the denominator, making the second term zero. The following Equation becomes:

$$k_{MF-x} = \frac{1}{\frac{1 - \frac{b}{h}}{k_m}} \dots\dots\dots (4.2)$$

Permeability due to matrix - fracture interactions for each grid block, calculated using **Equation 4.2** in both X and Y- direction is listed in **Table 4.12**. The table lists the calculated permeability ratio with respect to the coordinate system displayed in **Figure 4.10** and geometry parameters ($\frac{a}{h}$ and $\frac{b}{h}$) calculated using MATLAB for each grid block. Effective permeability for few grid blocks are left blank, indicating that those grid blocks does not contain matrix-fracture interactions. The red boundary defines the grid blocks containing fractures in red and blue boundary blocks define the fractures in blue.

Fracture – Fracture Interaction:

$$k_{ff} = \left(\frac{l_c}{l_f}\right) \frac{w^2}{12h} \dots\dots\dots (4.3)$$

Where, k_{ff} = effective permeability of the fracture cells,

l_c = length of representative path

l_f = length of curved fracture between two points

w = aperture size of fracture

h = cell size

For the reservoir model, the cell dimension, h is 40 *ft*, fracture width is considered constant at, $w = 1.0 \text{ mm}$ (0.003 *ft*) and the length ratio, suggested in Sakhaee-Pour and Wheeler (2013), $\frac{l_c}{l_f}$ is 1.29. A MATLAB code was generated to calculate the $\frac{l_c}{l_f}$ ratio for the reservoir model and the value obtained was same i.e. 1.29.

This defines $k_{ff} = 8.96 \text{ mD}$. With no variable in the **Equation 4.3**, a constant value

of 8.96 mD was defined for each grid block having fracture-fracture interactions either in X- or Y- direction.

Table 4.12: Effective permeability for the Matrix-Fracture interactions

Cell	$\frac{b}{h}$	$\frac{a}{h}$	$\frac{k_{MF-x}}{k_m}$	$\frac{k_{MF-y}}{k_m}$	Cell	$\frac{b}{h}$	$\frac{a}{h}$	$\frac{k_{MF-x}}{k_m}$	$\frac{k_{MF-y}}{k_m}$
1	0.14	0.75	1.16	4.00	1	0.73	0.50	3.70	2.00
2	0.49	1.00	1.95	-	2	0.24	0.25	1.32	1.33
3	0.41	1.00	1.68	-	3	1.00	0.50	-	2.00
4	0.11	0.13	1.12	1.14	4	1.00	0.18	-	1.21
5	0.73	1.00	3.70	-	5	0.86	0.10	7.40	1.11
6	0.49	0.50	1.95	2.00	6	0.19	0.05	1.23	1.05
7	0.49	0.50	1.95	2.00	7	1.00	0.80	-	5.00
8	0.73	0.63	3.70	2.67	8	0.54	0.75	2.18	4.00
9	0.92	0.75	12.33	4.00	9	0.49	0.68	1.95	3.08
10	0.11	0.13	1.12	1.14	10	0.11	0.13	1.12	1.14
11	0.41	1.00	1.68	-	11	0.86	1.00	7.40	-
12	0.32	1.00	1.48	-	12	0.14	0.10	1.16	1.11
13	0.73	1.00	3.70	-	13	0.81	0.80	5.29	5.00
14	0.19	0.20	1.23	1.25	14	0.14	0.18	1.16	1.21
15	0.68	0.25	3.08	1.33	15	1.00	0.68	-	3.08
16	0.19	0.13	1.23	1.14	16	0.24	0.05	1.32	1.05
17	1.00	0.88	-	8.00	17	0.49	0.18	1.95	1.21
18	0.14	0.13	1.16	1.14	18	1.00	0.45	-	1.82
19	1.00	1.00	-	-	19	1.00	0.23	-	1.29
20	0.14	0.13	1.16	1.14	20	0.73	0.45	3.70	1.82
21	0.86	1.00	7.40	-					
22	0.19	0.13	1.23	1.14					
23	0.73	0.88	3.70	8.00					
24	0.24	0.25	1.32	1.33					

The effective permeability of each fracture cell in the representative path is calculated from the dominating mechanism between k_{MF-x} and k_{FF} . This process is followed to calculate the effective permeability in both X and Y direction to account for complete anisotropy and to signify the importance of non –planar geometry.

Figure 4.11 shows the perforation plane of the reservoir model containing the two natural and induced fractures. The higher permeability zones indicate the natural fractures.

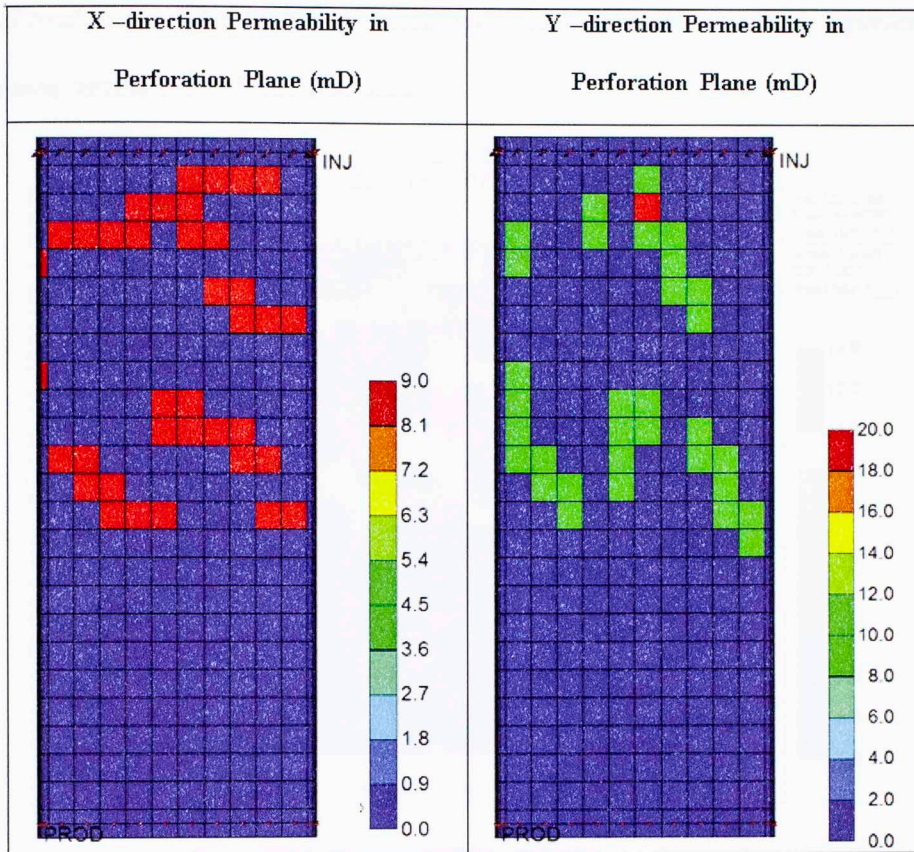


Figure 4.11: Perforation plane with natural and induced fractures

The reservoir model with fracture cells is simulated for CO₂ injection and hydrocarbon production for 30 years. The induced and natural fractures define the dominating flow path for CO₂ migration as compared to tight matrix. The fracture model was implemented in both homogeneous and heterogeneous model. Even in heterogeneous model, the grid blocks with effective permeability due to fracture-fracture interaction dominate the flow and pressure migration. **Figure 4.11** shows a heterogeneous model but as the matrix permeability order is very small, the permeability variations are invisible. **Figure 4.12** provides a better visualization of the differences in matrix and natural fracture permeability with permeability plotted on a

log normal scale. The higher permeability zones defined in yellow represent the simulated natural and induced fractures.

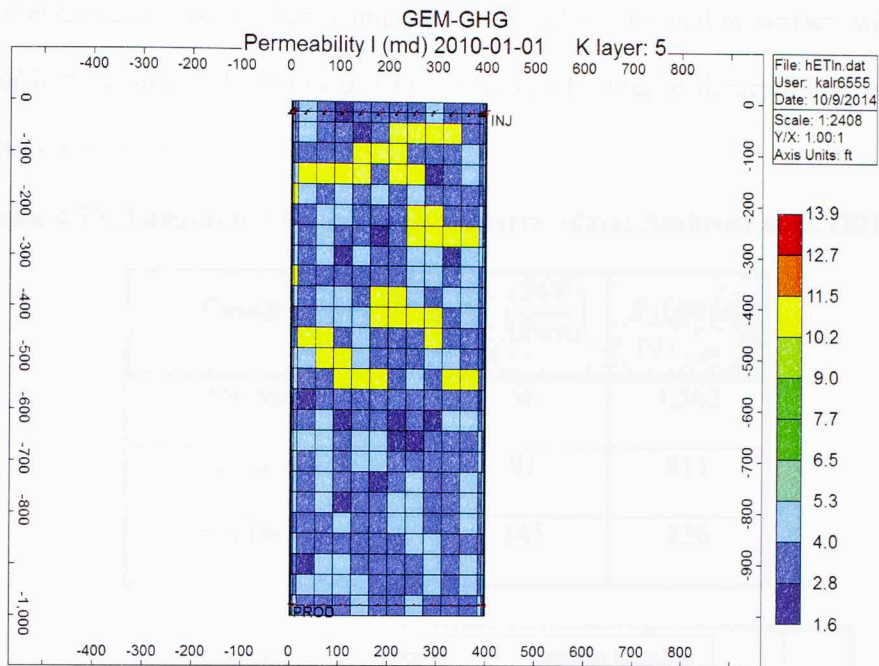


Figure 4.12: Permeability variation on log scale

4.4.3 ADSORPTION / DESORPTION MODEL WITH TOC

For this study, Extended Langmuir Isotherm model, discussed in 2.4.3 ADSORPTION/DESORPTION EFFECT ON OIL PRODUCTION, is employed to account for adsorption of CO₂ and desorption of hydrocarbon components in reservoir simulation. Desorption of methane and ethane molecules from the formation is considered in the model whereas the other higher C+ components are ignored as their desorption is very minimal. Also, since CO₂ is injected into the formation, adsorption parameters for CO₂ are also considered in the model. Adsorption parameters for these components are provided from the laboratory experiments from Ambrose et al. (2011). **Table 4.13** illustrates the constant adsorption parameters of

different components for Langmuir's Isotherm model. It can be observed in **Figure 4.13** that at higher reservoir pressure, adsorption capabilities of CO₂ are significantly higher when compared to hydrocarbon components. Therefore, formation surface will have more affinity towards adsorption of CO₂ molecules leading to desorption of methane and ethane molecules.

Table 4.13: Langmuir's Isotherm parameters (data: Ambrose et al. (2011))

<i>Component</i>	$V_L \left(\frac{SCF}{Ton} \right)$	$P_L (psia)$
Methane, C1	56	1,562
Ethane, C2	91	811
Carbon Dioxide, CO₂	145	836

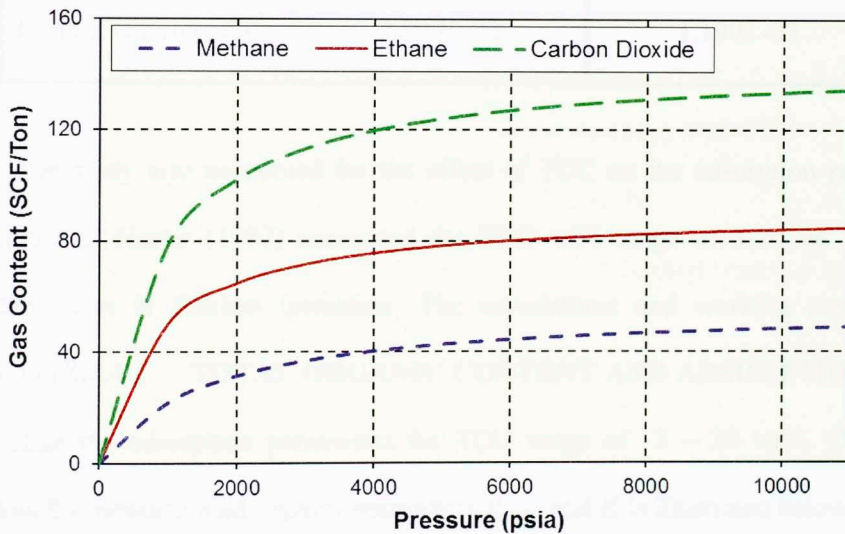


Figure 4.13: Extended Langmuir's Isotherm simulated in reservoir model (data: Ambrose et al. (2011))

Adsorption parameters from **Table 4.13** are modified in order to feed as an input to CMG-GEM. Maximum adsorbed mass is calculated from Langmuir's adsorption

capacity, V_L and unit conversions. Similarly, Langmuir's adsorption constant is inverse of langmuir's pressure, P_L . Also, Rock density of $120 \frac{lb}{ft^3}$ is used in reservoir model. The adsorption parameters calculated for input into CMG-GEM are illustrated in **Table 4.14**.

Table 4.14: Adsorption parameters input to GEM

ADSORPTION PARAMETERS IN GEM		
<i>Component</i>	Maximum Adsorbed	Langmuir Adsorption
	Mass, $M_L, \frac{gmole}{lb}$	Constant, $\frac{1}{P_L}, \frac{1}{psi}$
Methane, C1	3.04 E -02	6.41 E -04
Ethane, C2	4.95 E -02	1.24 E -03
Carbon Dioxide, CO₂	7.89 E -02	1.19 E -03

The study also accounted for the effect of TOC on the adsorption parameters. Schmoker and Hester (1983) accounted for TOC wt% range of 3-20 wt % for the Williston basin in Bakken formation. The correlations and working methodology described in **2.4.4 TOTAL ORGANIC CONTENT AND ADSORPTION** is used to calculate the adsorption parameters for TOC range of 3 – 20 wt%. Calculation workflow for measuring adsorption parameters V_{max} and K is illustrated below:

STEP 1: Calculate $1/K$ using Type 1 Kerogen **Equation 2.7**

$$\ln K = \frac{1241}{T} - 5.89 \text{ @ } T = 65 \text{ }^\circ\text{C} \dots\dots\dots (4.4)$$

Where, T = Temperature, Kelvin

K = Langmuir's constant, 1/MPa

$$\frac{1}{K} = 1335.5 \text{ psia } (P_L) \dots\dots\dots (4.5)$$

STEP 2: Calculate C8 Lewis Correlation constant using **Equation 2.14**

$$c8 = \log P_L + (c7.T_i) \dots\dots\dots (4.6)$$

Where, T_i = Isotherm temperature (65 °C)

P_L = Langmuir's constant at T_i , from **Equation 2.6**

$c7$ = 0.005

$$c8 = 3.4506 \dots\dots\dots (4.7)$$

STEP 3: Calculate 1/K at Bakken temperature (115 °C) using **Equation 2.12**

$$P_{LT} = 10^{(-c7.T+c8)} \dots\dots\dots (4.8)$$

$$P_{LT} = 746.19 \text{ psia} \dots\dots\dots (4.9)$$

STEP 4: Calculate V_{max} with varying TOC % @ T = 65 °C

$$V_{max} = 724 [0.0134 * TOC + 0.0148] \dots\dots\dots (4.10)$$

Where, V_{max} = Maximum adsorption capacity, SCF/Ton

TOC = Total Organic Content, wt %

STEP 5: Use Lewis Correlation to calculate V_{max} at Bakken reservoir temperature

$$V_{LT} = 10^{(-c3.T+c4)} \dots\dots\dots (4.11)$$

$$c4 = \log V_L + (c3.T_i) \dots\dots\dots (4.12)$$

Where, T_i = Isotherm temperature (65 °C)

V_L = Adsorption capacity at T_i , from **Equation 2.6**

T = Reservoir temperature (115 °C)

V_{LT} = Adsorption capacity at reservoir temperature

$c3$ = 0.0027

The calculations are illustrated in **Table 4.15**.

Table 4.15: Adsorption Parameter calculations

TOC wt%	$V_{max}@ 65\text{ }^{\circ}\text{C}$, $\frac{\text{SCF}}{\text{Ton}}$	c_4 Lewis Constant	$V_{max}@ 115\text{ }^{\circ}\text{C}$, $\frac{\text{SCF}}{\text{Ton}}$
3	39.8	1.776	29.1
5	59.2	1.948	56.2
10	107.7	2.208	78.7
15	156.2	2.369	114.1
20	204.7	2.487	145.0

Figure 4.14 displays the adsorption isotherm curves for varying TOC wt% calculated using the parameters in Equation 4.4 to Equation 4.12 and Table 4.15.

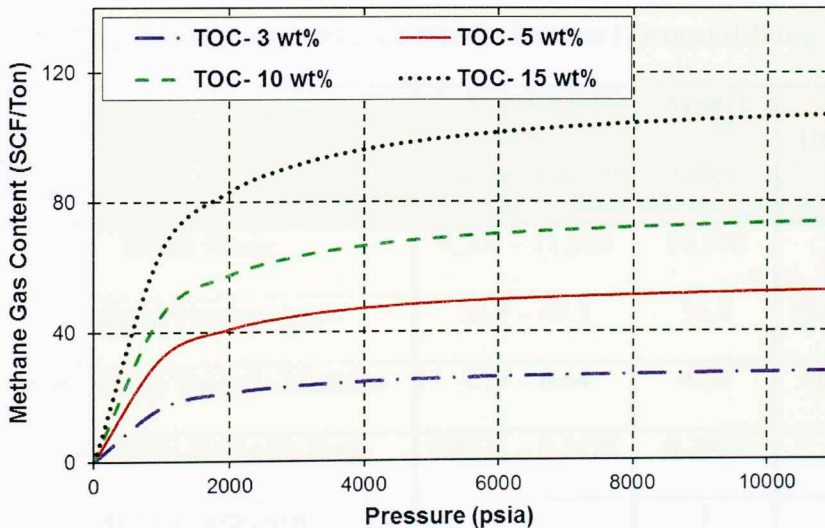


Figure 4.14: Methane adsorption isotherm curve with varying TOC wt%

4.4.4 GEOMECHANICAL COUPLING WITH RESERVOIR SIMULATOR

CMG-GEM provides the ability to couple Geomechanics module with the reservoir simulator model. The module was utilized to consider the stress dependent permeability effects into reservoir model. Natural fracture and induced fracture permeability will be significantly affected by stress changes in the formation and need to be encountered to better characterize the CO₂ flow migration in the reservoir.

Various laboratory studies have been carried out to study the geomechanical effects in the Bakken formation (Zeng and Jiang 2009, Zhou et al. 2008) and published results are tabulated in **Table 4.16**.

During CO₂ injection into formation, stress changes will also reactivate the natural fractures providing path for CO₂ to migrate into the matrix displacing oil towards the well perforations. Hence, stress dependent permeability will play a critical role in designing CO₂ injection profile into a tight formation for enhanced oil recovery.

Table 4.16: Stress parameters for Middle Bakken (Zeng and Jiang 2009)

Parameter	Value for Middle Bakken	Model value	Units
Depth Range	9,500 – 11,000	10,500	ft
Coulomb Friction Angle	36.8 – 49.3	36.8	Degree
In-situ Static Young's Modulus	4.79 – 6.64	4.79	M psi
In-situ Static Poisson's Ratio	0.2625 – 0.3425	0.2625	
Biot's Coefficient		1	

To evaluate the pressure dependent permeability and porosity of the fractures, Kurtoglu (2014) carried out multi-stress permeability test on three Middle Bakken core samples. Permeability was measured as a function of increasing effective stress (**Figure 4.15**).

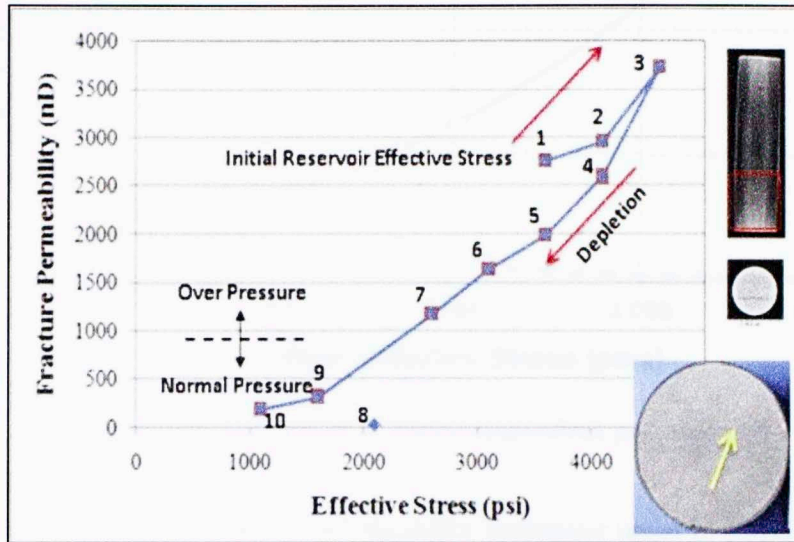


Figure 4.15: Permeability as a function of confining stress

In order to input this curve in reservoir simulation, the expansion and depletion curve in pressure range for Bakken are extrapolated, as illustrated in **Figure 4.16**. To input the extrapolated curve from **Figure 4.16** into CMG-GEM, permeability multiplier table in reference to stress change in X-, Y- and Z- direction can be input to the Geomechanics module as describes in **Table 4.17**.

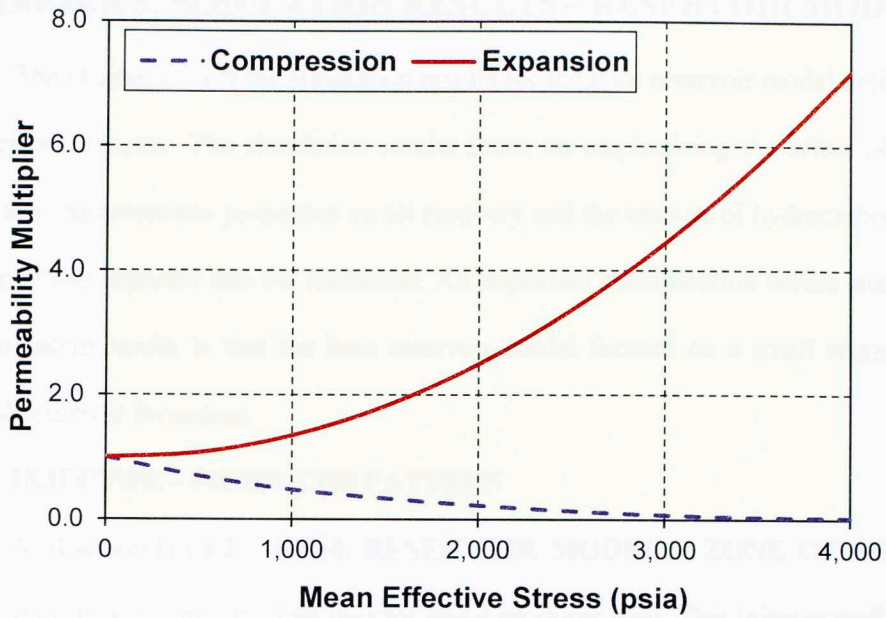


Figure 4.16: Extrapolated Stress dependent permeability curve

Table 4.17: Stress dependent permeability multiplier input to CMG-GEM

Effective Stress, psi	$\frac{k_x}{k_{x0}}$	$\frac{k_y}{k_{y0}}$	$\frac{k_z}{k_{z0}}$
-4000	7.200	7.200	7.200
-3000	4.450	4.450	4.450
-2500	3.375	3.375	3.375
-2000	2.500	2.500	2.500
-1000	1.350	1.350	1.350
-500	1.075	1.075	1.075
0	1.000	1.000	1.000
500	0.700	0.700	0.700
1000	0.480	0.480	0.480
2000	0.230	0.230	0.230
3000	0.080	0.080	0.080
4000	0.030	0.030	0.030

CHAPTER 5: SIMULATION RESULTS – RESERVOIR MODEL

The chapter covers the simulation results for the base reservoir model defined in the previous chapter. The simulation results focus on emphasizing the effect of shale formation characteristics properties on oil recovery and the amount of hydrocarbon pore volume of CO₂ injected into the formation. An important consideration before analyzing the simulation results is that the base reservoir model focuses on a small segment of original reservoir formation.

5.1 INJECTOR – PRODUCER PATTERN

As discussed in **4.2 BASE RESERVOIR MODEL – ZONE OF STUDY**, the reservoir model consists of an injector and a producer well. This injector well could previously be a producer well or there can be a case where an infill well is drilled to act as an injector well between two producer wells. The simulation was run for 30 years with simultaneous CO₂ injection and hydrocarbon production from separate wells. The reservoir properties for the model are described in average column of **Table 4.1** and grid dimensions in **Table 4.2**. To understand the significance of CO₂ injection, oil production in primary recovery is compared with oil production with CO₂ injection in **Figure 5.1**. Without CO₂ injection, total oil recovery was 7.4 % after 30 years of production. It increased to 53.2% with continuous CO₂ injection along with production. Total CO₂ injected was 113.1% HCPV (hydrocarbon pore volume).

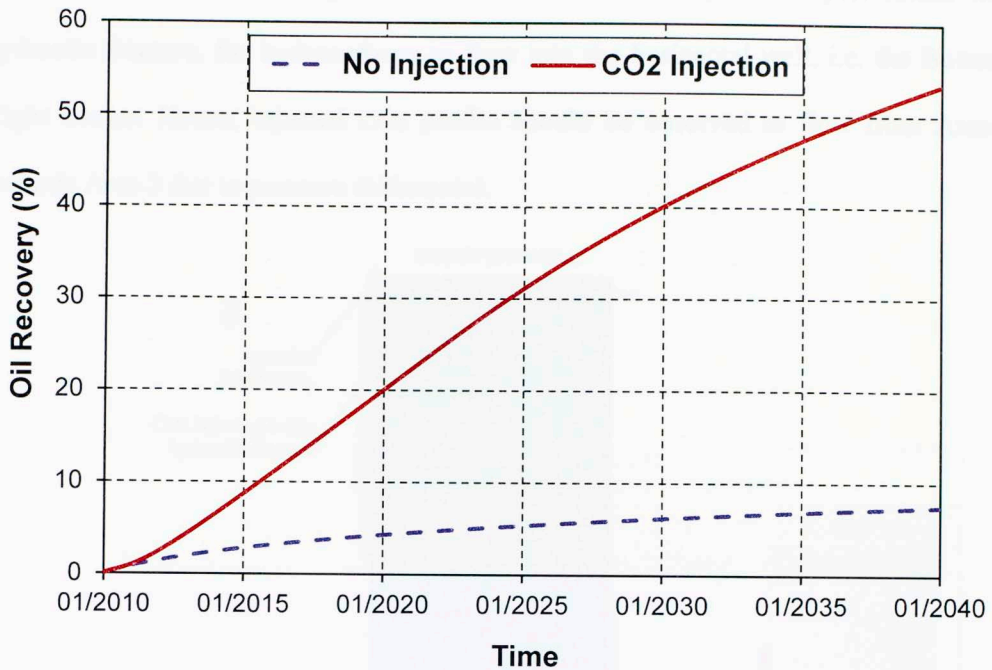


Figure 5.1: Oil Recovery comparison with and without CO₂ injection

The simulation results are very optimistic for a tight oil reservoir. This can be due to the fact that modeling was done only across a small zone to study CO₂ flow characteristics. The Zone of Study is a region between one perforation of an injector well and one perforation of a producer well. The lateral length of the horizontal wells in the reservoir model is 400 ft. Pu and Hoffman (2014) reported an incremental oil recovery of 35% in the Middle Bakken with a 15 stage injector well and a nearby producer well.

For understanding the reservoir profile for future simulation and sensitivity analysis, **Figure 5.2** provides an example of reservoir profile that is used to show simulation results obtained during this study for future work. **Area 1** is the injector perforation and the injector hydraulic fracture, through which CO₂ is injected into the

formation, i.e. from the Top-Left corner. **Area 2** is the producer perforation with hydraulic fracture, for hydrocarbons to flow into the horizontal well, i.e. the Bottom-Right corner. Hence, injected CO₂ profile should be observed to flow from Area 1 towards Area 2 due to pressure differential.

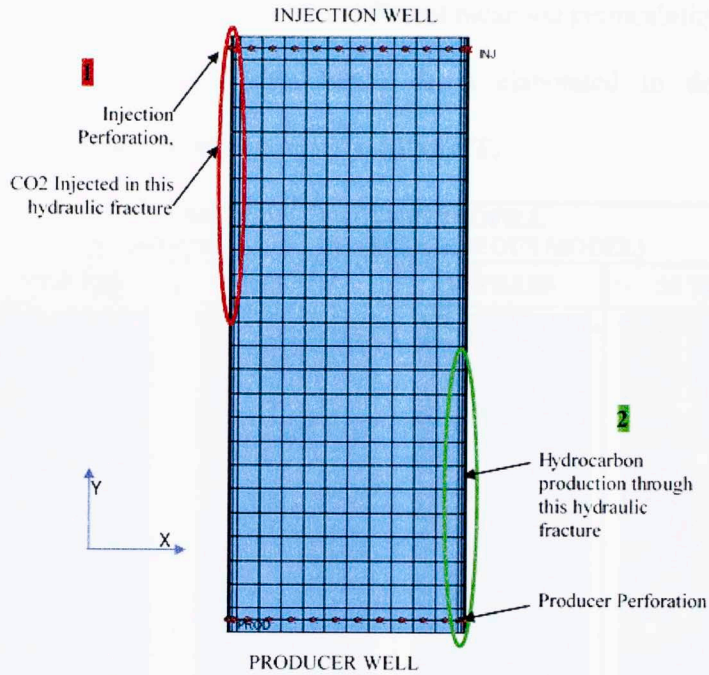


Figure 5.2: Reservoir profile in X-Y direction with injector and producer perforation

5.2 ANALYSIS OF RESERVOIR CHARACTERISTICS

The reservoir model is heterogeneous in nature and consists of simulated natural fractures as discussed in **4.4.2 NATURAL AND INDUCED FRACTURES EFFECT**. Tight oil/shale reservoirs are very heterogeneous in lithology with ultra—low matrix permeability, signifying the presence of natural fractures in the reservoir to account for major production. These characteristics are incorporated into the reservoir model.

5.2.1 HOMOGENEOUS V/S HETEROGENEOUS MODEL

The homogeneous reservoir model is defined as a single porosity model with constant reservoir permeability of 0.005 mD and porosity of 5 %. To incorporate reservoir heterogeneity, a reservoir model was built considering three different lithology layers within the depth of pay, each with a different mean log permeability and different permeability defined for each grid block. It is elaborated in detail in 4.4.1

RESERVOIR HETEROGENEITY EFFECT.

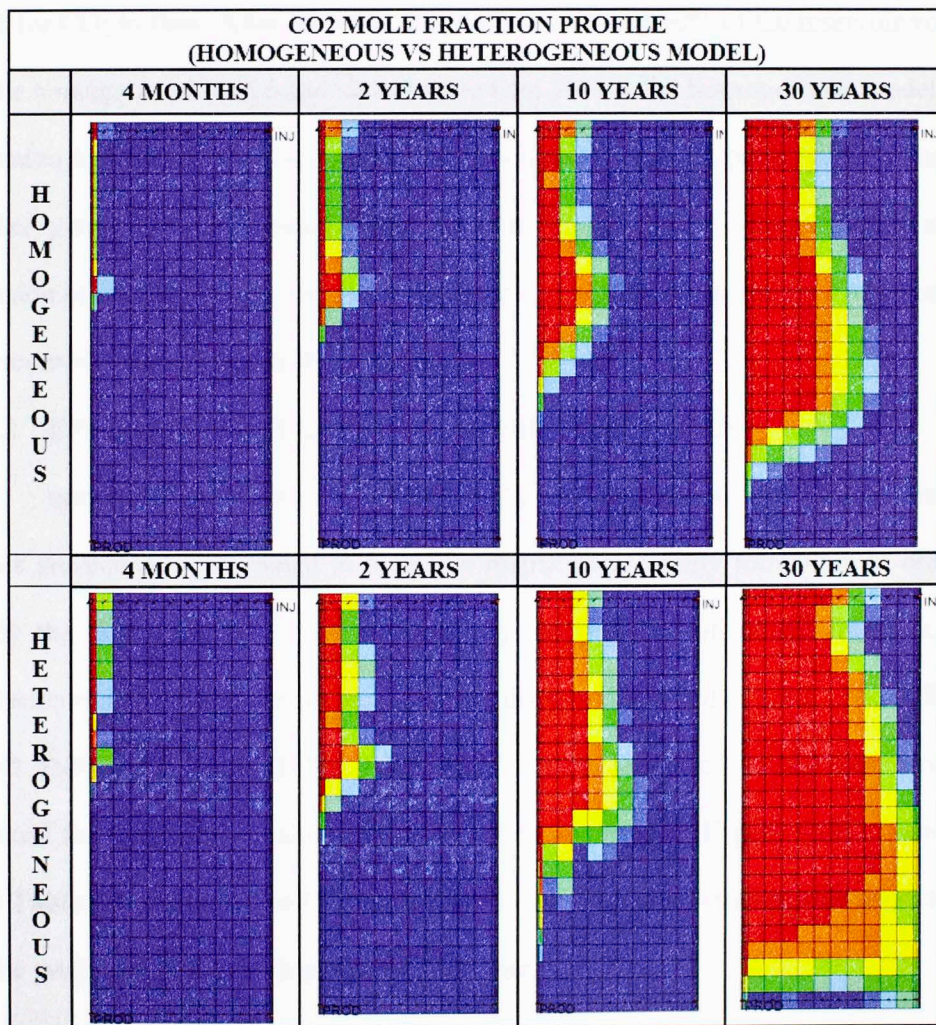


Figure 5.3: CO₂ flow profile for homogeneous and heterogeneous reservoir model

Figure 5.3 compares the injected CO₂ mole fraction flow profile in the reservoir model for the homogeneous and heterogeneous reservoir model in the perforation plane with time progression. The homogeneous model had a constant permeability of 0.005 mD and does not consider the effect of natural fractures in the model. It can be observed that even after 2 years of continuous injection, CO₂ was able to sweep less than 10% of the reservoir volume. On the other hand, in the heterogeneous model, CO₂ flow profile is advanced due to heterogeneity in the permeability values for various zones providing path for CO₂ to flow. After 30 years, CO₂ is able to sweep 60% of the reservoir volume in the homogeneous model and almost more than 80% in the heterogeneous model. The variation in permeability for each grid blocks cater to creating paths for flow through higher permeable grid blocks. Transmissibility in X- and Y- direction is a strong function of permeability in respective direction and will dominate the flow mechanics in the reservoir due to pressure differential.

5.2.2 EFFECT OF SIMULATED NATURAL FRACTURES

Instead of depending on Dual-Porosity models, natural and induced fracture zones are manually simulated in ultra-low matrix permeability formation, in order to study the flow behavior of CO₂ affected by the presence of natural fractures. The inclusion of natural fractures in the model are discussed in detail in **4.4.2 NATURAL AND INDUCED FRACTURES EFFECT**. Two connected natural fractures and induced fracture paths are simulated in the perforation plane (**Figure 4.10**). **Table 5.1** and **Table 5.2** illustrates the CO₂ mole fraction profile and pressure profile respectively in the perforation plane with progression of time.

Table 5.1: CO₂ mole fraction profile in the perforation plane affected by natural fractures

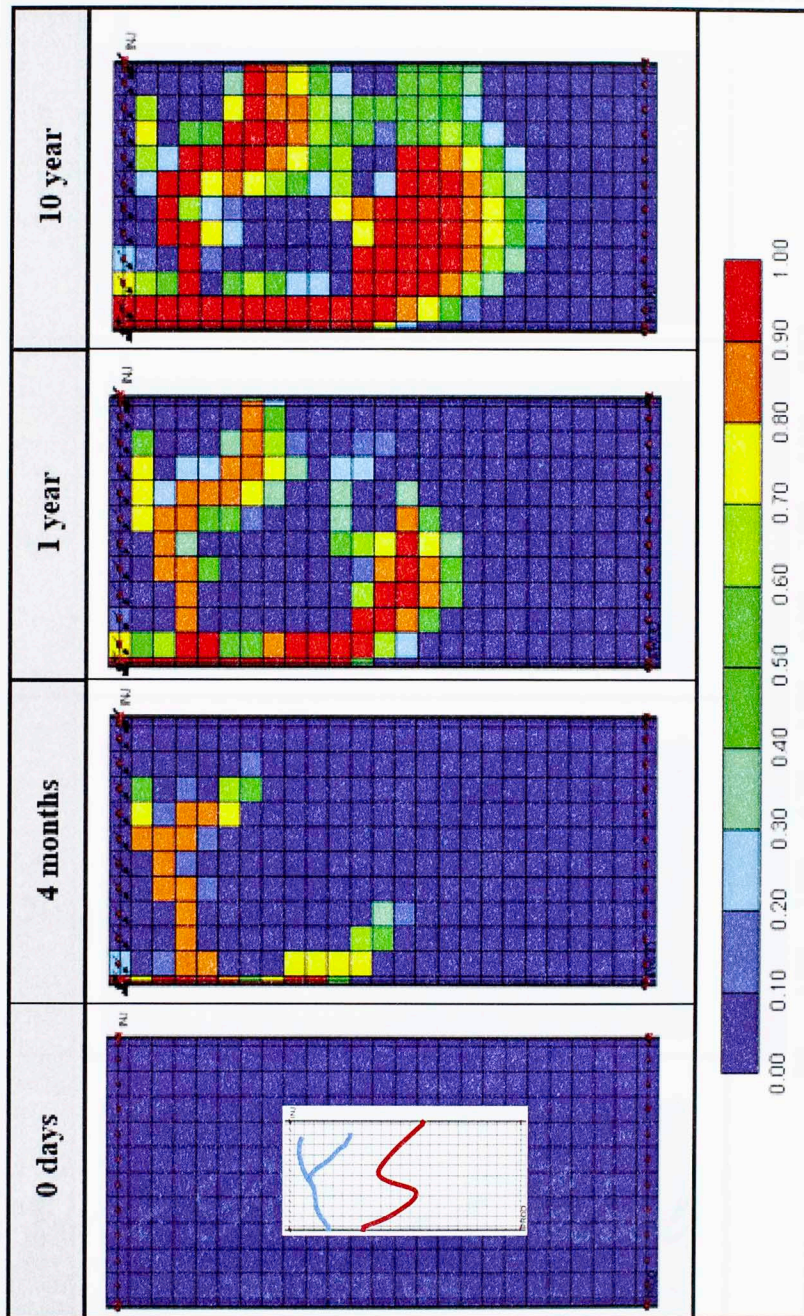
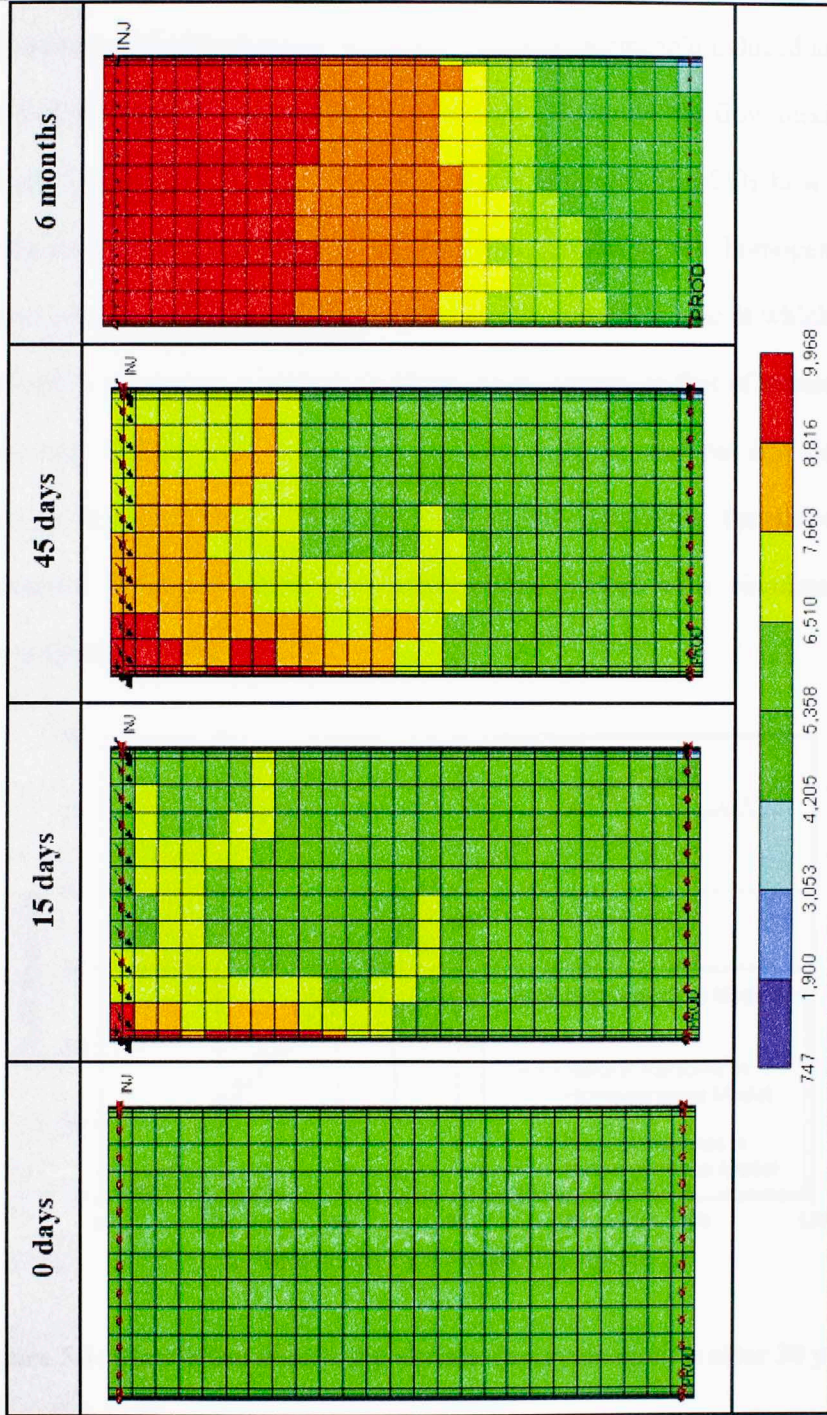


Table 5.2: Reservoir pressure profile in the Injector – Producer perforation plane



It can be observed in **Table 5.1** that CO₂ injected in the hydraulic fracture in the Top-Left corner takes the flow path created by the high permeable induced and natural fractures in the formation. The presence of fractures dominate the flow mechanism in the reservoir and hence, higher sweep efficiency is achieved. The CO₂ flow profile of natural fractures can be compared with the flow profile in the homogeneous and heterogeneous reservoirs in **Figure 5.3**. **Table 5.2** illustrates the rate at which reservoir pressure varies. The nature of flow follows the same pattern as that of natural fracture conducive path. Reservoir pressure drains near the producer zone but at a slow rate as compared to injection zone. The simulation results comparing the three models: Homogeneous, Heterogeneous, and Heterogeneous model with simulated natural fractures is illustrated in **Figure 5.4**

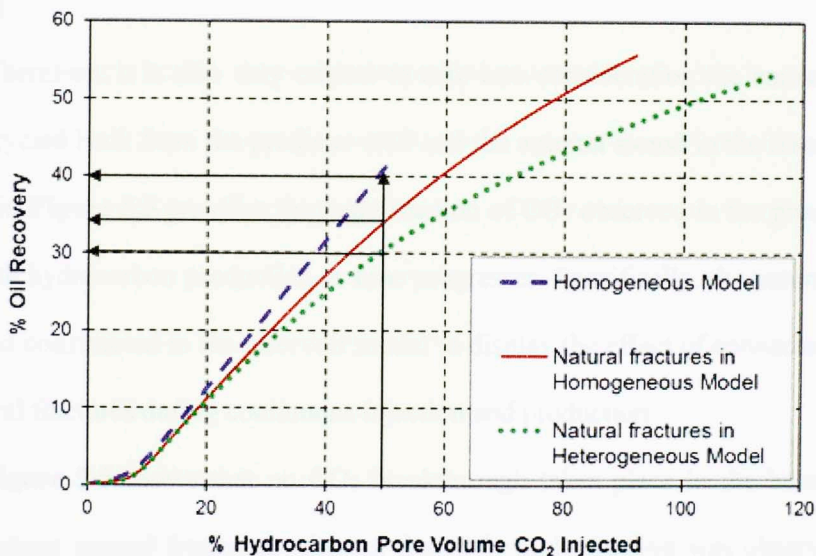


Figure 5.4: Simulation results for various reservoir models after 30 years

The major effect of the presence of natural fractures in a reservoir can be clearly observed in **Figure 5.4**. If, equal amount of CO₂ is injected into the three different

models, the vertical black line defines 50% HCPV CO₂ injection into the formation. **Figure 5.4** represents that the homogeneous reservoir displays maximum oil recovery followed by heterogeneous permeability reservoir model and the least oil recovery is achieved from the heterogeneous reservoir model containing natural fracture model. The difference in total oil recovery of 15% and double volume of CO₂ being injected due to the presence of natural fractures was a clear indication of the importance of presence of fractured media in tight formations that dominate the flow mechanisms. This is a very important parameter to be considered when planning CO₂ EOR in tight formations, which are naturally fractured and can provide flow paths for CO₂ to migrate through the matrix. Natural fractures improve the reservoir contact but they also allow CO₂ to migrate towards the producer well, leading to early CO₂ breakthrough and recycling.

Therefore, it is also very critical to take into consideration the amount of CO₂ being recycled back from the producer well and the amount stored in the reservoir. The analysis in **Figure 5.5** provides the mole fraction of CO₂ observed in the producer well along with hydrocarbon production as time progresses. Specifically, the natural fracture in red was constructed in the reservoir model to display the effect of connected induced and natural fractures during continuous injection and production.

Figure 5.5 shows that no CO₂ breakthrough takes place in the homogeneous model lacking natural fractures, whereas first CO₂ mole fraction was observed in the heterogeneous model containing natural fractures after 4 years of continuous injection and production. After 10 years, almost 50% of hydrocarbon production consists of CO₂ for a heterogeneous reservoir.

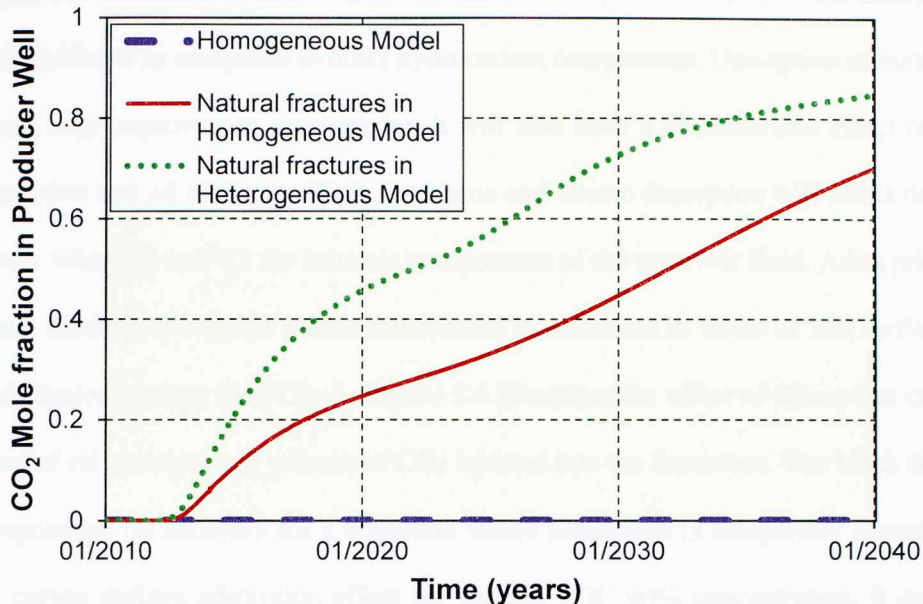


Figure 5.5: CO₂ mole fraction in the producer well for various reservoir models

Heterogeneity also plays a significant role for migration of CO₂ or/and hydrocarbon fluids within the reservoir to the producer well. While comparing a homogeneous and heterogeneous reservoir model containing natural fractures, CO₂ breakthrough for both models occurs at the same time due to natural fractures, but then considerably less amount of CO₂ mole fraction was observed in the homogeneous model containing natural fractures with time progression.

5.2.3 EFFECT OF ADSORPTION / DESORPTION

The study considers the adsorption and desorption effect for methane, ethane and carbon dioxide molecules. Adsorption capability of CO₂ is significantly higher than hydrocarbon components. Formation surface will have more affinity towards adsorption of CO₂ molecules leading to desorption of methane and ethane molecules. As CO₂ is injected into the formation, it comes into contact with the formation matrix. Some molecules of CO₂ will be adsorbed onto the matrix surface, thereby forcing

hydrocarbon molecules to desorb from the same. Desorption of methane and ethane are more significant as compared to other hydrocarbon components. Desorption of methane will not only improve gas recovery but it will also have a characteristic effect on oil composition and oil recovery. Higher methane and ethane desorption will affect the oil recovery when C1 and C2 are intrinsic components of the reservoir fluid. Adsorption is a strong function of organic matter content and is correlated in terms of TOC wt% and gas adsorption content (SCF/Ton). **Figure 5.6** illustrates the effect of adsorption on the amount of oil recovery and volume of CO₂ injected into the formation. The black dotted line represents oil recovery for a condition where adsorption is completely absent and other curves defines adsorption effect for various TOC wt% concentration. It can be observed that adsorption modeling does not significantly affect the oil recovery, but due to adsorption of CO₂, higher hydrocarbon pore volume of CO₂ was injected into the formations. Higher organic content (TOC) has greater capabilities of CO₂ adsorption and more desorption of hydrocarbon components, leading to higher oil recovery as compared to reservoir containing lower organic content. Adsorption effects are significant in the later life of the reservoir with lower pressure. Significant drop in pressure triggers the adsorption/desorption mechanisms. **Figure 5.7** shows the observed CO₂ mole fraction profile in the producer well of reservoir models without adsorption physics and with adsorption based on TOC wt%. It can be observed that higher amount of CO₂ was produced for the reservoir model with no adsorption effect. With consideration of adsorption, the mole fraction of CO₂ in the produced fluid is reduced and also delayed with time progression. Less amount of CO₂ was produced with

adsorption consideration in the reservoir model, indicating a higher amount of CO_2 being sequestered into the formation.

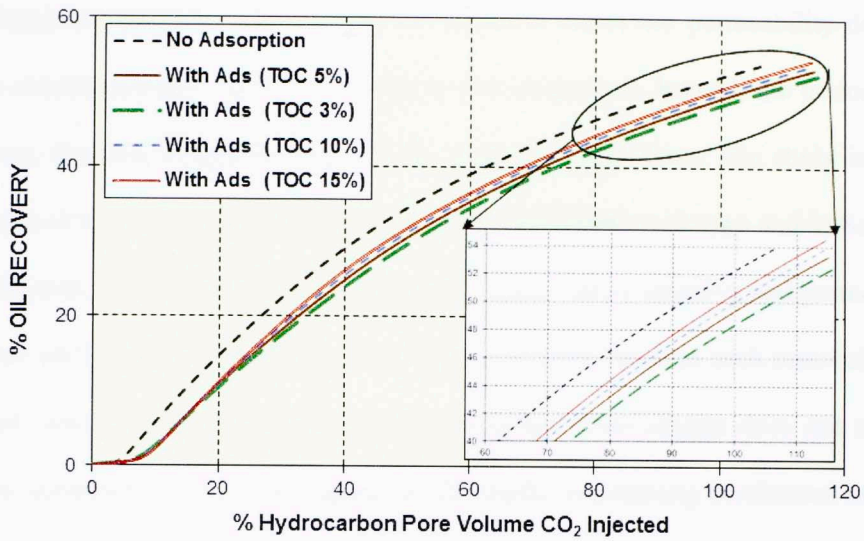


Figure 5.6: Oil recovery with adsorption effects with respect to TOC wt%

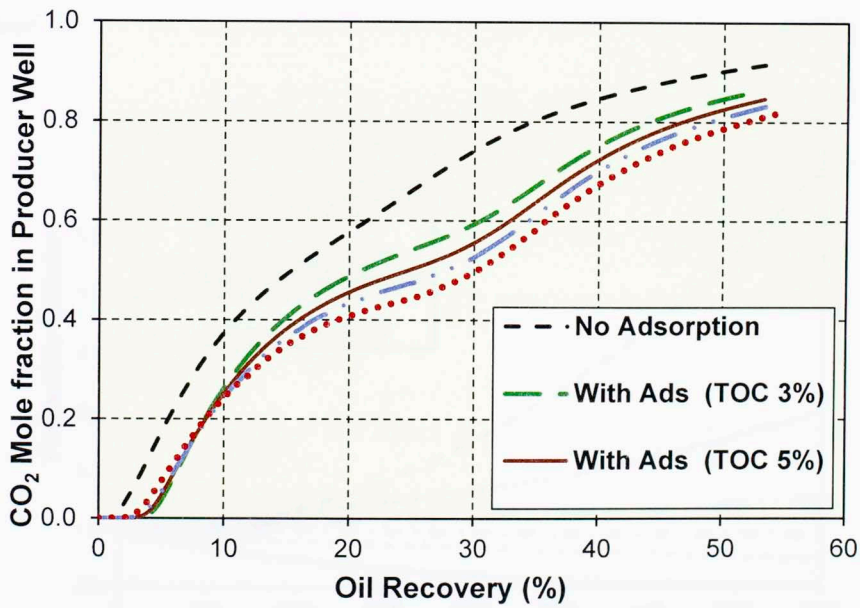


Figure 5.7: Variation in CO_2 production due to adsorption effects

5.2.4 EFFECT OF STRESS DEPENDENT PERMEABILITY

In this study, geomechanical analysis is primarily focused on considering the stress dependent permeability effect in the reservoir. Reservoir permeability does not remain constant during continuous injection and production. Instead, the permeability is a strong function of mean effective stress changing with time. The study included three types of rock formations: 1) Stiff rock type, 2) Medium rock type and 3) Soft rock type. Soft rock type means that the formation is highly stress sensitive and permeability variations will be significant based on the mean effective stress in each reservoir zone. Stiff rock means that the formation is very tight that stress change does not strongly affect the permeability of the formation. In this study, considering continuous injection and production, mean effective stress will vary in different reservoir zones and considering the changes in permeability with mean effective stress is critically very important.

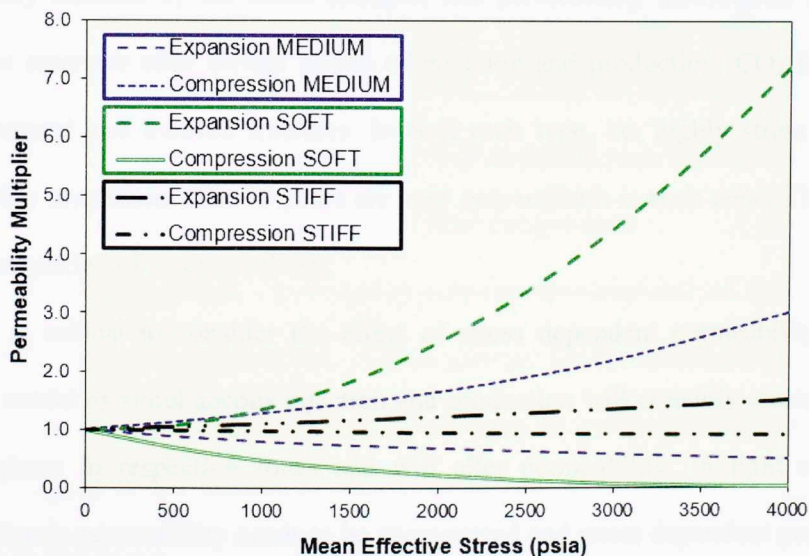


Figure 5.8: Permeability multiplier for different rock types

Figure 5.8 defines the permeability multiplier for the Soft, Medium and Stiff rock type geomechanical model. Permeability multiplier is defined as a ratio of current permeability to original permeability. Expansion curves define the increment in permeability with increasing mean effective stress and compression curves define the reduction in permeability with increasing mean effective stress in the reservoir zone. These two curves are defined for each rock type in the reservoir model, as the formation will experience both phenomenon in different zones like near injection zones and the producer zones.

The permeability variations in the reservoir with time progression will strongly affect the flow mechanisms of CO₂. Permeability defines the path for fluid to flow within the reservoir. **Figure 5.9** compares the CO₂ migration in the reservoir between a highly stress sensitive and less stress sensitive rock. The CO₂ flow profile with time progression are very different for the two cases. In Stiff rocks, permeability is not significantly affected by the stress changes, and permeability distribution is uniform within the reservoir after certain period of injection and production. CO₂ follows the path of natural and induced fractures. In Soft rock type, i.e. highly stress sensitive, permeability alterations after 10 years are very non-uniform in each zone. This defines the flow migration of reservoir fluids.

It is critical to consider the effect of stress dependent permeability into the reservoir model as simultaneous injection and production will certainly create different stress regimes in respective zones and will alter permeability. In tight rocks, any modification in permeability needs to be encountered and stress dependent permeability is one of the most important characteristic.

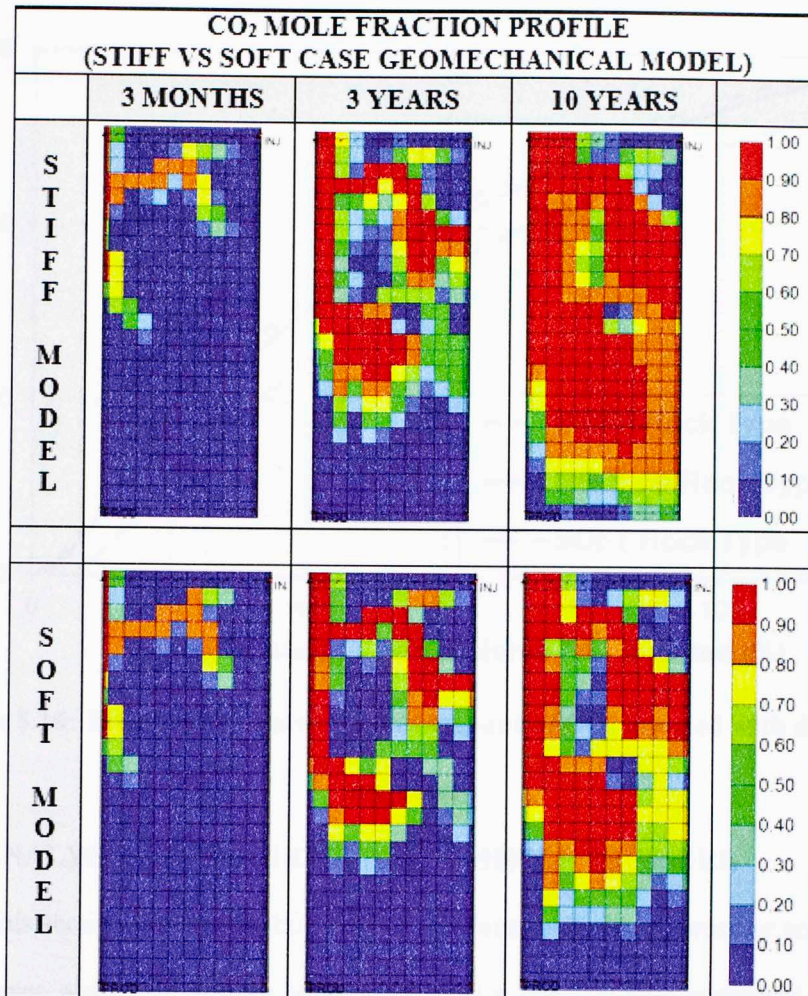


Figure 5.9: CO₂ mole fraction profile for Soft and Stiff rock type geomechanical model with time progression

Figure 5.10 provides a comparison between the simulated oil recoveries with amount of hydrocarbon pore volume of CO₂ injected for different rock types. Highly stress sensitive reservoir model has less oil recovery as compared with other models. The main reason is the significant permeability change in the natural and induced fractures; hence, higher pressure drop in the producer zones, thereby causing reservoir pressure to stabilize in earlier time as compared to stiff rocks.

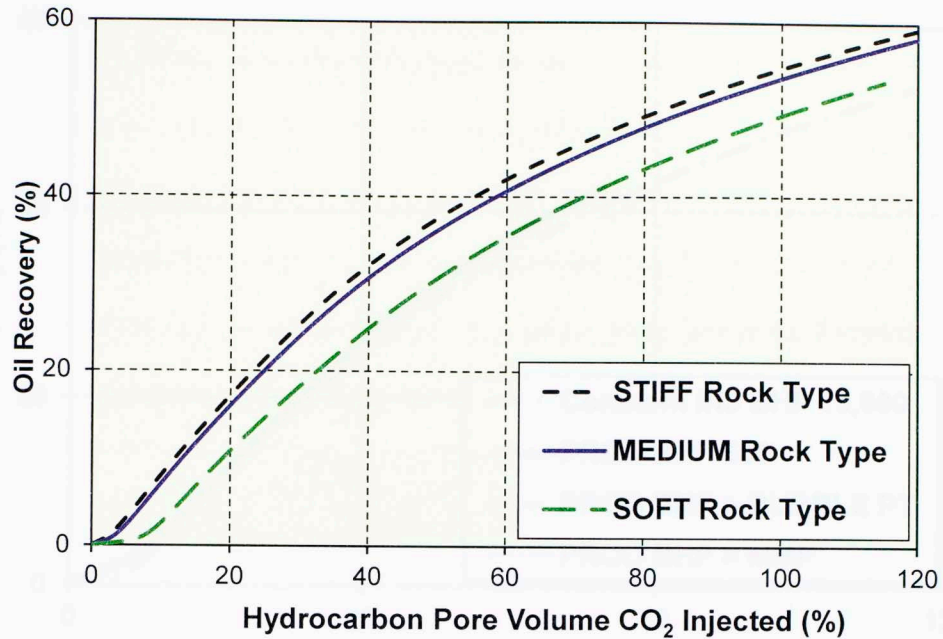


Figure 5.10: Effects on oil recovery and amount of CO₂ injected with different rock types

5.3 ANALYSIS OF PRODUCER BOTTOMHOLE PRESSURE

This section focuses on the effect of minimum bottomhole pressure constraint of the producer well. The injector well operates at a constant rate constraint of 17,000 ft³/day during the simulation time. Three cases with varying producer well constraint of minimum bottomhole pressure were simulated. Model 1 has a minimum producer bottomhole pressure of 500 psia. Model 2 is simulated with producer minimum bottomhole pressure above the bubble point pressure i.e. 3,000 psia is used above the bubble point pressure of 2,800 psia. Model 3 is simulated above the Minimum Miscibility Pressure. The producer well minimum bottomhole pressure was constrained at 4,500 psia above the MMP of 4,235 psia.

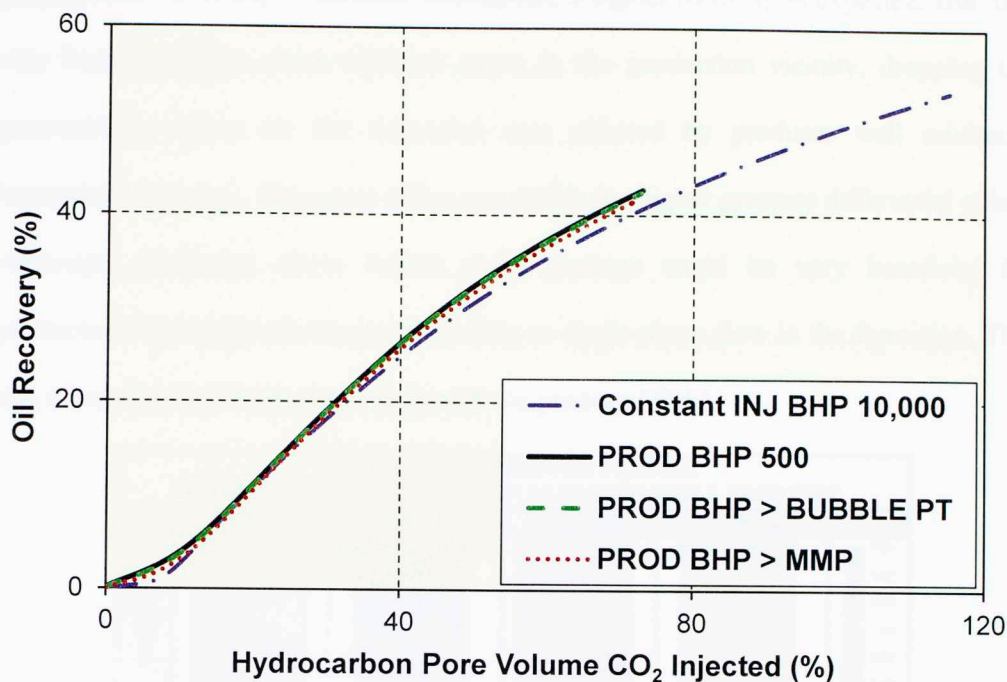


Figure 5.11: Simulation results of producer bottomhole pressure analysis

It can be observed in **Figure 5.11** that the higher amount of CO₂ was able to be injected with the injector well constraint of constant bottomhole pressure of 10,000 psia. This also led to a higher incremental oil recovery as compared to simulation models with injection rate constraint and changing producer bottomhole pressure. No change in oil recovery was observed with changing producer well constraint of minimum bottomhole pressure. This can be attributed to two important effects. First, the effect of producer bottomhole pressure is observed in a small extent of near wellbore vicinity. The pressure in the reservoir formation is mainly dominated by the injection pressure. This effect is elaborated in **Figure 5.12**, displaying the formation pressure with time progression for the three simulation models with different producer well constraint of minimum bottomhole pressure. The second is the effect of stress dependent

permeability. With higher pressure differential, a higher recovery is expected. But, this also leads to higher mean effective stress in the production vicinity, dropping the permeability values for the formation area affected by producer well minimum bottomhole pressure. This stress effect can nullify the higher pressure differential effect. Although, producing above bubble point pressure could be very beneficial for production from tight oil reservoirs, leading to single phase flow in the formation. This can mitigate early CO₂ breakthrough with the produced fluid.

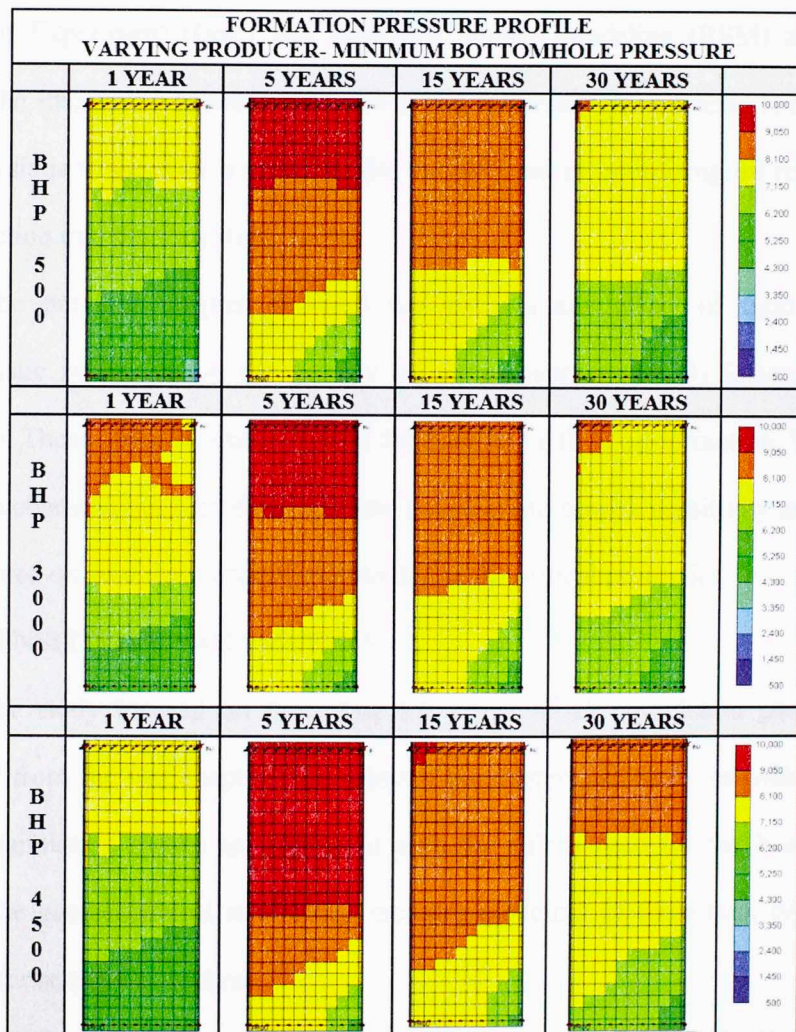


Figure 5.12: Reservoir pressure profile for producer bottomhole pressure analysis

CHAPTER 6: SENSITIVITY ANALYSIS

The chapter covers the study of sensitivity analysis carried out on critical parameters required to define completion practices that may help optimize field application of CO₂ injection in tight oil formations. The sensitivity analysis is implemented by two methods. First method analyzed each parameter individually and reproduced the results in terms of a tornado chart, defining the critical parameters. Second method analyzed the uncertain parameters simultaneously, implementing the Design of Experiment (DoE) and Response Surface Modeling (RSM) approach to counter the interaction between parameters and influential parameters. The motive of this analysis is to generate a proxy model that will aid in optimizing oil recovery and CO₂ injection into the formation.

The previous chapter provided the analysis and effect of tight formation characteristic properties on the amount of oil recovery and CO₂ injected into the formation. Those properties were crucial for modeling a tight oil formation. With all the formation characteristics implemented into the reservoir model, sensitivity analysis was implemented on completion parameters to define the critical properties.

6.1 SENSITIVITY PARAMETERS

The study focused on evaluating the effect of 11 completion parameters as identified from the last chapter. The selected parameters are analyzed within a range and the simulation results are compared with the values used for the base reservoir model. The geomechanical model that includes modeling of three rock types is also included for sensitivity analysis.

Table 6.1: Parameters for sensitivity analysis

	PARAMETER	SYMBOL	MINIMUM	BASE CASE	MAXIMUM
1	Geomechanics- Stress Dependent Permeability	Geo_Mech	Stiff Rock type	Medium Rock	Soft Rock type
2	Distance between Injector and producer well (Y plane), ft	Dist_Well	500	1,000	1,500
3	Distance between Injector and Producer fracture, (X plane), ft	Dist_Frac	200	400	800
4	K_v/K_h	K_v/K_h	0.01	0.1	1
5	Producer fracture Permeability, mD	Prod_Perm	10	70	150
6	Producer fracture half-length, ft	Prod_HL	200	400	600
7	Injector fracture Permeability, mD	Inj_Perm	70	230	400
8	Injector Fracture Half Length, ft	Inj_HL	200	400	600
9	Injection Bottomhole Pressure, psia	Inj_BHP	7,000	10,000	11,000
10	Production Bottomhole Pressure, psia	Prod_BHP	200	500	1,000

Adsorption effect with respect to changes in TOC wt% were analyzed in previous chapter. The adsorption effect is modeled in the base reservoir model with 5 wt% TOC. It was concluded that not much significant effect of adsorption on oil recovery and is not considered as a parameter for sensitivity analysis. The lateral

distance between the injector hydraulic fracture and the producer hydraulic fracture is also a parameter that will affect the well placement in field planning. The distance between wells (well spacing) is a critical parameter and is included for analysis.

Sensitivity analysis determines the effect of parameters on the objective function within the applicable range during the simulation. For this study, two objective functions are defined:

1. Oil Recovery
2. Hydrocarbon Pore Volume of CO₂ Injected

Therefore, sensitivity analysis is implemented for both the objective functions independently with the above stated 10 parameters. Two different workflows are used for sensitivity analysis. Method one analyzed One-Parameter-At-A-Time (OPAAT) and generated results are represented in terms of a tornado chart that defines the critical parameters. Method two analyzed the uncertain parameters simultaneously, implementing the Design of Experiment (DoE) and Response Surface Modeling (RSM) approach to counter the interaction between parameters and influential parameters.

For sensitivity analysis, CMG-CMOST Sensitivity Analysis engine is used to run numerous cases with several combinations within the parameter range. **Figure 6.1** provides the workflow adopted for this study for both the objective functions.

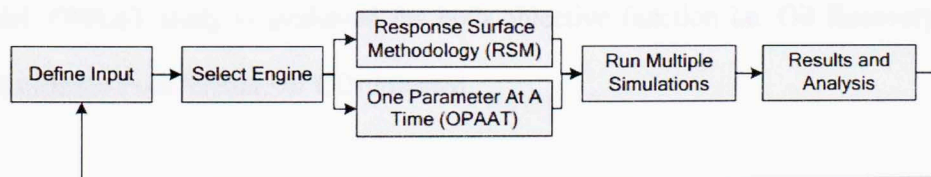


Figure 6.1: Study workflow for sensitivity analysis (CMG-CMOST 2013)

6.2 ONE-PARAMETER-AT-A-TIME (OPAAT) STUDY

The results provided the effect of each parameter on the objective functions, creating a Tornado chart. Tornado chart will rank the critical parameters based on their effect on the objective function in a decreasing order. The simulation results in **5.2.2**

EFFECT OF SIMULATED NATURAL FRACTURES show that the presence of natural fractures plays a critical role in the reservoir model and affects flow dynamics to a great extent. For these reasons, OPAAT study was implemented for two reservoir models:

1. Heterogeneous model containing natural fractures
2. Heterogeneous model without natural fractures

6.2.1 OPAAT WITH NATURAL FRACTURE MODEL

The base reservoir model described in **Table 6.1** consists of simulated natural fractures. OPAAT analysis was implemented on the reservoir model by running sensitivity analysis within the applicable range of each parameter one at a time and comparing their effect on the objective function and the simulated results of the base case. The simulation involved 23 runs to result in generation of the effect of 10 parameters. The tornado chart ranks the parameters in decreasing order of effectiveness and the base line represents the objective function calculated for the base case reservoir model. OPAAT study is evaluated for both objective function i.e. Oil Recovery and Hydrocarbon Pore Volume of CO₂ Injected.

Figure 6.2: Oil recovery -Tornado Chart (OPAAT with NF)

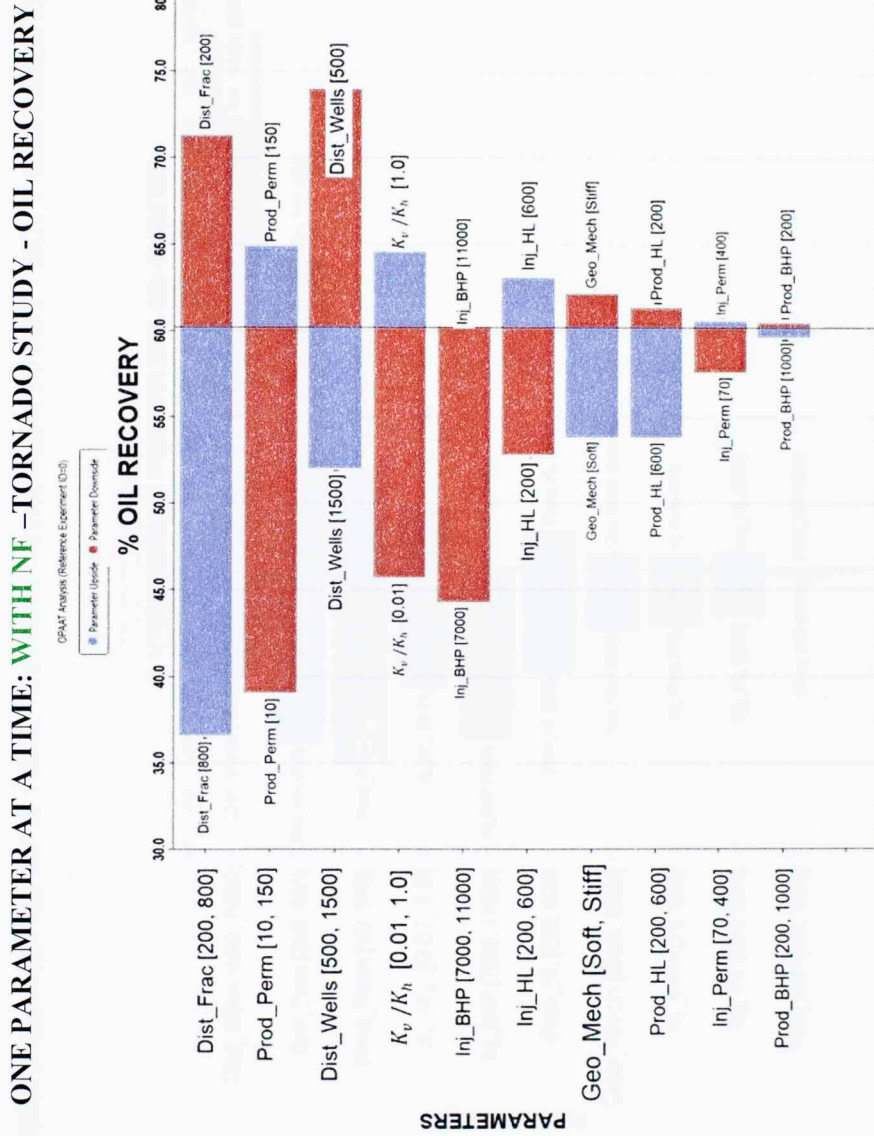


Figure 6.3: HCPV CO₂ Injected -Tornado Chart (OPAAT with NF)
ONE PARAMETER AT A TIME: WITH NF –TORNADO STUDY - HCPV CO₂ INJECTED

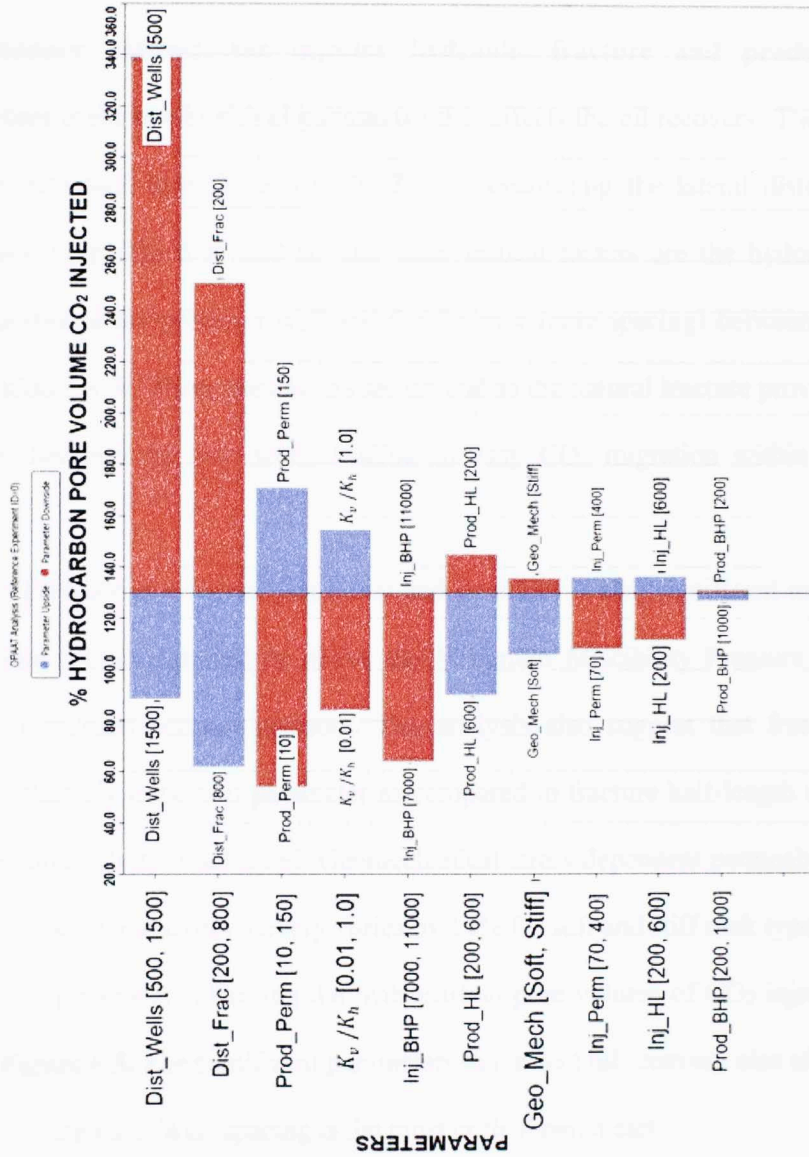


Figure 6.2 and **Figure 6.3** shows the Tornado Chart for Oil recovery and Hydrocarbon Pore Volume of CO₂ Injected respectively for the heterogeneous reservoir model containing simulated natural fractures. The oil recovery factor chart shows that the **lateral distance between the injector hydraulic fracture and producer hydraulic fracture** is the **most critical parameter** that affects the oil recovery. The oil recovery factor increased from 36.6% to 71.2% by decreasing the lateral distance between fractures from 800 ft to 200 ft. The other critical factors are the hydraulic fracture permeability of the producer well and the distance (acre spacing) between the injector and producer well. These parameters are critical as the natural fracture provides connective path between the two wells leading to easy CO₂ migration within the reservoir.

Injection pressure is a critical parameter and its effect is also significant on oil recovery. Injection pressure should be above the Minimum Miscibility Pressure and lower than the formation fracture pressure. The analysis also suggest that fracture permeability is relatively important parameter as compared to fracture half-length until infinite fracture conductivity is achieved. Geomechanical stress dependent permeability is also a critical parameter and oil recovery varies by 15% for soft and stiff rock type.

The critical parameters affecting the hydrocarbon pore volume of CO₂ injected is displayed in **Figure 6.3**. The significant parameters that affect oil recovery also affect the amount of CO₂ injected. Well spacing is the most critical parameter.

Tornado charts were also created for simulation time of 1 year instead of 30 years. It was found that in the early life of simultaneous injection and production, stress

dependent permeability and injection rate are the most critical parameters and their effect minimizes with time progression to 30 years.

For OPAAT analysis, 23 runs were carried out to produce the Tornado Chart. **Figure 6.4** shows the simulated results i.e. HCPV CO₂ Injected and Oil recovery for the 23 cases to produce the Tornado Chart.

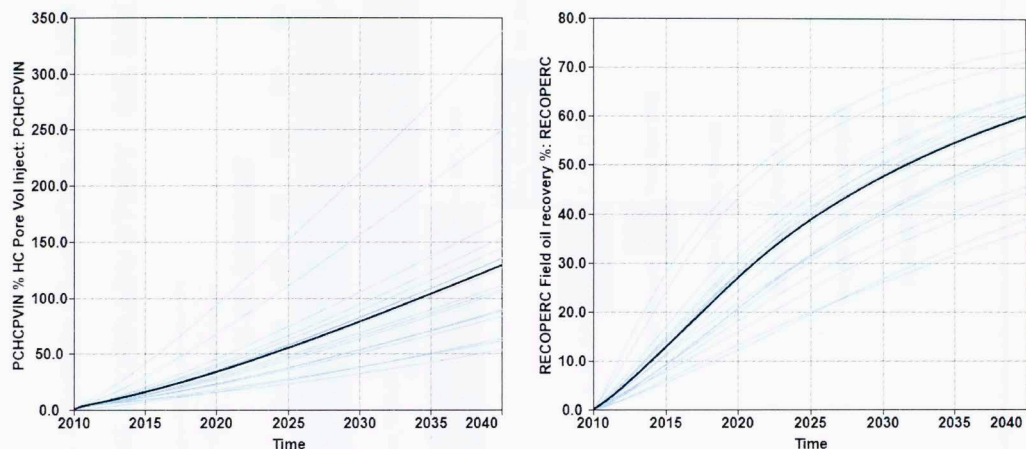


Figure 6.4: HCPV CO₂ Injected and Oil recovery for OPAAT with NF cases. The black line represents the base case results

6.2.2 NO NATURAL FRACTURE MODEL – OPAAT ANALYSIS

Second OPAAT analysis was carried out on a heterogeneous reservoir model without natural fractures. This hypothesis in the OPAAT analysis with natural fractures provides significant emphasis on parameters like producer fracture permeability and fracture half lengths for the injector and producer. These properties are more significant because the presence of natural fractures provide conducive pathway between the producer and injector wells and flow migration was maintained with pressure drop. So OPAAT analysis was repeated again for a reservoir model without natural fractures.

Figure 6.5: Oil recovery -Tornado Chart (OPAAT- No NF)
 ONE PARAMETER AT A TIME: **NO NF** -TORNADO STUDY - OIL RECOVERY

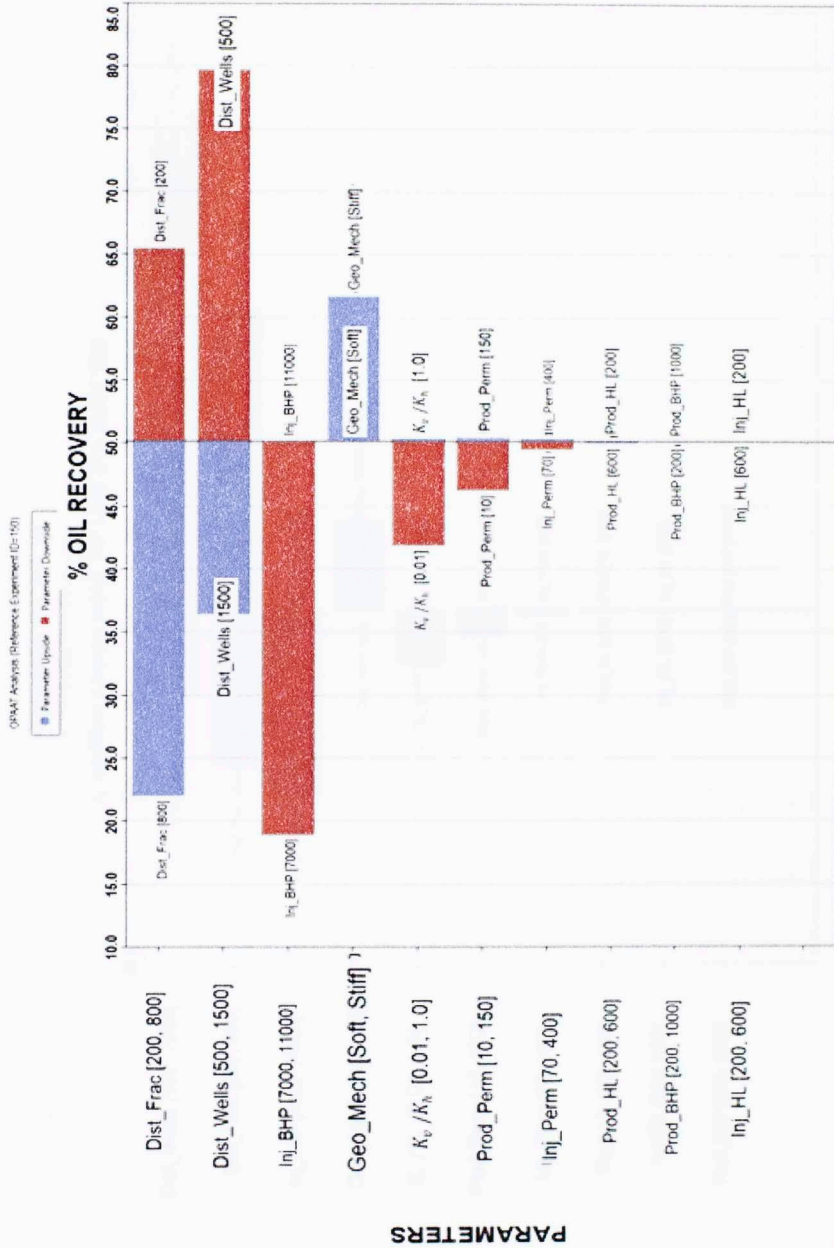


Figure 6.6: HCPV CO₂ Injected -Tornado Chart (OPAAT- No NF)
 ONE PARAMETER AT A TIME: **NO NF** –TORNADO STUDY - HCPV CO₂ INJECTED

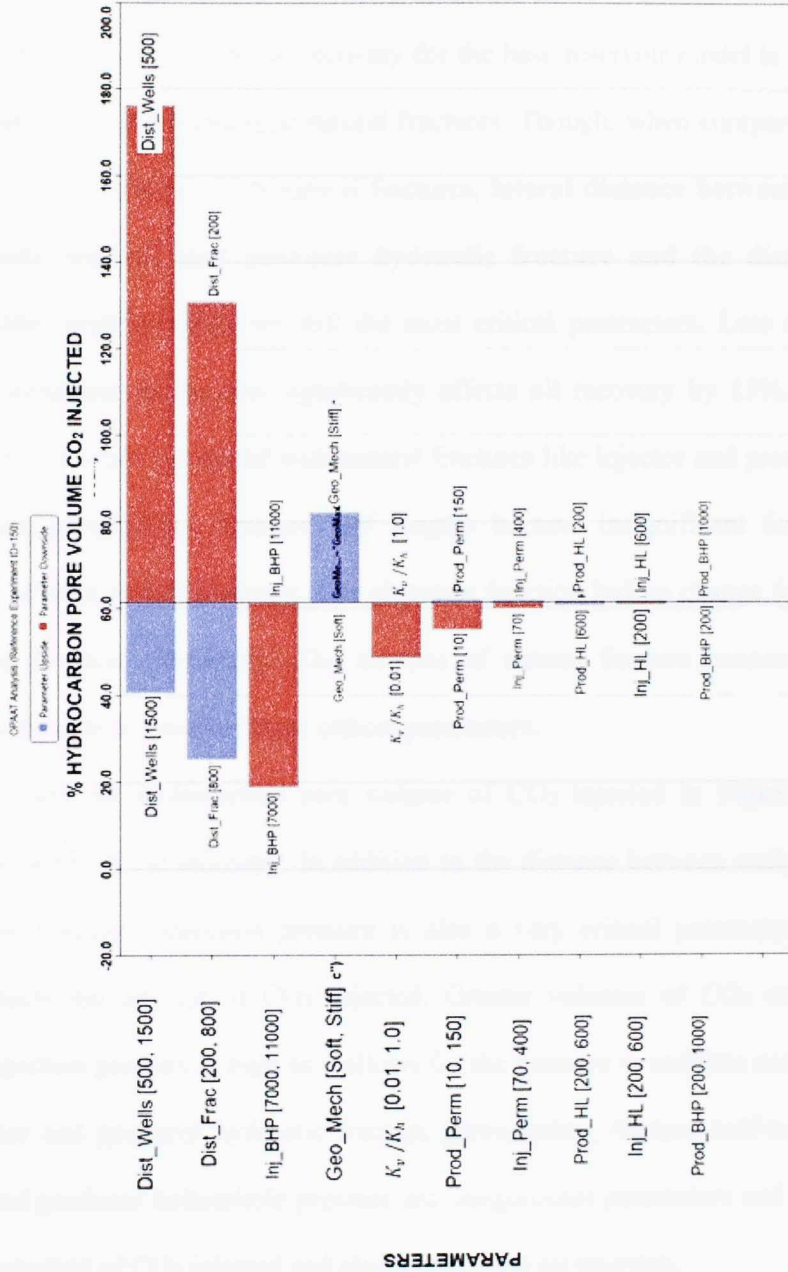


Figure 6.5 and **Figure 6.6** illustrate the Tornado chart for oil Recovery and hydrocarbon pore volume of CO₂ injected respectively for the heterogeneous reservoir model without natural fractures. The oil recovery for the base reservoir model is 15% less than the reservoir model containing natural fractures. Though, when compared to **Figure 6.2** i.e. OPAAT analysis with natural fractures, **lateral distance between the injector hydraulic fracture and producer hydraulic fracture and the distance between the wells (well spacing)** are still the most critical parameters. Less stress dependent geomechanical model also significantly affects oil recovery by 15%. The critical parameters for reservoir model with natural fractures like injector and producer hydraulic fracture permeability, fracture half lengths became insignificant for the reservoir model without natural fractures. The objective function had no change for the applicable range of these parameters. The absence of natural fracture connectivity strongly reduces the effectiveness of these critical parameters.

Tornado chart for hydrocarbon pore volume of CO₂ injected in **Figure 6.6** illustrate similar trends of oil recovery. In addition to the distance between wells and distance between fractures, injection pressure is also a very critical parameter and significantly affects the amount of CO₂ injected. Greater volumes of CO₂ can be injected if the injection pressure is high as it allows for the pressure to stabilize near the reservoir. Injector and producer hydraulic fracture permeability, fracture half-length, injection rate, and producer bottomhole pressure are insignificant parameters and have no effect on the amount of CO₂ injected and also incremental oil recovery.

For this OPAAT analysis, 23 simulation runs, as earlier, were carried out to produce the Tornado Chart as shown in **Figure 6.7**.

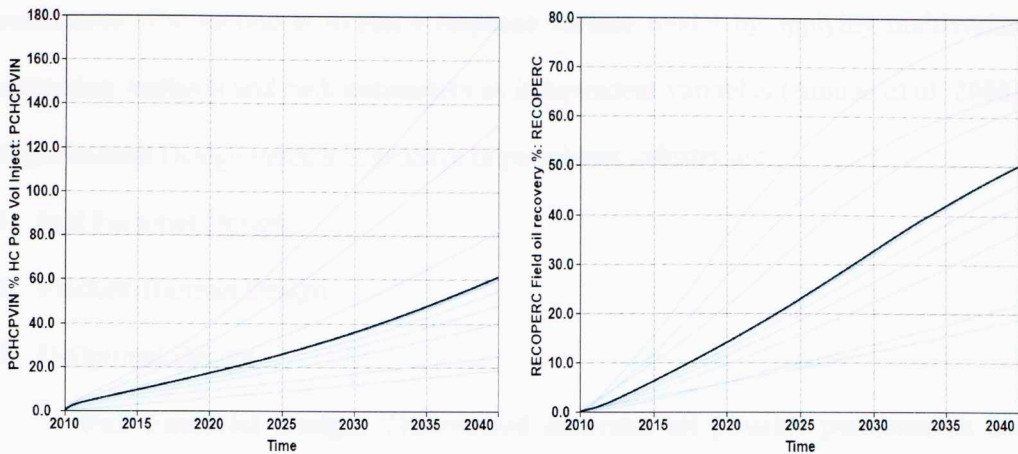


Figure 6.7: HCPV CO₂ injected and oil recovery for OPAAT without NF cases;

black line represents the results for the base case reservoir model.

6.3 RESPONSE SURFACE MODELING APPROACH

A response surface model is defined as a proxy model developed by multiple regression of all the uncertain parameters that affect the objective function. The term ‘response’ refers to the measurable variables and the model is an approximation to define the relationship between the parameters within a specified uncertainty domain to the response (objective function). The response surface is a proxy for the reservoir simulator that allows fast estimation of the response. In order to generate a response surface model, 11 parameters analyzed for the OPAAT analysis are taken into consideration. Multiple runs are generated by combination of several parameters. These combinations are based on the Design of Experiment (DoE) approach.

6.3.1 DESIGN OF EXPERIMENT (DOE)

Experimental Design is a technique developed to get maximum unbiased information regarding changes in a response model by altering the input parameters. It is carried out in two steps. The first is to identify and rank the key parameters and

constraints. The second is to run a response surface model by applying multivariate regression methods and rank parameters as independent variables (Amudo et al. 2008).

Experimental Design models in practice in petroleum industry are:

1. Full Factorial Design
2. Plackett-Burman Design
3. D-Optimal Design

Full Factorial Design: The method generates all possible permutations and combinations for the factors to be considered. The drawback is that the design generates unaccounted number of combinations for large number of parameters. For example, to vary N parameters at L values, the number of simulation runs will be L^N and this may become computationally difficult. Therefore, the other two methods are used to reduce the number of simulations; and hence, computational requirement.

Plackett-Burman Design: It is a widely used approach to attain maximum accuracy of the factors for dependent variables. For N parameters, the number of simulation runs will be P , where P a multiple of 4 and P is greater than N . The drawback of the method is that it is a two level design. It ignores interactions and quadratic effects of the parameters on the response surface. It is used in the early phase of modeling when uncertainties of all the affecting parameters are unknown. This model is used to study the effect of main factors and in situations where the two-way interactions can be ignored. A mathematical model can be developed to model how the changes in a variable can affect the process. With the benefit of changing any variable in the process, proxy models can be further optimized to attain higher productivity.

D-Optimal Design: It is a 3-level experimental model, so it considers interactions and quadratic effects in the response surface. The model screens the less effective variables, combines the important parameters and selects the best outcome (Okenyi and Omeke 2012). D-optimal design minimizes the overall variance of the regression coefficients by maximizing the determinant of $|XX'|$. The number of simulation runs is higher when using this type of model and increases multiple folds with increasing number of factors. For N number of factors, the total runs are:

$$\text{Number of Runs} = (N + 1) * (N + 2)/2 \quad \dots\dots\dots (6.1)$$

This model is usually applied after Plackett-Burman model so that main factors are considered and then this model is applied for better results. D-optimal model allows factors to have multiple levels. D-Optimal design is a rigorous design based on quadratic regression. It includes square terms and linear terms.

6.3.2 RSM WORKFLOW

CMG-CMOST sensitivity analysis engine module is again used for the Response Surface Modeling (RSM) as well. CMOST offers a workflow for RSM with some tune ups. CMOST provides the ability to select OPAAT or RSM sensitivity analysis approach. The general procedure is to apply OPAAT model, define the critical parameters. These critical parameters are then analyzed through RSM approach. For this study, 11 parameters are used for both models to get a wider perspective of generating a proxy model. This allows to observe the effect of each parameter, their interaction with other parameters and the ranking in which they affect the objective functions i.e. Oil Recovery and HCPV of CO₂ injected.

CMOST-RSM has the ability to polynomial fit the simulation results by three methods:

1. Linear Regression

$$y = a_0 + a_1x_1 + a_2x_2 + \dots + a_kx_k \dots\dots\dots (6.2)$$

2. Linear + Quadratic Regression

$$y = a_0 + \sum_{j=1}^k a_j x_j + \sum_{j=1}^k a_{jj} x_j^2 \dots\dots\dots (6.3)$$

3. Linear + Quadratic + Interaction Terms Regression

$$y = a_0 + \sum_{j=1}^k a_j x_j + \sum_{j=1}^k a_{jj} x_j^2 + \sum_{i<j} \sum_{j=2}^k a_{ij} x_i x_j \dots\dots\dots (6.4)$$

Where, y = objective function

a_0 = intercept

$a_1, a_2 \dots a_k$ = coefficient of linear terms

a_{jj} = coefficient of quadratic terms

a_{ij} = coefficient of parameter interaction terms

x = input parameters

For this study, **D-optimal Design** methodology is used to define the uncertainty between the parameters and to generate the number of simulation runs. This design will not only identify the key parameters, but will also consider the interaction effect and quadratic effect of parameters (Devegowda and Gao 2007). The RSM polynomial fit of higher order i.e. **Linear + Quadratic + Interaction parameters** terms is used to generate a proxy model to validate the simulation results.

The workflow for Response Surface Model is:

1. Define the objective function i.e. oil Recovery and HCPV of CO₂ injected
2. Evaluate uncertainty factors and its distribution affecting the objective function.

3. Analyze the parameters (heavy hitter) that will highly influence the response of the optimizing parameter (OPAAT analysis).
4. Use Design of Experiments (D-Optimal Design) to generate simulation cases
5. Run CMOST-RSM model for all simulation cases.
6. Generate proxy model for each objective function

Before running RSM engine, desired accuracy in the proxy model needs to be specified in CMOST. Based on this, the engine will create the number of experiments required and try to achieve the minimum accuracy defined. **Figure 6.8** illustrates the input for defining accuracy for the proxy model in CMOST.

▲ Response Surface Methodology	
Interested Terms	Linear + Quadratic + Interaction
Acceptable R-Square	0.85
Acceptable R-Square Adjusted	0.8
Acceptable R-Square Prediction	0.7
Acceptable Relative Error of Proxy Verifications (%)	10
Percentage Limit of Extra Experiments for Improving Proxy (%)	25

Figure 6.8: Snapshot of RSM Model accuracy input parameters

For this study, it was desired to achieve a proxy model considering the effect of interaction parameters. The minimum accuracy requirements are defined in similar way. An acceptable R-Square of 0.85 is defined in the engine. The aim of CMOST is to create experiments to achieve this minimum requirement. Once, the initial accuracy is achieved, more experiments are generated to achieve a higher R-square value. The engine STOP function depends on these two critical parameters: generating a proxy model as defined and achieving the minimum accuracy required.

RSM approach will first try to fit a linear relationship between the objective function and each critical parameter. If a parameter has a non-linear relationship with

the objective functions, a quadratic term (x^2) will define the relation. If modifying 2 parameters at the same time has a stronger effect than the sum of their individual linear or quadratic effects, a cross term (xy) will define the relationship with the objective function.

6.3.3 RSM PROXY MODEL VALIDATION

It is very critical to validate the proxy model generated using the response surface approach. The proxy model will be used instead of running simulation, so it is necessary to first validate the results of proxy model with actual simulation results. Proxy models are verified by:

1. Response Surface Verification Plot
2. Summary of Fit Table

Response Surface Verification Plot is a cross plot showing the relation between the predicted response from proxy model and the simulated response for each experimental run. The plot has a unit slope unit line. The variance of the data points when the unit slope line is considered as a reference shows the error/residual for that particular experiment and the points that fall on the unit slope data are exact match i.e. predicted response matches exactly with the simulated response (CMG-CMOST 2013).

Figure 6.9 provides an illustration of a response surface verification plot for predicted and simulated oil recovery. The dark blue line is the unit slope line. Significant number of points lie on the unit slope line indicating a good proxy model.

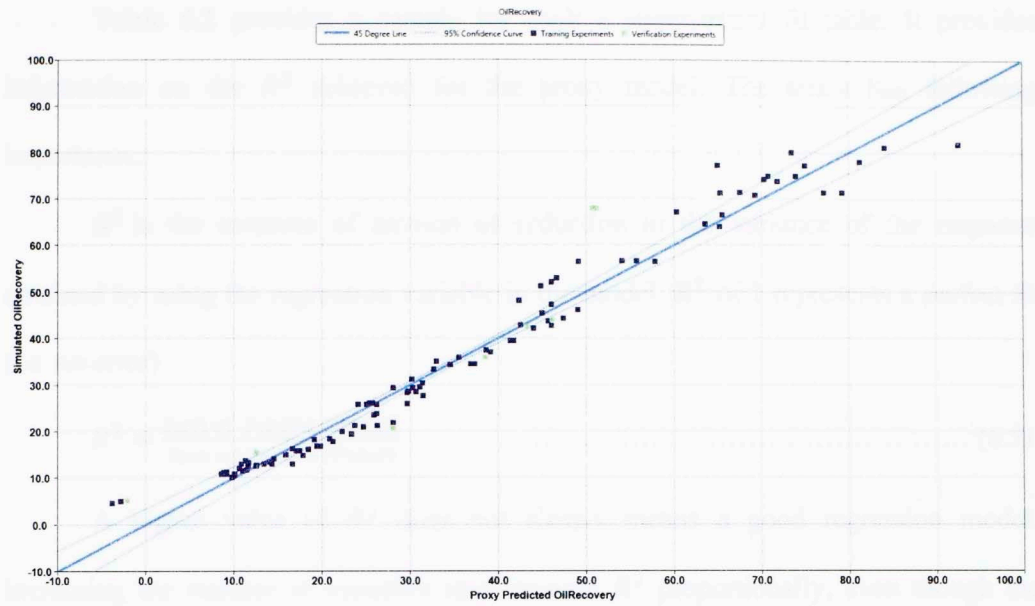


Figure 6.9: Sample response surface verification plot

Summary of Fit Table consists of several R^2 calculations indicating the accuracy of the generated proxy model. Initially, minimum accuracy required for the polynomial fit is defined before running RSM engine.

Table 6.2: Sample summary of fit table

SUMMARY OF FIT	
R^2	0.9756
R^2 - Adjusted	0.9701
R^2 - Predicted	0.9614
Mean of Response	34.7909
Standard Error	3.8612

Table 6.2 provides a sample for such a summarized fit table. It provides information on the R^2 achieved for the proxy model. The terms has following importance.

R^2 is the measure of amount of reduction in the variance of the response obtained by using the regression variable in the model. R^2 of 1 represents a perfect fit (i.e. no error)

$$R^2 = \frac{\text{Sum of Square (Model)}}{\text{Sum of Square (Total)}} \dots\dots\dots (6.5)$$

A higher value of R^2 does not always means a good regression model. Increasing the number of variables also increase R^2 proportionally, even though the added variable may not be statistically significant. Further verification of R^2 value is required.

R^2 - Adjusted, is the manipulated R^2 to make it comparable over models with different numbers of regression variables by using the degrees of freedom in its computation. When **R^2 - Adjusted** and R^2 values are significantly different, it indicates that the model has non-significant terms in the proxy equation.

$$R^2_{\text{Adjusted}} = 1 - \frac{n-1}{n-p} (1 - R^2) \dots\dots\dots (6.6)$$

Mean of Response is the averaged out value for all the response results. It is important as a base model for prediction because all other models are compared to it.

Standard Error estimates the standard deviation of the random error.

For this study, response surface modeling approach was implemented for two objective functions: Oil Recovery and HCPV of CO₂ Injected respectively. It must be noted that RSM approach only considers completion parameters to generate a proxy model. It means that only those parameters which are relative to operations are

considered for this study. Formation properties are not evaluated in this study as these properties cannot be changed and each reservoir has its characteristic set of defined formation and petrophysical properties. Therefore, the importance and usefulness of proxy model is only after a reservoir model is built for the particular formation and then for operations. There is a need to carry out sensitivity analysis to have confidence on predicted recoveries from a formation. Stress dependent permeability and adsorption properties defined for the base model are kept constant and not considered for proxy model approach. **Table 6.3** provides the variable range between maximum and minimum value for the uncertainty parameters used for generating a proxy model.

Table 6.3: Uncertainty parameters for RSM approach

	SYMBOL	MINIMUM	BASE CASE	MAXIMUM
1	Dist_Well	500	1,000	1,500
2	Dist_Frac	200	400	800
3	K_v/K_h	0.01	0.1	1
4	Prod_Perm	10	70	150
5	Prod_HL	200	400	600
6	Inj_Perm	70	230	400
7	Inj_HL	200	400	600
8	Inj_BHP	7,000	10,000	11,000
9	Prod_BHP	200	500	1,000

6.3.4 OIL RECOVERY – RSM

The objective function was defined as Oil recovery for thirty years of simultaneous injection and production. Ten uncertainty parameters, defined in **Table 6.3** are considered in the CMOST-RSM engine.

The input is defined to produce a proxy model which considers interaction and quadratic terms. The Reduced Quadratic Model is utilized to create a tornado chart to indicate the significance of each uncertainty and also improve the proxy model. The polynomial fit consists of linear terms, quadratic terms and parameter interaction terms. Each term has its own statistical significance affecting the objective function. The reduced quadratic model initially generates a proxy model consisting of all quadratic terms and interaction terms. The model then removes the statistically insignificant terms from the proxy equation. This will significantly improve the model by maximizing the $R^2_{Adjusted}$ term.

The number of simulation runs required can be calculated from **Equation 6.1**:

$$\text{Number of Runs} = (N + 1) * (N + 2)/2 \quad \dots\dots\dots (6.1)$$

From **Equation 6.1**, 66 simulation runs are required. The engine generated 212 simulation runs based on the number of parameters and the minimum accuracy ($R^2 = 0.85$) defined in CMOST. Out of 212 runs, 108 runs terminated successfully with convergence. The remaining runs were unable to converge the geomechanical stability. This means that the results for oil recovery and HCPV of CO₂ injected are based on the response of 108 experimental runs. The number of runs is strong enough to generate a proxy model depending on 10 uncertainties. **Figure 6.10** summarizes the effect estimate of uncertainty parameters on oil recovery generated by RSM engine.

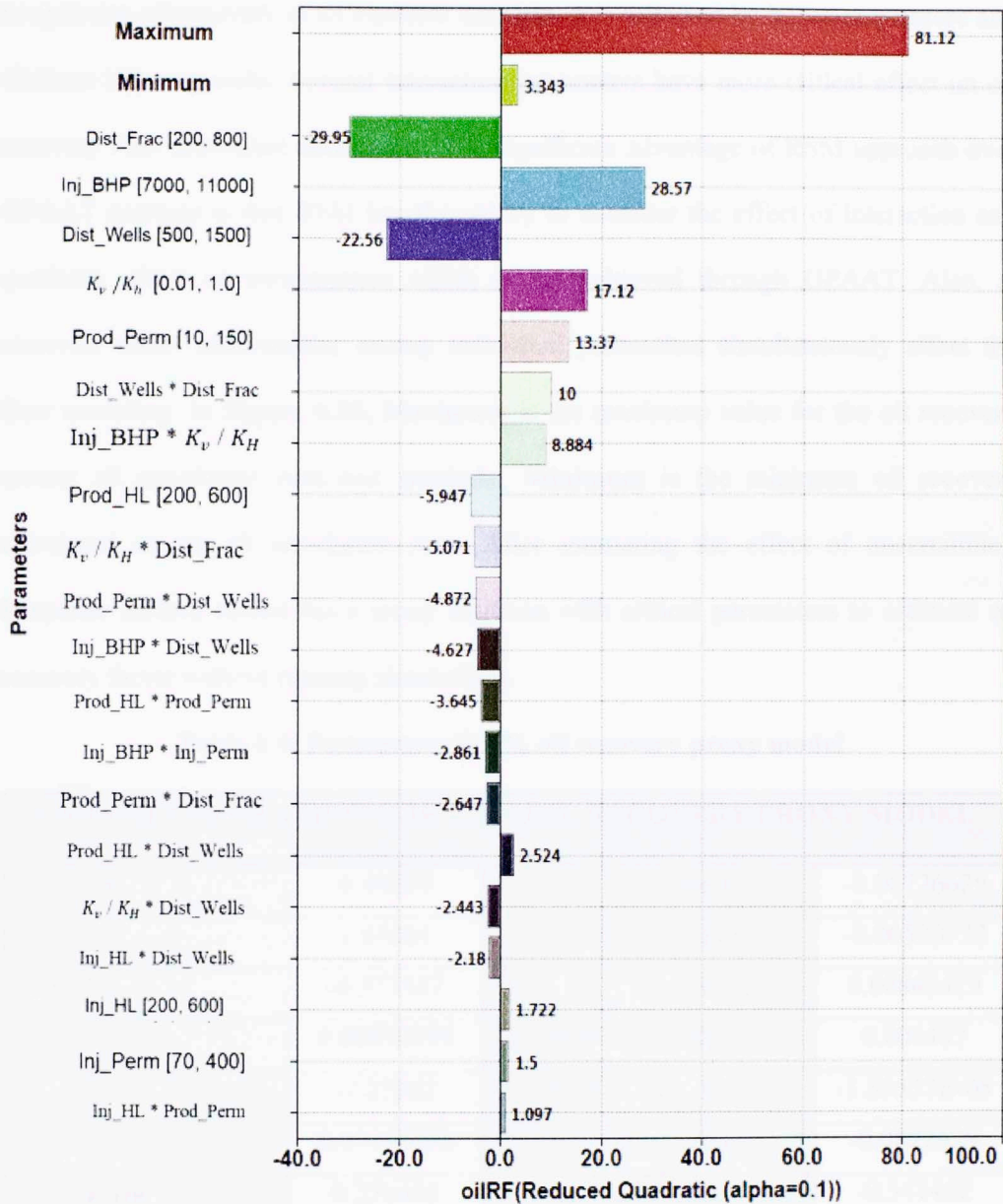


Figure 6.10: Effect estimate of uncertainty parameters on oil recovery (%)

It can be observed that RSM approach also follows the similar trend observed in OPAAT analysis. With huge number of simulation runs, RSM approach defined lateral distance between injector and producer hydraulic fracture as the most critical parameter

to optimize oil recovery in a CO₂-EOR scenario. It is followed by injection pressure and distance between wells. Several interaction parameters have more critical effect on oil recovery than individual uncertainty. The significant advantage of RSM approach over OPAAT analysis is that RSM has the ability to consider the effect of interaction and quadratic effect of uncertainties which is not achieved through OPAAT. Also, at reservoir scale, uncertainties among individual parameters simultaneously affect the flow modeling. In **Figure 6.10, Maximum** is the maximum value for the oil recovery among all simulation runs and similarly, **Minimum** is the minimum oil recovery calculated among all simulation runs. After estimating the effect of uncertainties, Response surface model fits a proxy equation with critical parameters to estimate oil recovery factor without running simulations.

Table 6.4: Parameters for % oil recovery proxy model

PARAMETERS & COEFFICIENTS – OIL RECOVERY PROXY MODEL			
Intercept	6.49569	Inj_HL * Dist_Wells	-0.00726629
Inj_HL	1.67601	Prod_HL * Prod_Perm	-0.00520772
Prod_HL	-0.573547	Prod_HL * Dist_Wells	0.00841419
Inj_BHP	0.00812039	Inj_BHP * K_v / K_H	0.004487
K_v / K_H	-7.27162	Inj_BHP * Dist_Wells	-3.85557E-05
Inj_Perm	0.00454593	K_v / K_H * Dist_Wells	-0.0822629
Prod_Perm	0.256618	K_v / K_H * Dist_Frac	-0.341462
Dist_Wells	-0.460401	Prod_Perm * Dist_Wells	-0.00116003
Dist_Frac	-1.00127	Prod_Perm * Dist_Frac	-0.00126049
Inj_HL * Inj_BHP	-0.000143063	Dist_Wells * Dist_Frac	0.0111152
Inj_HL * Prod_Perm	0.00156644		

Table 6.4 defines the critical parameters analyzed by RSM engine and their coefficients to generate a proxy equation. The end result of RSM approach was to generate a proxy equation as a function of uncertainty parameters. The generated proxy equation is modeled with 20 uncertain terms defines as:

$$\begin{aligned}
 \% \text{ OIL RECOVERY} = & 6.49569 + (1.67601 * \text{Inj_HL}) - (0.573547 * \\
 & \text{Prod_HL}) + (0.00812039 * \text{Inj_BHP}) - (7.27162 * K_v / K_H) - (0.00454593 * \\
 & \text{Inj_Perm}) + (0.256618 * \text{Prod_Perm}) - (0.460401 * \text{Dist_Wells}) - (1.00127 * \\
 & \text{Dist_Frac}) - (0.000143063 * \text{Inj_HL} * \text{Inj_BHP}) + (0.00156644 * \text{Inj_HL} * \\
 & \text{Prod_Perm}) - (0.00726629 * \text{Inj_HL} * \text{Dist_Wells}) - (0.00520772 * \\
 & \text{Prod_HL} * \text{Prod_Perm}) + (0.00841419 * \text{Prod_HL} * \text{Dist_Wells}) + (0.004487 * \\
 & \text{Inj_BHP} * K_v / K_H) - (3.85557E - 05 * \text{Inj_BHP} * \text{Dist_Wells}) - (0.0822629 * \\
 & K_v / K_H * \text{Dist_Wells}) - (0.341462 * K_v / K_H * \text{Dist_Frac}) - (0.00116003 * \\
 & \text{Prod_Perm} * \text{Dist_Wells}) - (0.00126049 * \text{Prod_Perm} * \text{Dist_Frac}) + \\
 & 0.0111152 * \text{Dist_Wells} * \text{Dist_Frac}) \\
 & \dots\dots\dots (6.7)
 \end{aligned}$$

It is very critical to validate the proxy model generated by the response surface model approach. Statistical analysis of the proxy equation is elaborated in **APPENDIX D**.

Table 6.5: Validation 1: Oil recovery proxy model

SUMMARY OF FIT - OIL PROXY MODEL	
R^2	0.983
R^2 - Adjusted	0.978
R^2 - Predicted	0.964
Mean of Response	25.15
Standard Error	2.879

Table 6.5 is the summary of fit table for proxy model generated for oil recovery. The proxy model had $R^2 = 0.98$ which defines a very good fit. Also, difference between R^2 and $R^2_{adjusted}$ is also very minimal, indicating that no insignificant parameter is used to generate the proxy model and all parameters in the **Equation 6.7** are statistically significant.

Second validation was the response surface verification plot with a unit slope line. **Figure 6.11** shows the verification plot for oil recovery proxy model. The plot relates simulated oil recovery with proxy predicted oil recovery. Many simulation runs fall on the 45° line indicating a good match for the proxy model. The green dots in the plot were verification runs given by RSM engine to validate the proxy equation generated using this study. 4 out of 5 verification runs by proxy model predicted exact simulated oil recovery.

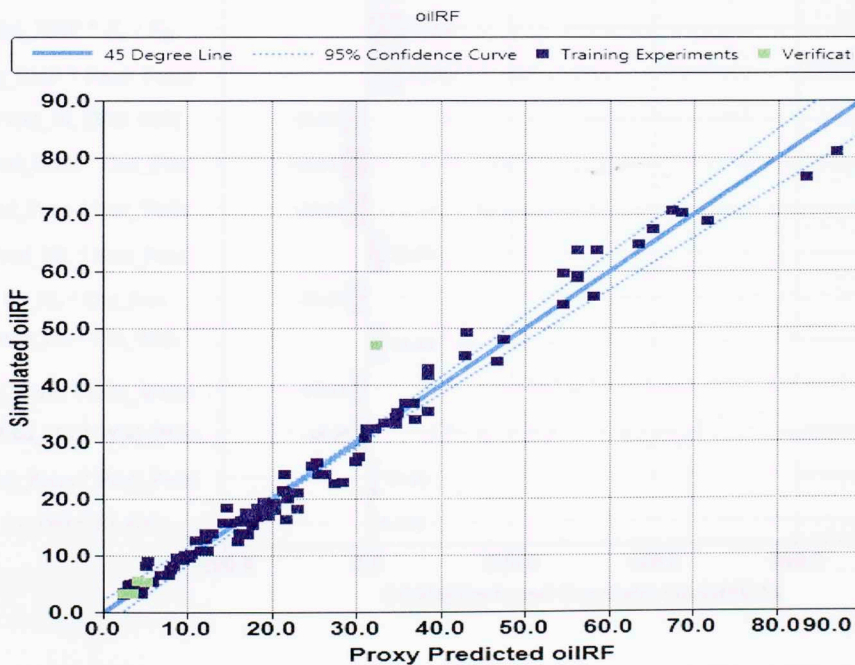


Figure 6.11: Validation 2: Oil recovery proxy model verification plot

6.3.5 HCPV CO₂ INJECTED – RSM

The RSM engine run for this study has two objective functions i.e. Oil recovery and HCPV CO₂ injected in the formation. RSM engine individually modeled each objective function and provided the proxy model.

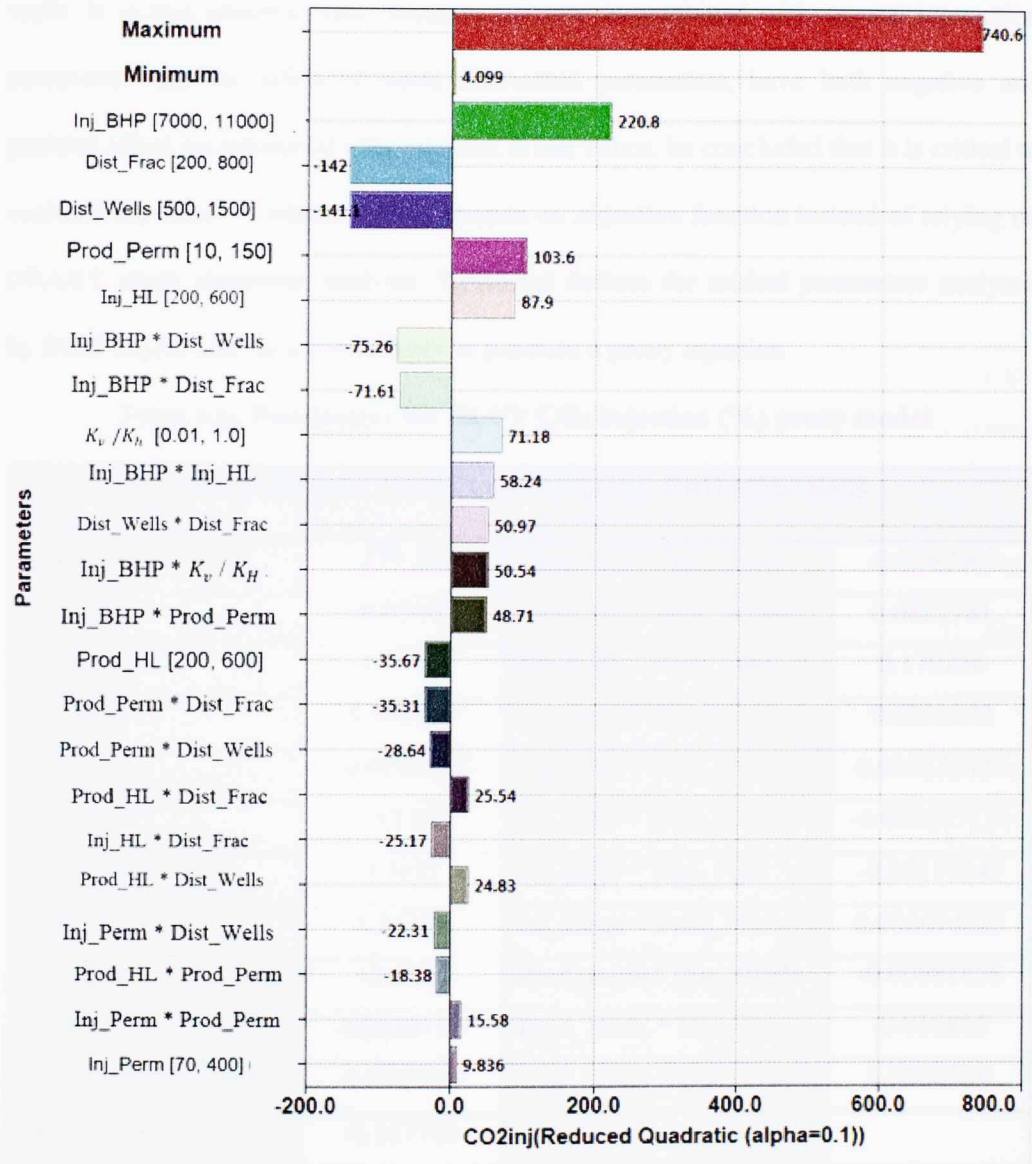


Figure 6.12: Effect estimate of uncertainty parameters on HCPV of CO₂ injected

Figure 6.12 illustrates the effect estimation of uncertainty parameters on Hydrocarbon Pore Volume of CO₂ injected. With 108 simulation runs, RSM model estimated injection pressure as the most critical parameter for both HCPV CO₂ injected and oil recovery. It is followed by distance between fractures and distance between wells. It is also observed that injection pressure is combined with several interaction parameters and the effect of these interaction parameters, have both negative and positive effect on amount of CO₂ injected. It can hence, be concluded that it is critical to evaluate the effect of interaction parameters on objective function instead of relying on OPAAT single parameter analysis. **Table 6.6** defines the critical parameters analyzed by RSM engine and their coefficients to generate a proxy equation.

Table 6.6: Parameters for HCPV CO₂ Injection (%) proxy model

COEFFICIENTS IN TERMS OF ACTUAL PARAMETERS			
Intercept	-279.502	Prod_HL * Prod_Perm	-0.0262607
Inj_HL	-8.05005	Prod_HL * Dist_Wells	0.0827781
Prod_HL	-11.3156	Prod_HL * Dist_Frac	0.170256
Inj_BHP	0.070509	Inj_BHP * K_v / K_H	0.0255272
Inj_Perm	-0.0241408	Inj_BHP * Prod_Perm	0.000173949
K_v / K_H	-157.847	Inj_BHP * Dist_Wells	-0.000627134
Prod_Perm	0.3192	Inj_BHP * Dist_Frac	-0.00119349
Dist_Wells	1.34283	Inj_Perm * Prod_Perm	0.000674325
Dist_Frac	3.84585	Prod_Perm * Dist_Wells	-0.00681858
Inj_HL * Inj_BHP	0.0029119	Prod_Perm * Dist_Frac	-0.016815
Inj_HL * Dist_Wells	-0.0743607	Dist_Wells * Dist_Frac	0.0566389
Inj_HL * Dist_Frac	-0.167783		

The proxy equation generated for HCPV of CO₂ injected by the RSM engine:

$$\begin{aligned}
 \text{HYDROCARBON PORE VOLUME CO}_2 \text{ INJECTED} = & -279.502 - \\
 & (8.05005 * \text{Inj_HL}) - (11.3156 * \text{Prod_HL}) + (0.070509 * \text{Inj_BHP}) - \\
 & (157.847 * K_v / K_H) + (0.3192 * \text{Prod_Perm}) + (1.34283 * \text{Dist_Wells}) + \\
 & (3.84585 * \text{Dist_Frac}) + (0.0029119 * \text{Inj_HL} * \text{Inj_BHP}) - (0.0743607 * \\
 & \text{Inj_HL} * \text{Dist_Wells}) - (0.167783 * \text{Inj_HL} * \text{Dist_Frac}) - (0.0262607 * \\
 & \text{Prod_HL} * \text{Prod_Perm}) + (0.0827781 * \text{Prod_HL} * \text{Dist_Wells}) + (0.170256 * \\
 & \text{Prod_HL} * \text{Dist_Frac}) + (0.0255272 * \text{Inj_BHP} * K_v / K_H) + (0.000173949 * \\
 & \text{Inj_BHP} * \text{Prod_Perm}) - (0.000627134 * \text{Inj_BHP} * \text{Dist_Wells}) - \\
 & (0.00119349 * \text{Inj_BHP} * \text{Dist_Frac}) - (0.00681858 * \text{Prod_Perm} * \\
 & \text{Dist_Wells}) - (0.016815 * \text{Prod_Perm} * \text{Dist_Frac}) + (0.0566389 * \\
 & \text{Dist_Wells} * \text{Dist_Frac}) \dots\dots\dots (6.8)
 \end{aligned}$$

Even though a single RSM engine was run for both the objective functions, it is critical to validate the proxy model for each objective function. **Table 6.7** is the summary of fit table for the proxy model generated for HCPV of CO₂ Injected. The proxy model had $R^2 = 0.95$ which defines a very good fit but not better than the oil recovery fit. Also, difference between R^2 and $R^2_{adjusted}$ is also very minimal, indicating that no insignificant parameter is used to generate the proxy model and all parameters in the **Equation 6.8** are statistically significant. Statistical analysis of the proxy equation is elaborated in **APPENDIX D**.

Table 6.7: Validation 1: HCPV CO₂ Injection proxy model

SUMMARY OF FIT- HCPV CO ₂ INJECTION	
R^2	0.9445
R^2 - Adjusted	0.9269
R^2 - Predicted	0.8993
Mean of Response	146.42
Standard Error	43.69

Second validation is the response surface verification plot with a unit slope line.

Figure 6.13 illustrates the verification plot for HCPV of CO₂ injected proxy model.

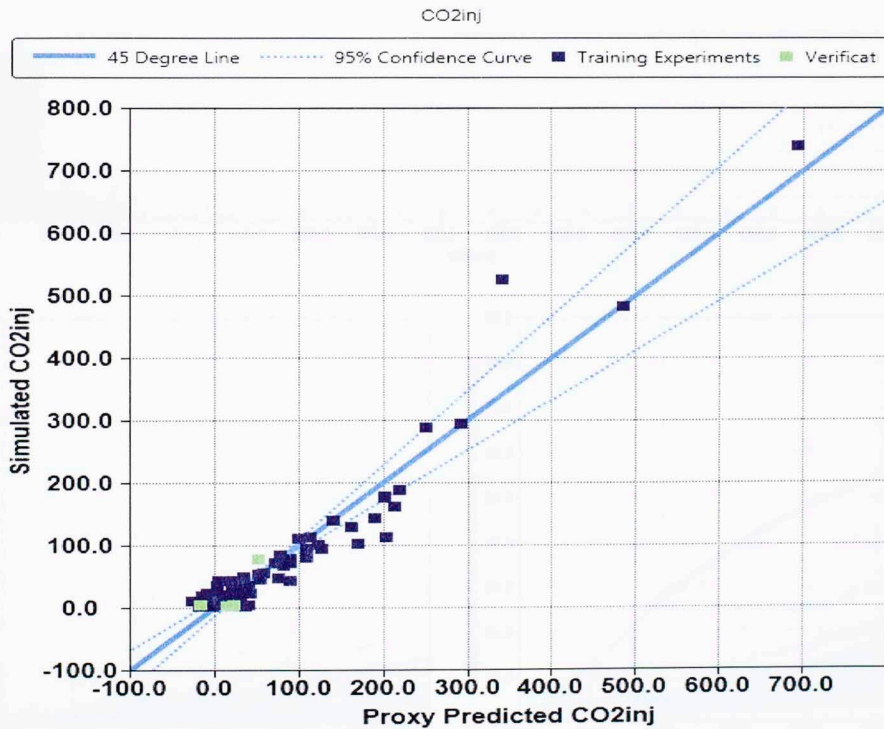


Figure 6.13: Validation 2: HCPV CO₂ injection proxy model verification plot

From the response surface model approach, a wider perspective of the simulation results could be analyzed and the range of objective function with dependence on uncertainty could be easily predicted. **Figure 6.14** illustrates the histogram of the simulated oil recovery factor and HCPV of CO₂ injected for all experimental runs in RSM analysis. Major count of oil recovery is for less than 20% and major count of HCPV of CO₂ injected is for less than 50 % volume of CO₂ injected.

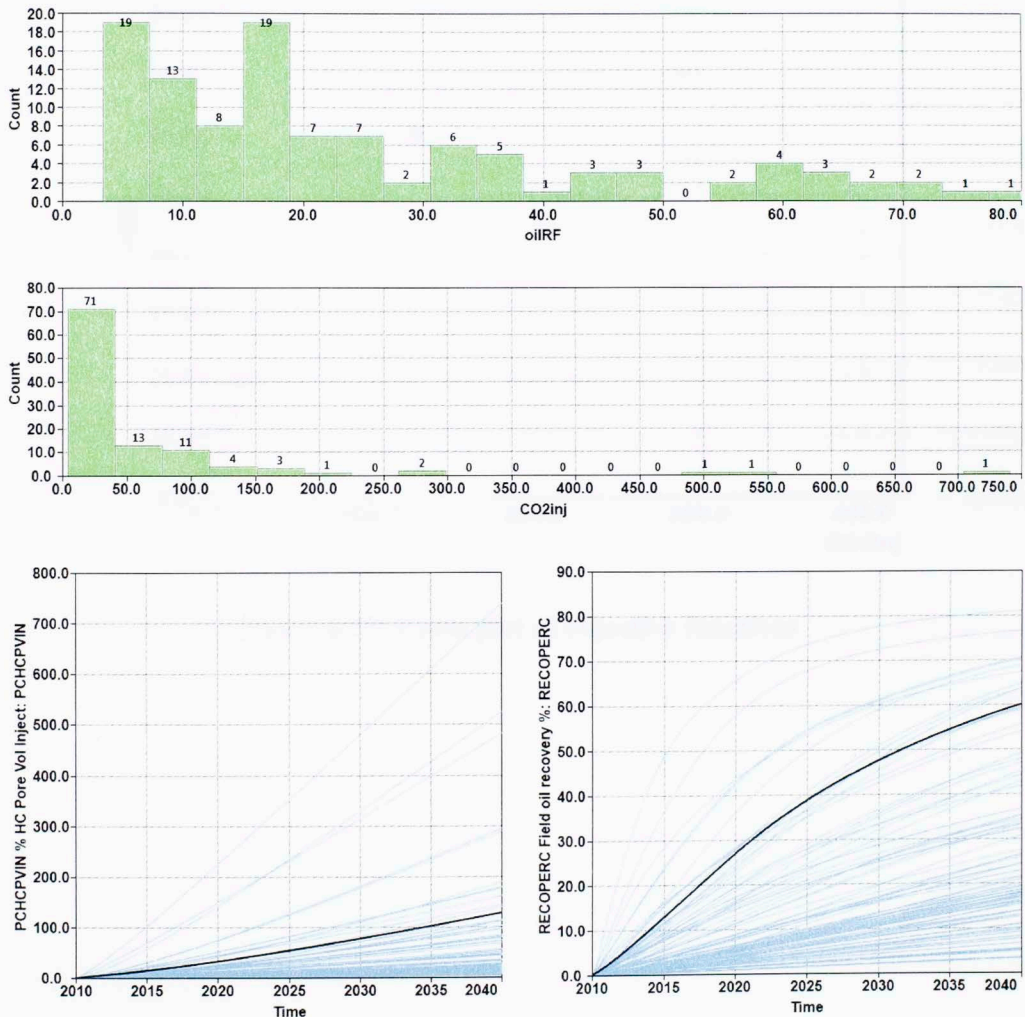


Figure 6.14: Histogram and simulation results of RSM engine

For final analysis, a cross plot was generated from all experimental runs as shown in **Figure 6.15**. The plot defines CO₂ utilization factor for improving oil recovery. In general CO₂ utilization factor of **3:1** can be observed from this cross plot. It signifies that for every **3%** hydrocarbon pore volume of CO₂ injected into the Middle Bakken formation can lead to an incremental oil recovery of **1%**.

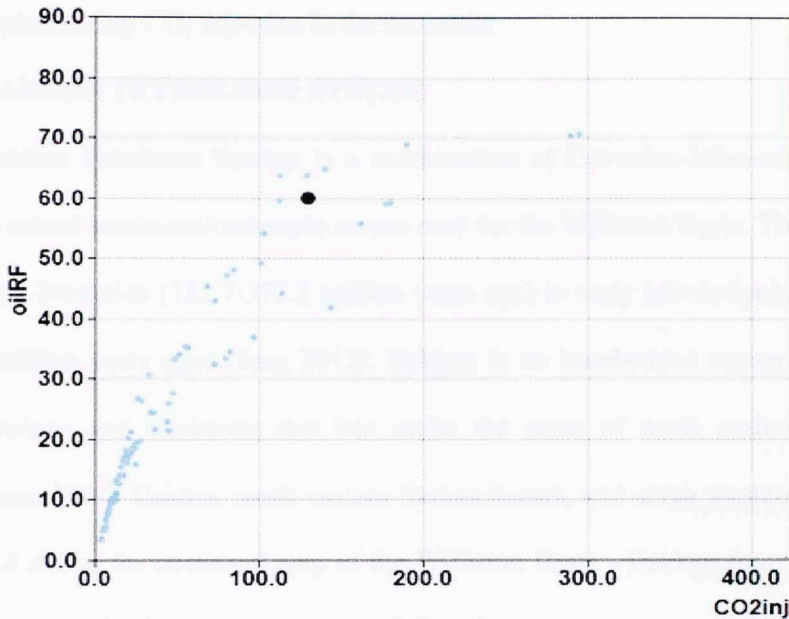


Figure 6.15: Cross plot of objective functions

Chapter 7: CASE STUDY- CO₂ INJECTION -PARSHALL FIELD

This chapter implements the CO₂ injection study proposed in previous chapters on a real field case in Parshall field, Bakken formation. A reservoir model was developed with one proposed injector well and one producer well to see the effect of CO₂ injection. History matching technique was used to define the optimum parameters before implementing CO₂ injection in the reservoir.

7.1 BAKKEN PETROLEUM SYSTEM

Bakken Petroleum System is a combination of Devonian-Mississippian black shale and mixed sandstone/carbonate source rock for the Williston Basin. The formation is from late Devonian (382.7-372.2 million years ago) to early Mississippian age (358-9-323.2 million years ago) (Sarg 2012). Bakken is an interbedded sequence of black shale, siltstone and sandstone that lies under the areas of north eastern Montana, northwestern North Dakota, south eastern Saskatchewan, and south western Manitoba.

Figure 7.1 shows the structural map of the Williston Basin - Bakken formation spread across 200,000 miles in North America and Canada.

The Bakken formation is categorized as unconventional due to low porosity and low permeability of the reservoir. The natural fracture connectivity in the system has led to the formation of reservoir ‘sweet spots’. Crude oil shale is the dominant product of fossil from Bakken with shale gas as a by-product. Recent production statistics from North Dakota Oil & Gas Division in July 2014 accounts for 1.04 million barrels of oil production per day from Bakken formation (EIA-DPR 2014). Production from Bakken quantifies 28% of total North America oil production. The efficient use of techniques

like multi-stage hydraulic fracturing and horizontal drilling targeted to Middle Bakken resulted in the significant production numbers shown in **Figure 7.2**.

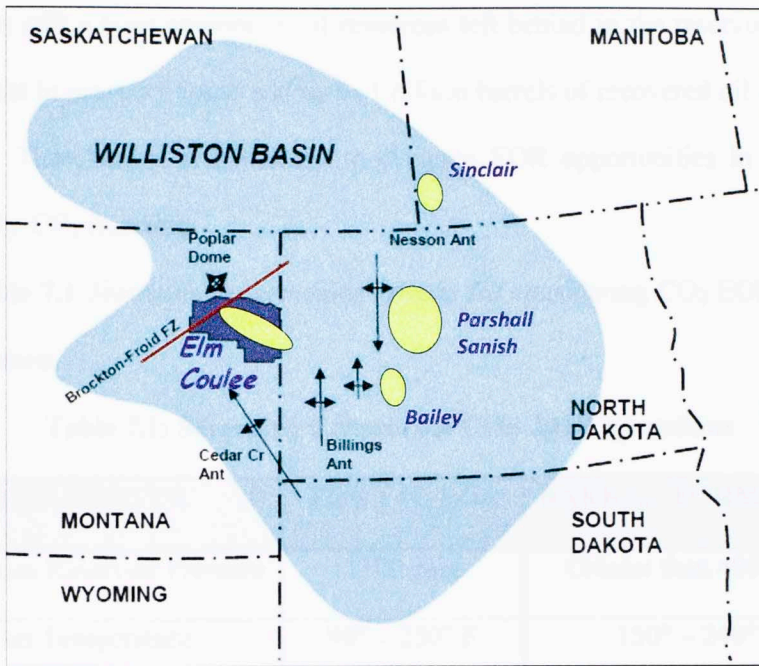


Figure 7.1: Regional Structural Map of the Williston Basin, Bakken Formation;

Blue patch is the regional limit of Bakken and yellow spots are major fields

Bakken Region
Oil production

thousand barrels/day

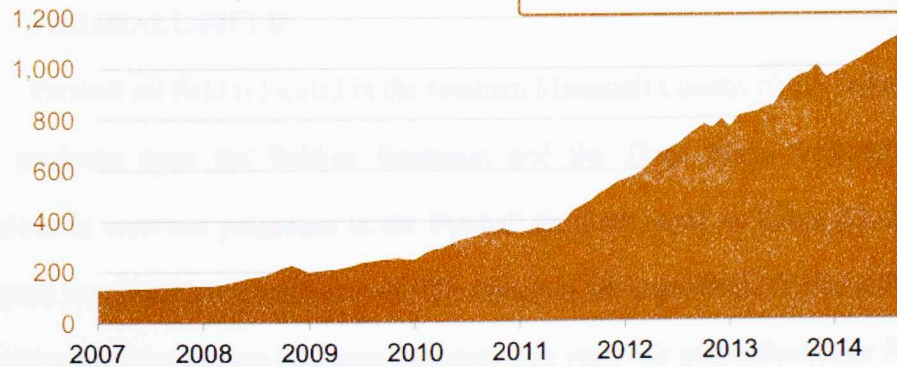


Figure 7.2: Oil production status from Bakken formation (EIA-DPR 2014)

Even though there is a significant amount of oil production from Bakken formation, it only accounts for 10-15% of total oil recovery from the field. This means that there is still a huge amount of oil resources left behind in the reservoir. Even 1% improvement in recovery could add up to 1 billion barrels of recovered oil (Sorensen et al. 2013a). Therefore, it is necessary to evaluate EOR opportunities in the Bakken formation by CO₂ injection.

Table 7.1 illustrates the screening criteria for considering CO₂ EOR in Bakken shale formation.

Table 7.1: Screening Criteria for CO₂- EOR operations

PARAMETER	FOR CO ₂ EOR	BAKKEN FORMATION
Minimum Reservoir Pressure	1100 psia	Greater than 4000 psia
Reservoir Temperature	90° – 250° F	150° – 240° F
Oil Gravity Range	27° - 48 °API	36° - 44 °API
Minimum Oil Saturation	Greater than 25%	Greater than 75%
Water flood Results	Necessary	No Water flooding results

7.2 PARSHALL FIELD

Parshall oil field is located in the southern Mountrail County, North Dakota. The field produces from the Bakken formation and the Three Forks formation. The variations in reservoir properties in the Parshall field are listed in **Table 7.2**. Several operators are planning on prospects of CO₂ injection for improving oil production, but until now, no pilot project has been initiated. The reservoir properties make Parshall field a good candidate for CO₂-EOR opportunities.

Table 7.2: Reservoir properties of Parshall field

PARAMETER	PARSHALL FIELD		Unit
	MIN	MAX	
Reservoir Pressure	6,000	8,000	psia
Permeability	0.0001	1.90	mD
Average Porosity	4	10	%
Oil API Gravity	36	45	°API
Gas Specific Gravity	0.77	0.96	
Average Water Saturation	25	45	%
Solution GOR	500	1,500	SCF/STB
Bubble Point	1,800	4,000	psia

7.3 FIELD SCALE RESERVOIR MODEL

A two well injector-producer system was simulated using the formation and well completion information available through DrillingInfo and North Dakota Oil and Gas Portal. Two wells, PARSHALL 20-03H and BARTELSON 1-3H, are modeled as injector and producer respectively. PARSHALL 20-03 was producing hydrocarbons from June 2006 and was recompleted in 2014 as an injector. Information on the well and its nearby wells could be found through the state portal database. The formation properties for the field model are described in **Table 7.3**. The Middle Bakken reservoir is at a target depth of 10,500 ft with pay zone thickness of 40 ft. Homogeneous reservoir with permeability of 0.005 mD and average porosity of 5% was considered.

Table 7.3: Formation properties for Parshall field model

Parameter	Average	Unit
Reference Depth	10,500	<i>ft</i>
Initial Reservoir Pressure	6,000	<i>psia</i>
Pay Zone Thickness	40	<i>ft</i>
Total Compressibility	6.4 E-06	$\frac{1}{psia}$
Reservoir Temperature	240	°F
Oil API Gravity	42	°API
Reservoir Permeability	0.005	<i>mD</i>
k_v/k_h	0.1	
Reservoir Porosity	5.0	%
Initial Water Saturation	0.30	

Figure 7.3 shows the aerial view of the selected wells in the Parshall field. For simulation purposes, the zone marked as red is simulated with PARSHALL 20-03H as CO₂ injector well and BARTESON 1-3H as the producer well. Both wells are completed parallel with 5,000 lateral length and 2,000 apart from each other. PARSHALL 20-03H was completed with a 15 stage fracture design with 4 shots per foot of perforation per cluster having cluster spacing of 60 ft and stage spacing of 140 ft. BARTESON 1-3H was completed with a 6 stage fracture design with 5 shots per foot of perforation per cluster having cluster spacing of 140 ft and stage spacing of 300 ft. Reservoir simulation model was generated with this available information about the formation and the completion technique, as shown in **Figure 7.4**. The reservoir

description is already defined in APPENDIX A, but grid and well properties are changed to accommodate Parshall well characteristics.

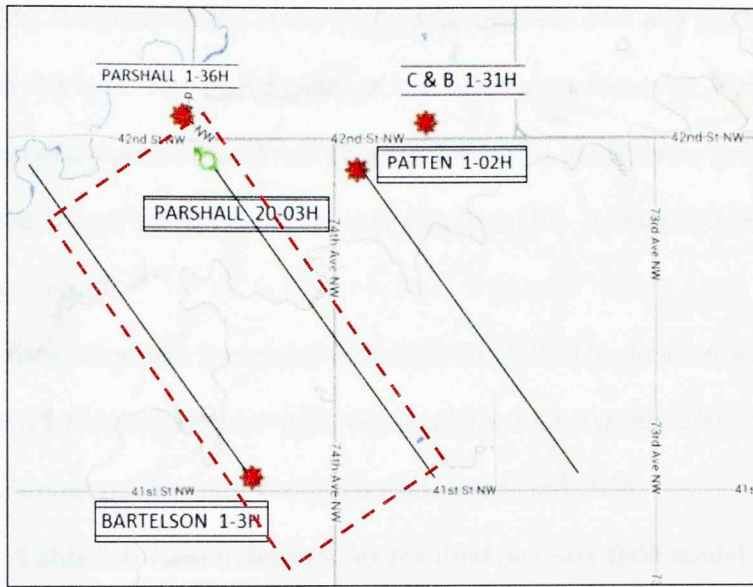


Figure 7.3: Aerial view of selected zone in the Parshall field, with red zone simulated as a two well Inj-Prod system

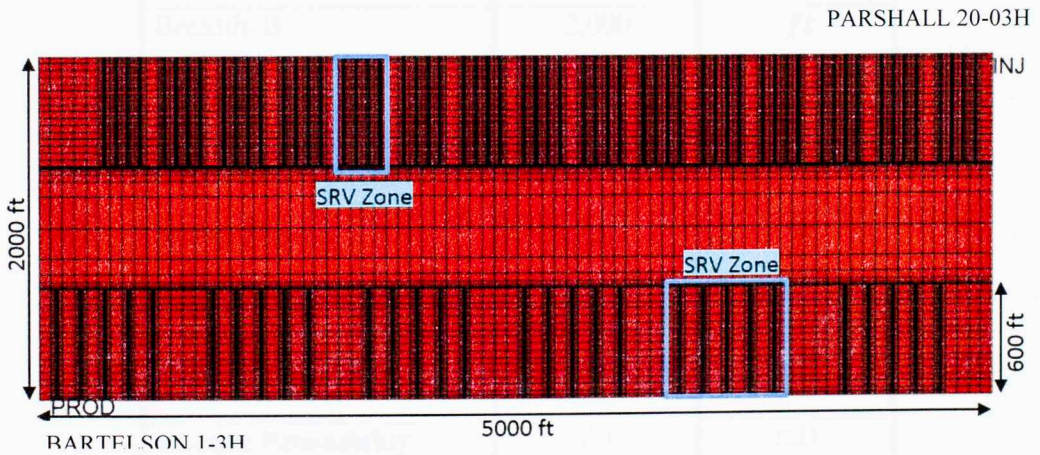


Figure 7.4: X-Y cross section perforation plane of field reservoir model

A Dual-Porosity model is used to account for the presence of naturally fractured formation. The hydraulic fractures were simulated in the fractured media with fracture

half - length of 600 ft. Logarithmically-spaced-local-grid refinement was utilized around the hydraulic fractures, with a width of 2 ft width representing a 0.0292 ft fracture width. The permeability in the injector fracture was 14.5 mD and the producer fracture with 7.3 mD. The permeability in the Stimulated Reservoir Volume (SRV) around the created fracture was 2 mD (**Figure 7.4**). Also, logarithmic grid refinement was generated around the hydraulic fracture tips to nullify convergence issues due to permeability contrast.

The simulation time frame was from 2007 to 2025. The duration was chosen as the production rate history for the wells was available from January 2007 to December 2013. The reservoir performance was further simulated until 2025.

Table 7.4: Grid definition for the dual porosity field model

GRID PROPERTIES		
Length, L	5,600	<i>ft</i>
Breadth, B	2,000	<i>ft</i>
Thickness, h	40	<i>ft</i>
Number of Grid Blocks	NX, NY, NZ	80, 50, 10
Matrix Porosity	5	%
Fracture Porosity	0.5	%
Matrix Permeability	0.005	mD
Fracture Permeability	0.1	mD
SRV Permeability	2.0	mD
Producer Minimum BHP	500	psia
Producer Maximum Rate	2,000	STB/Day

7.4 HISTORY MATCHING APPROACH

Production rate history data for 6 years of production was available for the wells modeled for this study. History matching approach could enable effective matching of simulation results with the available production history. CMG-CMOST was used for history matching after implementing sensitivity analysis. CMOST generated simulation runs from uncertain parameters with an objective function to closely match the production history and determine the formation parameter values from the optimal solution. This approach increased the confidence in the simulation results to predict future performance and also to evaluate EOR prospects. Production rate history of BARTELSON 1-3H is tabulated in **APPENDIX C**. Daily oil and gas production rates were available through North Dakota Oil and Gas Portal (NDIC 2013).

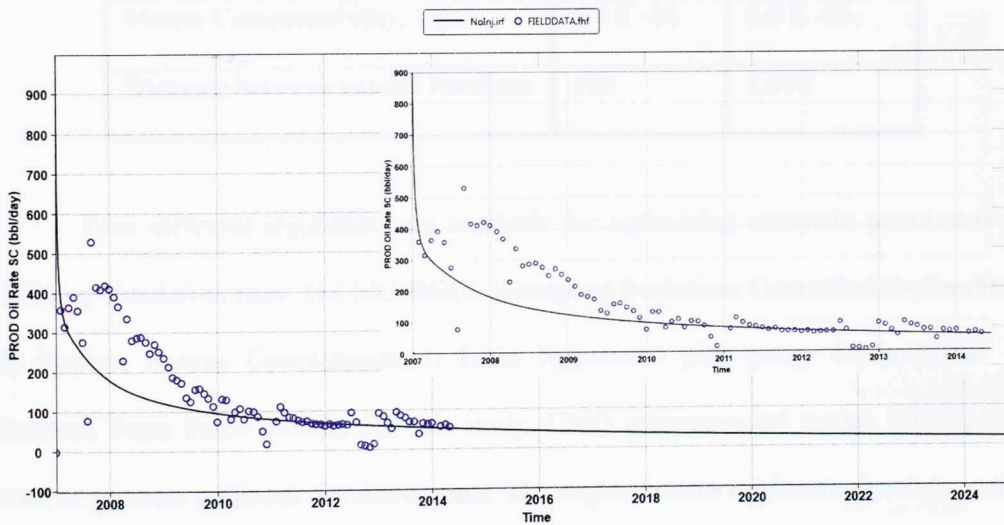


Figure 7.5: Simulation production rate and the rate history match

The simulation model was run without CO₂ injection to forecast the production performance of the model on primary recovery. Available production rate history was implemented into the reservoir model to match the simulation results as shown in

Figure 7.5. With initial match of the simulation results, uncertain parameters are defined in the history matching engine to evaluate optimum formation properties to compliment rate production history. The uncertain parameters with their respective ranges are listed in **Table 7.5.**

Table 7.5: History match parameters for field study

UNCERTAINTY PARAMETERS FOR HISTORY MATCH		
Parameter	Minimum	Maximum
Matrix Permeability, mD	0.003	0.05
Matrix Porosity, %	2.0	12.0
Fracture Porosity, %	0.5	2.0
K_v/K_H	0.01	1.0
Matrix Compressibility, 1/psia	4.8 E -06	8.0 E -06
Distance between natural fractures	100	1,000

Four different algorithms are available for optimizing uncertain parameters in defining simulation runs: 1) CMG DECE (Designed Evolution, Controlled Exploration) 2) Particle Swarm Optimization 3) Latin Hypercube plus proxy Optimization 4) Random Brute Force Search. For this study, CMG recommended model, DECE, was used to generate optimum simulation runs. The engine creates minimum simulation runs required to define an optimum result. Additional runs are generated to validate the history match results. CMG-DECE is elaborated in **APPENDIX D.**

It is critical to evaluate the error due to history match while defining the optimum uncertain parameters for simulation of the field production history.

$$\text{History Match Error} = \sqrt{\frac{\sum_{t=1}^N (Y_t^S - Y_t^M)^2}{N_t}} \dots\dots\dots (7.1)$$

This error is calculated by the square root of the difference between the squared simulated and measured objective function (CMG-CMOST 2013). The error is the arithmetic weighing average over the number of simulation runs.

History match engine generated 120 runs to evaluate the optimum parameters and the simulated results are shown in **Figure 7.6**. The optimum solution is in close agreement to the production rate history (objective function). The optimum values for the formation uncertainty parameters are listed in **Table 7.6**. The history match engine generated matrix permeability of 0.0093 mD and matrix porosity of 4.25%. The global history match error with oil production rate was 13.2%.

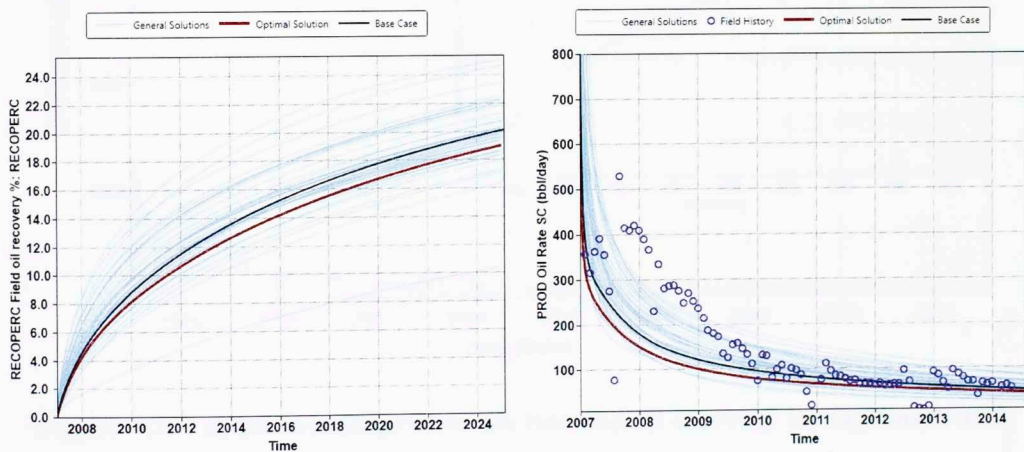


Figure 7.6: History match results for oil recovery and oil production rate

Table 7.6: Optimum parameters from history match

Parameter	Optimum	Unit
Matrix Permeability	0.0093	mD
Matrix Porosity	4.25	%
Fracture Porosity	1.1	%
K_v/K_H	0.01	
Matrix Compressibility	4.95 E -06	1/psia
Distance between natural fractures	694	ft

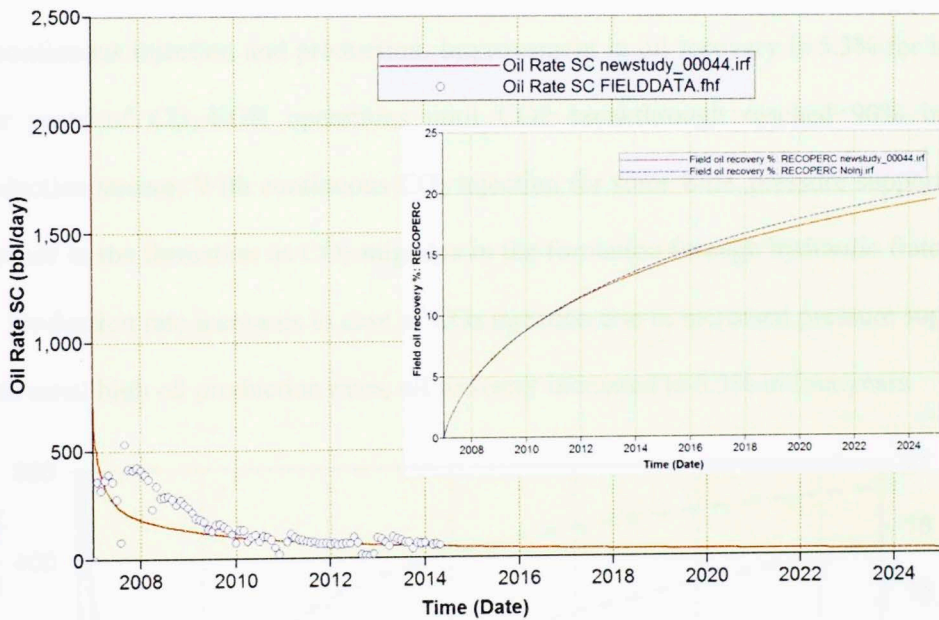


Figure 7.7: Comparison of production rate and oil recovery for Optimum and Base case solution

Figure 7.7 shows the optimum solution with the base case reservoir model simulation result. The difference in oil recovery with the optimum solution is 1.5% less than the base case result, but the optimum solution considers a good match with the rate production history.

7.5 CO₂-EOR PROSPECTS IN PARSHALL FIELD

After defining an optimum solution with history match engine, reservoir model with optimum parameters, as defined in **Table 7.6**, were used to implement CO₂-EOR prospects. PARSHALL 20-03H modeled in the reservoir was considered as 100% CO₂ injector with maximum injection rate defined at 1 MMSCF/Day and maximum injection pressure of 10,000 psia. **Figure 7.8** provides the comparison between field oil recovery achieved with and without CO₂ injection from producer well.

CO₂-EOR accounted for 3.2% improvement in oil recovery with thirteen years of continuous injection and production. Improvement in oil recovery is 5.3% for initial four years of CO₂-EOR operations until CO₂ breakthrough reached 90% in the production stream. With continuous CO₂ injection for some time, pressure support will increase in the formation as CO₂ migrates in the formation through hydraulic fractures. Oil production rate increases in case of CO₂ injection due to increased pressure support. With initial high oil production rates, oil recovery increased to 5.3% in four years.

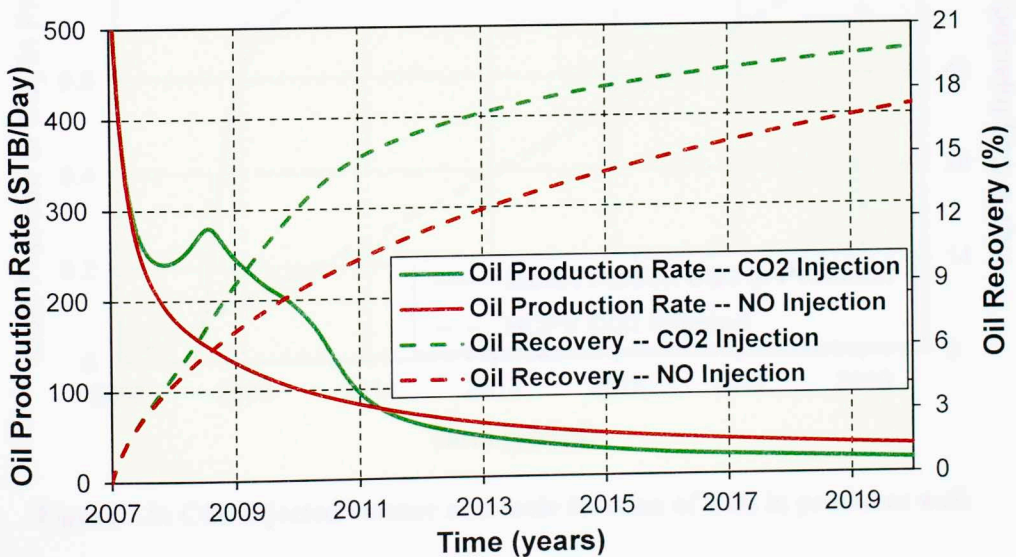


Figure 7.8: Parshall field CO₂-EOR simulation results with primary recovery

It is observed in **Figure 7.8** oil production rate decreased after four years below the rate achieved without CO₂ injection. It is attribution to 90% CO₂ breakthrough in the producer fluid reducing oil production. In the reservoir model, first mole of CO₂ breakthrough in the producer well was observed after 1.5 years of continuous injection and production (**Figure 7.9**). After 4 years, CO₂ breakthrough was beyond 90%. Total amount of CO₂ sequestered in the formation accounted for 69.2 % of hydrocarbon pore volume. This again validates the CO₂ utilization factor of 3:1 for Middle Bakken formation as observed for the base reservoir model.

It is critical to consider the time frame for CO₂ injection in improving oil recovery. For initial 1 year of CO₂-EOR operations, no improvement in oil recovery could be observed. Oil recovery increased after continuous 1 year of injected and ramped the oil production by 5.3% within four years.

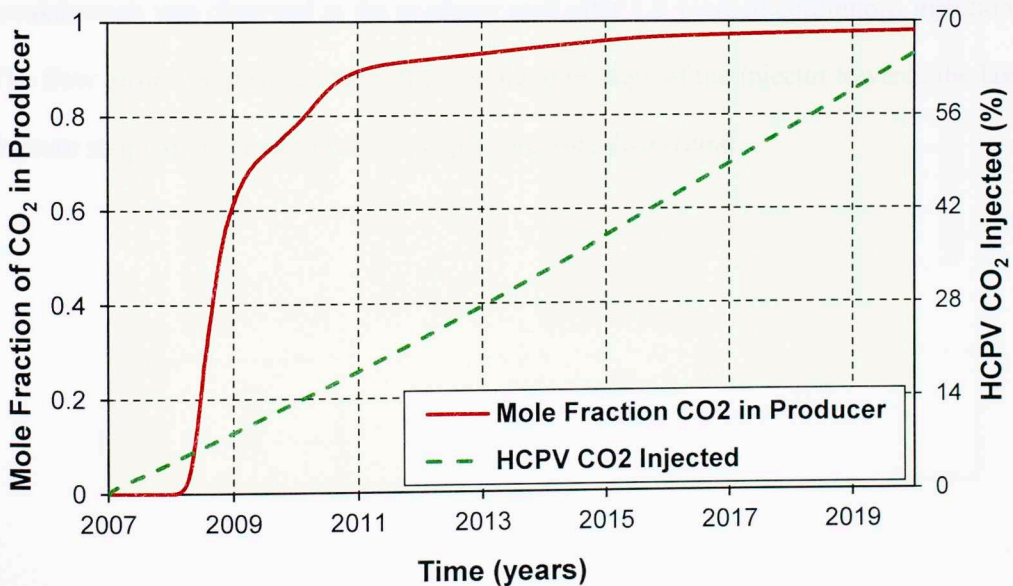
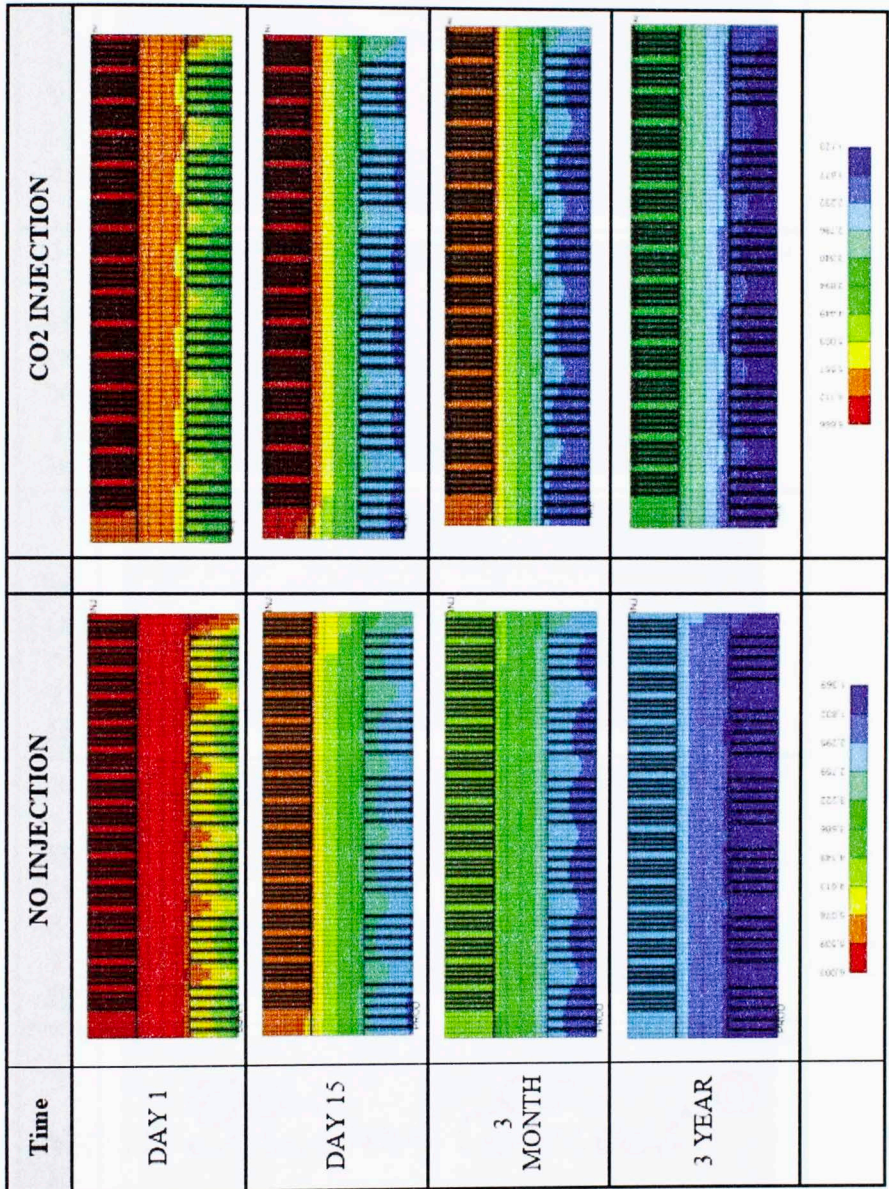


Figure 7.9: CO₂ injected volume and mole fraction of CO₂ in producer well

Figure 7.10 illustrates the pressure profile for the field model, comparing the pressure profile with CO₂ injection and no injection, for initial three years of simulation. CO₂ injection creates pressure supported drive in the formation that aids CO₂ in displacement of oil towards producer that has pressure drawdown limited to the near wellbore area. With no pressure drive, the reservoir pressure drains relatively quickly and attains pressure stability as it reaches the bottomhole pressure, leading to insignificant production rates.

Figure 7.11 shows the CO₂ mole fraction profile in the reservoir as CO₂ is injected through the injector well with 60 fracture stages. The fracture conductivity is high enough to provide relatively smooth fluid movement through the Stimulated Reservoir Volume (SRV). The presence of natural fractures is emulated by the dual porosity model and the flow profile is observed in the fractured media. CO₂ breakthrough was observed in the producer well after 1.5 years of continuous injection. The flow profile is observed from the first fracture stage of the injector towards the last fracture stage of the producer due to higher pressure differential.

Figure 7.10: Pressure profile for field model: NO Injection & CO₂ Injection



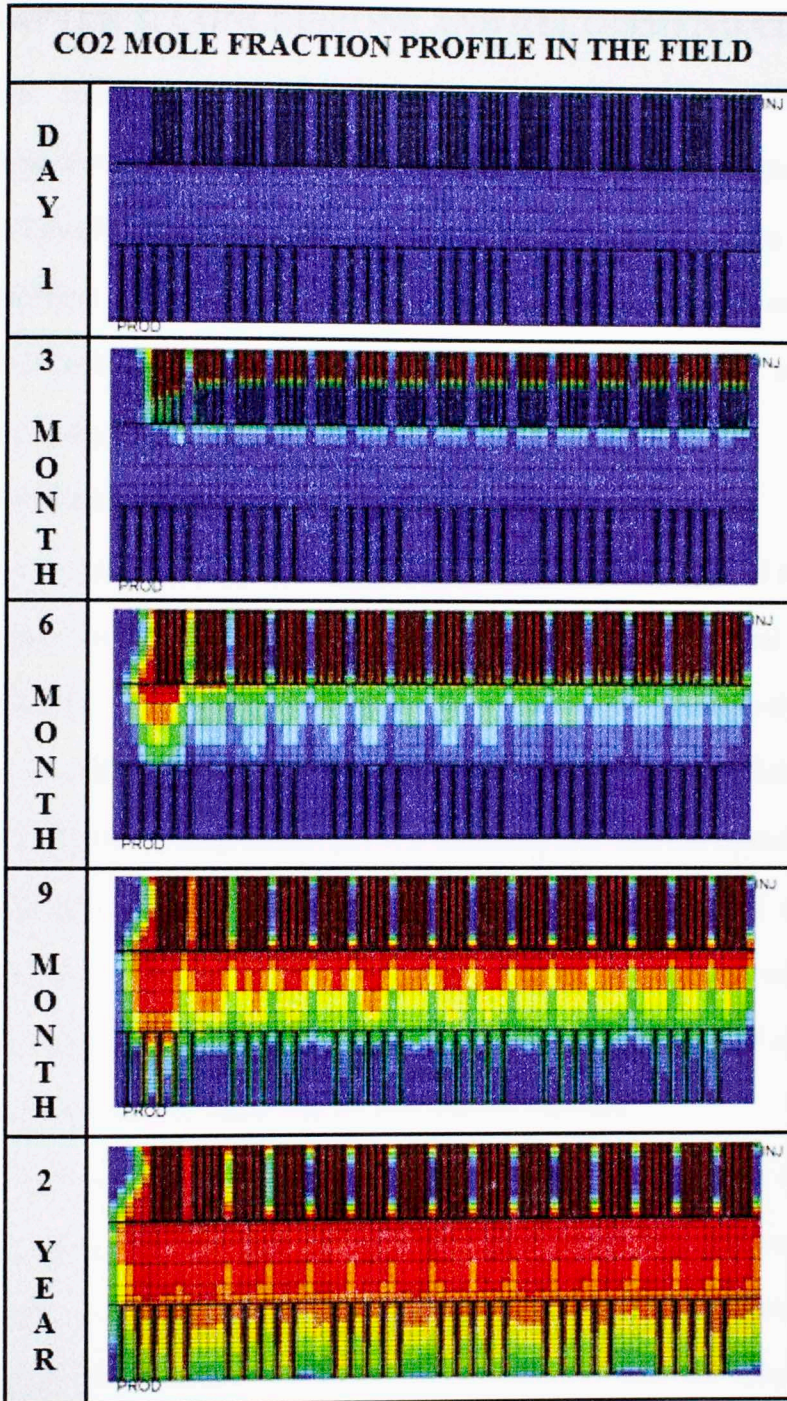


Figure 7.11: CO₂ mole fraction profile with time progression in the field model

CHAPTER 8: CONCLUSIONS AND RECOMMENDATIONS

This study evaluates the effectiveness of CO₂ injection for enhanced hydrocarbon recovery and formation CO₂ sequestration capacity for tight reservoirs. The work identifies the most favorable reservoir properties and operating envelope for field application of CO₂-EOR in tight formations. Single porosity compositional reservoir simulation model is employed to model CO₂ injection, while incorporating various physical processes into the model.

8.1 CONCLUSIONS

The research concluded that facilitating oil recovery from tight oil reservoirs by CO₂ injection could be greater than primary depletion depending on natural and induced fracture network connectivity. The presence of natural fractures significantly affects the flow migration of CO₂ in the reservoir, directly impacting the sweep efficiency. Major conclusions of incorporating various physical processes into reservoir model are:

1. Adsorption of CO₂ is significantly higher than hydrocarbon components. Formation surfaces tend to have more affinity towards adsorption of CO₂ molecules than hydrocarbon molecules leading to desorption of methane and ethane molecules, improving the hydrocarbon recovery.
2. Formation with higher total organic content (TOC) have a greater capability of CO₂ adsorption and more desorption of hydrocarbon components, leading to higher oil recovery as compared to reservoirs containing lower organic content.
3. Highly stress sensitive reservoir model achieves less oil recovery, when compared with homogeneous permeability. The main reason could be the

significant permeability changes in the natural and induced fractures, higher pressure drop in the producer zones.

4. Heterogeneity in the reservoir rock and permeability anisotropy are very critical for unconventional tight oil formations and needs to be considered in reservoir simulation studies. It significantly affects the oil recovery as well as CO₂ breakthrough time in the production stream.

Sensitivity analysis of the critical parameters by OPAAT and RSM approach provides significant understanding of critical parameters. Major conclusions are:

1. The lateral distance between the injector hydraulic fracture and producer hydraulic fracture are the most critical parameters that affect oil recovery. Other critical factors are hydraulic fracture permeability of the producer well and then the distance (acre spacing) between the injector and producer well.
2. Stress dependent permeability and injection rate are important initially, but their effect decreases with time progression.
3. The presence of natural fracture connectivity strong affects the importance of hydraulic fracture permeability's and fracture half lengths in the reservoir model. These parameters become insignificant in the absence of natural and induced fractures in the formation.
4. Significant advantage of RSM approach over OPAAT analysis is that the former has the ability to consider the effect of interaction and quadratic terms of uncertainties. Also, at reservoir scale, uncertainties among individual parameters simultaneously affect the flow modeling. However, OPAAT analysis is very

critical for initial understanding of critical parameters in order to define their uncertainties. The top significant parameters from OPAAT analysis could be utilized to generate RSM proxy model.

5. RSM model estimated injection pressure as the most critical parameter for both – the amount of HCPV CO₂ injected and the oil recovery. It is followed by distance between fractures and distance between wells. It was also noticed that when injection pressure was combined with several interaction parameters, the affect of these interaction parameters had negative as well as positive effect on amount of CO₂ injected. It can hence be concluded that it is critical to evaluate the effect of interaction parameters on objective function instead of relying on OPAAT single parameter analysis.
6. CO₂ utilization factor of 3:1 was evaluated using the base reservoir model for improving oil recovery in the Middle Bakken formation. It signifies that for every 3% HCPV of CO₂ injected into the formation, an incremental oil recovery of 1% could be achieved.
7. It is For Parshall field CO₂-EOR operations, no improvement in oil recovery could be observed for initial 1.2 years of continuous injection. Oil recovery increased after continuous 1.2 year of injection and ramped the oil production by 5.3% within four years. The rate decreased after 90% CO₂ breakthrough was observed in the produced fluid.
8. For Parshall field CO₂-EOR operations, total amount of CO₂ sequestered in the formation accounted for 69.2 % of hydrocarbon pore volume leading to an oil

recovery of 21%. This again validates the CO₂ utilization factor of 3:1 for Middle Bakken formation as observed for the base reservoir model.

8.2 RECOMMENDATIONS FOR FUTURE RESEARCH

A range of future research opportunities prevail in directions of laboratory experiments and improving reservoir simulation of CO₂ fluid migration in the reservoir.

1. There is a need to better characterize the presence of natural fractures in the formation through high end laboratory experiments and core analysis. Also, SEM analysis of the natural fractures should be incorporated into the simulation models.
2. Consideration of pore size distribution in the reservoir formation is very critical for tight/shale formations and could be considered for future study.
3. Experiments to estimate the relative permeability curves and capillary pressure must be performed. The experimental results should serve as the input for the rock-fluid parameters in reservoir simulation.
4. A general recommendation is to incorporate the laboratory measurements on the core data to incorporate geomechanical studies in reservoir simulation as the changes in porosity and permeability will strongly depend on formation characteristics and type of fractures in the formation.
5. In field scale reservoir modeling, it was difficult to incorporate adsorption and diffusion physics due to numerical instability and numerical dispersion effects. But these parameters are critical for fluid migration and recommended to include in future research.

6. This study could also be used to evaluate the effectiveness of injecting the produced gas back into the formation instead of CO₂ injection. Produced gas could also achieve miscibility with the reservoir fluid and improve production. This could also mitigate the flaring issues and environmental issues relative to greenhouse gas emission after breakthrough.

REFERENCES

- Adekunle, O. 2014. Experimental Approach to Investigate Minimum Miscibility Pressures in the Bakken. MS Thesis, Colorado School of Mines, Golden, Colorado.
- Al Ismail, M., Hol, S., Reece, J. S. and Zoback, M. D. 2014. The Effect of CO₂ Adsorption on Permeability Anisotropy in the Eagle Ford Shale. Paper SPE-2014-1921520-MS presented at the SPE/AAPG/SEG Unconventional Resources Technology Conference (URTEC), Denver, Colorado, USA, 25-27 August <http://dx.doi.org/10.15530/urtec-2014-1921520>.
- Alramahi, B. and Sundberg, M. 2012. Proppant Embedment And Conductivity of Hydraulic Fractures in Shales. Paper ARMA-2012-291 presented at the 46th US Rock Mechanics/Geomechanics Symposium, Chicago, Illinois, 24-27 June.
- Ambrose, R. J., Diaz-Campos, M., Akkutlu, I. Y. and Sondergeld, C. H. 2010. New Pore-scale Considerations for Shale Gas in Place Calculations. Paper SPE-131772-MS presented at the SPE Unconventional Gas Conference, Pittsburgh, Pennsylvania, USA, 27-29 March. <http://dx.doi.org/10.2118/131772-MS>.
- Ambrose, R. J., Hartman, R. C. and Akkutlu, I. Y. 2011. Multi-Component Sorbed Phase Considerations for Shale Gas-in-Place Calculations. Paper SPE-141416-MS presented at the SPE Production and Operations Symposium, Oklahoma City, Oklahoma, USA, 27-29 March. <http://dx.doi.org/10.2118/141416-MS>.
- Amudo, C., May, R., Graf, T., Dandekar, R., Harris, N. and Ben Amor, F. 2008. Experimental Design and Response Surface Models as a Basis for the Stochastic History Match-A Case Study on Complex Reservoirs in the Niger Delta. Paper IPTC-12665-MS presented at the International Petroleum Technology Conference, Kuala Lumpur, Malaysia, 3-5 December. <http://dx.doi.org/10.2523/12665-MS>.
- Angus, S., Armstrong, B. and de Reuck, K. M. 1976. International Thermodynamic Tables of the Fluid State - 3 Carbon Dioxide. *Pergamon Press, Pergamon, New York, Oxford (Reprint)*.
- Baker, R. 2013. A Global Perspective for IOR and Primary in Unconventional Tight Oil and Gas Reservoirs. Overview of Tight Oil/Shale Oil Worldwide.
- Beliveau, D. 1993. "Honey, I Shrunk the Pores!". PETSOC-93-08-01. <http://10.2118/93-08-01>.
- Breit, V. S., Stright Jr, D. H. and Dozzo, J. A. 1992. Reservoir Characterization of the Bakken Shale from Modeling of Horizontal Well Production Interference Data.

- Paper SPE-24320-MS presented at the SPE Rocky Mountain Regional Meeting, Casper, Wyoming, 18-21 May. <http://dx.doi.org/10.2118/24320-MS>.
- Bumb, A. and McKee, C. 1988. Gas-Well Testing in the Presence of Desorption for Coalbed Methane and Devonian Shale. *SPE Formation Evaluation* **3** (01): 179-185. <http://dx.doi.org/10.2118/15227-PA>.
- Bustin, R. M., Bustin, A. M., Cui, A., Ross, D. and Pathi, V. M. 2008. Impact of Shale Properties on Pore Structure and Storage Characteristics. Paper SPE-119892-MS presented at the SPE Shale Gas Production Conference, Fort Worth, Texas, USA, 16-18 November. <http://dx.doi.org/10.2118/119892-MS>.
- Chang, Y., Coats, B. and Nolen, J. 1998. A Compositional Model for CO₂ Floods Including CO₂ Solubility in Water. *SPE Reservoir Evaluation & Engineering* **1** (02): 155-160. SPE-35164-PA. <http://dx.doi.org/10.2118/35164-PA>.
- Chase, M. W. 1998. NIST-JANAF Thermochemical Tables. *Journal of Physical and Chemical Reference Data* **4** (9): 1963.
- Chawathe, A., Sun, H., Shi, X., Li, L. and Hoteit, H. 2014. Understanding Shale Gas Production Mechanisms Through Reservoir Simulation. Paper SPE-167753-MS presented at the SPE/EAGE European Unconventional Resources Conference and Exhibition, Vienna, Austria, 25-27 February. <http://dx.doi.org/10.2118/167753-MS>.
- Cipolla, C. L., Lolon, E. P., Erdle, J. C. and Rubin, B. 2010. Reservoir Modeling in Shale-Gas Reservoirs. *SPE Reservoir Evaluation & Engineering* **13** (04): 638-653. SPE-125530-PA. <http://dx.doi.org/10.2118/125530-PA>.
- Cipolla, C. L., Warpinski, N. R., Mayerhofer, M. J., Lolon, E. and Vincent, M. C. 2008. The Relationship Between Fracture Complexity Reservoir Properties and Fracture Treatment Design. Paper SPE-115769-MS presented at the SPE Annual Technical Conference and Exhibition, Denver, Colorado, USA, 21-24 September. <http://dx.doi.org/10.2118/115769-MS>.
- Clark, A. J. 2009. Determination of Recovery Factor in the Bakken Formation Mountrail County ND. Paper SPE-133719-STU presented at the SPE Annual Technical Conference and Exhibition, New Orleans, Louisiana, 4-7 October. <http://dx.doi.org/10.2118/133719-STU>.
- CMG-CMOST. 2013. CMOST User Manual. *Computer Modeling Group Ltd.* **2013.20**.
- CMG-GEM. 2013. GEM User Manual. *Computer Modeling Group Ltd.* **2013.20**.
- CMG-WINPROP. 2013. WINPROP User Manual. *Computer Modeling Group Ltd.* **2013.20**.

- Cramer, D. D. 1986. Reservoir Characteristics and Stimulation Techniques in the Bakken Formation and Adjacent Beds Billings Nose Area Williston Basin. Paper SPE-15166-MS presented at the SPE Rocky Mountain Regional Meeting, Billings, Montana, 19-21 May. <http://dx.doi.org/10.2118/15166-MS>.
- Das, M., Jonk, R. and Schelble, R. 2012. Effect Of Multicomponent Adsorption/Desorption Behavior on Gas-In-Place (GIP) and Estimated Ultimate Recovery (EUR) in Shale Gas Systems. Paper SPE-159558-MS presented at the SPE Annual Technical Conference and Exhibition, San Antonio, Texas, USA, 8-10 October. <http://dx.doi.org/10.2118/159558-MS>.
- Dechongkit, P. and Prasad, M. 2011. Recovery Factor and Reserves Estimation in the Bakken Petroleum System (Analysis of the Antelope Sanish and Parshall fields). Paper SPE-149471-MS presented at the Canadian Unconventional Resources Conference, Alberta, Canada, 15-17 November. <http://dx.doi.org/10.2118/149471-MS>.
- Devegowda, D. and Gao, H. 2007. Integrated Uncertainty Assessment for Unconventional Gas Reservoir Project Development. Paper SPE-111203-MS presented at the Eastern Regional Meeting, Exington, Kentucky USA, 17-19 October. <http://dx.doi.org/10.2118/111203-MS>.
- Duan, Z. and Mao, S. 2006. A Thermodynamic Model for Calculating Methane Solubility, Density and Gas Phase Composition of Methane-Bearing Aqueous Fluids from 273 to 523K and from 1 to 2000 bar. *Geochimica et Cosmochimica Acta* **70** (13): 3369-3386. <http://10.1016/j.gca.2006.03.018>.
- EIA-DPR. 2014. Drilling Productivity Report - For Key Tight Oil and Shale Gas Regions, accessed September 2014.
- EIA, U. 2013. Technically Recoverable Shale Oil and Shale Gas Resources: An Assessment of 137 Shale Formations in 41 Countries Outside the United States (2013a).
- EIA, U. 2014. Annual Energy Outlook 2014 with Projections to 2040. *US Energy Information Administration, Washington, DC DOE/EIA-0383*.
- Hall, F. E., Chunhe, Z., Gasem, K. A. M., Robinson Jr, R. L. and Dan, Y. 1994. Adsorption of Pure Methane Nitrogen and Carbon Dioxide and their Binary Mixtures on Wet Fruitland Coal. Paper SPE-29194-MS presented at the SPE Eastern Regional Meeting, Charleston, West Virginia, USA, 8-10 November. <http://dx.doi.org/10.2118/29194-MS>.
- Hoffman, B. T. 2012. Comparison of Various Gases for Enhanced Recovery from Shale Oil Reservoirs. Paper SPE-154329-MS presented at the SPE Improved Oil

Recovery Symposium, Tulsa, Oklahoma, USA, 14-18 April.,
<http://dx.doi.org/10.2118/154329-MS>.

IHS. 2012. America's New Energy Future: The Unconventional Oil and Gas Revolution and the US Economy. **1: National Economic Contributions**.

Klusman, R. W. 2003. Evaluation of Leakage Potential from a Carbon Dioxide EOR/Sequestration Project. *Energy Conversion and Management* **44** (12): 1921-1940. [http://10.1016/S0196-8904\(02\)00226-1](http://10.1016/S0196-8904(02)00226-1).

Kucuk, F. and Sawyer, W. K. 1980. Transient Flow in Naturally Fractured Reservoirs and its Application to Devonian Gas Shales. Paper SPE-9397-MS presented at the SPE Annual Technical Conference and Exhibition, Dallas, Texas. <http://dx.doi.org/10.2118/9397-MS>.

Kurtoglu, B. 2014. Integrated Reservoir Characterization and Modeling in Support of Enhanced Oil Recovery for Bakken. Ph.D. , Colorado School of Mines, Golden, Colorado.

Langmuir, I. 1916. The Constitution and Fundamental Properties of Solids and Liquids. Part I Solids. *Journal of the American Chemical Society* **38** (11): 2221-2295.

LeFever, J. A. 2005. Oil production from the Bakken Formation: A Short History: North Dakota Geological Survey Newsletter. **32** (1): 5-10.

LeFever, J. A. 2011. Horizontal Drilling in the Williston Basin, United States and Canada. *The Bakken-Three Forks Petroleum System in the Williston Basin-Rocky Mountain Association of Geologists*: 508-529.

Lewis, R., Ingraham, D., Percy, M., Williamson, J., Sawyer, W. and Frantz, J. 2004. New Evaluation Techniques for Gas Shale Reservoirs. Paper presented at the Schlumberger Reservoir Symposium

Lie, S. H. 2013. Diffusion as an Oil Recovery Mechanism During CO₂ Injection in Fractured Reservoirs.

Liu, F., Ellett, K., Xiao, Y. and Rupp, J. A. 2013. Assessing the Feasibility of CO₂ Storage in the New Albany Shale (Devonian–Mississippian) with Potential Enhanced Gas Recovery Using Reservoir Simulation. *International Journal of Greenhouse Gas Control* **17**: 111-126. <http://10.1016/j.ijggc.2013.04.018>.

Maldal, T. and Tappel, I. 2004. CO₂ Underground Storage for Snøhvit Gas Field Development. *Energy* **29** (9-10): 1403-1411. <http://10.1016/j.energy.2004.03.074>.

- Mengal, S. A. and Wattenbarger, R. A. 2011. Accounting for Adsorbed Gas in Shale Gas Reservoirs. Paper SPE-141085-MS presented at the SPE Middle East Oil and Gas Show and Conference, Manama, Bahrain, 25-28 September. <http://dx.doi.org/10.2118/141085-MS>.
- Michael, K., Golab, A., Shulakova, V., Ennis-King, J., Allinson, G., Sharma, S. and Aiken, T. 2010. Geological Storage of CO₂ in Saline Aquifers—A Review of the Experience from Existing Storage Operations. *International Journal of Greenhouse Gas Control* **4** (4): 659-667. <http://10.1016/j.ijggc.2009.12.011>.
- Mihcakan, M. 1994. Minimum Miscibility Pressure Rising Bubble Apparatus and Phase Behavior. Paper SPE-27815-MS presented at the SPE/DOE Improved Oil Recovery Symposium, Tulsa, Oklahoma, 17-20 April. <http://dx.doi.org/10.2118/27815-MS>.
- Mills, R. M. 2008. *The Myth of the Oil Crisis: Overcoming the Challenges of Depletion, Geopolitics, and Global Warming*, Greenwood Publishing Group (Reprint).
- NDIC, N. D. I. C. 2013. Director's Cut, North Dakota Production Statistics Website, <https://www.dmr.nd.gov/oilgas/directorscut/directorscut-2014-09-12.pdf>, accessed September 20, 2014.
- Nojabaei, B., Johns, R. T. and Chu, L. 2013. Effect of Capillary Pressure on Fluid Density and Phase Behavior in Tight Rocks and Shales. *SPE Reservoir Evaluation & Engineering* **16** (03): 281 - 289. <http://dx.doi.org/10.2118/159258-PA>.
- Occidental Petroleum Corporation. 2014. Permian CO₂ EOR, <http://www.oxy.com/OurBusinesses/OilAndGas/UnitedStates/Pages/Permian.aspx>, accessed September 20, 2014.
- Okenyi, K. C. and Omeke, J. 2012. Well Performance Optimization using Experimental Design Approach. Paper SPE-162973-MS presented at the Nigeria Annual International Conference and Exhibition, Lagos, Nigeria, 6-8 August. <http://dx.doi.org/10.2118/162973-MS>.
- Pitman, J. K., Price, L. C. and LeFever, J. A. 2001. *Diagenesis and Fracture Development in the Bakken Formation, Williston Basin: Implications for Reservoir Quality in the Middle Member*, US Department of the Interior, US Geological Survey (Reprint).
- Plains CO₂ Reduction PCOR Partnership. 2014. Intergrated Approach, <http://www.undeerc.org/pcor/co2sequestrationprojects/IntegratedApproach.aspx>, accessed September 20, 2014.

- Poling, B. E., Prausnitz, J. M., John Paul, O. C. and Reid, R. C. 2001. *The Properties of Gases and Liquids*, Vol. 5. New York, McGraw-Hill (Reprint).
- Pu, W. and Hoffman, T. B. 2014. EOS Modeling and Reservoir Simulation Study of Bakken Gas Injection Improved Oil Recovery in the Elm Coulee Field, Montana. Paper SPE-2014-1922538-MS presented at the SPE/AAPG/SEG Unconventional Resources Technology Conference, Denver, Colorado, USA, 25-27 August. <http://dx.doi.org/10.15530/urtec-2014-1922538>.
- Sakhaee-Pour, A. and Wheeler, M. F. 2013. Fracture Cell for Flow Modeling. Paper SPE-167183-MS presented at the SPE Unconventional Resources Conference Canada, Calgary, Alberta, Canada, 5-7 November. <http://dx.doi.org/10.2118/167183-MS>.
- Sarg, J. F. 2012. The Bakken – An Unconventional Petroleum and Reservoir System. *Oil & Natural Gas Technology*.
- Schmoker, J. W. and Hester, T. C. 1983. Organic Carbon in Bakken Formation, United States Portion of Williston Basin. *AAPG Bulletin* **67** (12): 2165-2174.
- Shoaib, S. and Hoffman, B. T. 2009. CO₂ Flooding the Elm Coulee Field. Paper SPE-123176-MS presented at the SPE Rocky Mountain Petroleum Technology Conference, Denver, Colorado, 14-16 April. <http://dx.doi.org/10.2118/123176-MS>.
- Shook, M., Li, D. and Lake, L. W. 1992. Scaling immiscible flow through permeable media by inspectional analysis. *In Situ; (United States)* **16:4**: 311-350. OSTI ID: 6928846.
- Sieminski, A. 2014. Outlook for US Shale Oil and Gas. Paper presented at the National Capital Area Chapter - U.S. Association for Energy Economics
- Simenson, A. 2010. Depositional Facies and Petrophysical Analysis of the Bakken Formation: Parshall Field, Mountrail County, North Dakota. MS, Colorado School of Mines, Golden, Colorado.
- Sondergeld, C. H., Ambrose, R. J., Rai, C. S. and Moncrieff, J. 2010. Micro-Structural Studies of Gas Shales. Paper SPE-131771-MS presented at the SPE Unconventional Gas Conference, Pittsburgh, Pennsylvania, USA, 23-25 February. <http://dx.doi.org/10.2118/131771-MS>.
- Sonnenberg, S. A. 2011. TOC and Pyrolysis Data for the Bakken Shales, Williston Basin, North Dakota and Montana. *The Bakken-Three Forks Petroleum System in the Williston Basin*: 308-331.

- Sorensen, J., Harju, J., Hawthorne, S., Braunberger, J., Liu, G., Smith, S. and Steadman, E. 2013a. Concepts for CO₂ EOR in the Bakken Formation. *19th Annual CO₂ Flooding Conference, EERC*.
- Sorensen, J. A., Hawthorne, S. B., Harju, J. A., Melzer, S., Gorecki, C. D. and Steadman, E. N. 2013b. Hydrocarbon Mobilization Mechanisms from Upper Middle and Lower Bakken Reservoir Rocks Exposed to CO₂. Paper SPE-167200-MS presented at the SPE Unconventional Resources Conference Canada, Calgary, Alberta, Canada, 5-7 November. <http://dx.doi.org/10.2118/167200-MS>.
- Sorensen, J. A., Schmidt, D. D., Smith, S. A., Knudsen, D. J., Steadman, E. N. and Harju, J. A. 2009. Plains CO₂ Reduction (PCOR) Partnership (Phase II)–Williston Basin Field Demonstration, Northwest McGregor CO₂ Huff ‘N’ Puff–Regional Technology Implementation Plan (RTIP). *Energy & Environmental Research Center 2010-EERC-04-10* (Task 2 – Deliverable D55).
- Terzaghi, K. 1943. *Theoretical Soil mechanics*. New York City, John Wiley & Sons (Reprint).
- Thompson, J. M., Okouma Mangha, V. and Anderson, D. M. 2011. Improved Shale Gas Production Forecasting Using a Simplified Analytical Method–A Marcellus Case Study. Paper SPE-144436-MS presented at the North American Unconventional Gas Conference and Exhibition, The Woodlands, Texas, USA, 14-16 June. <http://dx.doi.org/10.2118/144436-MS>.
- Wan, T., Sheng, J. J. and Soliman, M. Y. 2013. Evaluate EOR Potential in Fractured Shale Oil Reservoirs by Cyclic Gas Injection. Paper SPE-168880-MS presented at the Unconventional Resources Technology Conference, Denver, Colorado, USA, 12-14 August. <http://dx.doi.org/10.1190/URTEC2013-187>.
- Wang, R., Zhao, R., Yan, P. and Freeman, D. 2009. Effect of Stress Sensitivity on Displacement Efficiency in CO₂ Flooding for Fractured Low Permeability Reservoirs. *Journal of Petroleum Science* **6** (3): 277-283. <http://10.1007/s12182-009-0044-6>.
- Wang, X., Luo, P., Er, V. and Huang, S.-S. S. 2010. Assessment of CO₂ Flooding Potential for Bakken Formation Saskatchewan. Paper SPE-137728-MS presented at the Canadian Unconventional Resources and International Petroleum Conference, Calgary, Alberta, Canada, 19-21 October. <http://dx.doi.org/10.2118/137728-MS>.
- Wang, Z. and Krupnick, A. 2013. A Retrospective Review of Shale Gas Development in the United States: What Led to the Boom? *Resources for the Future Discussion Paper DP 13* (12). <http://dx.doi.org/10.2139/ssrn.2286239>.

- Warren, J. E. and Root, P. J. 1963. *The Behavior of Naturally Fractured Reservoirs*. Pittsburgh, PA, Gulf Research & Development Company (Reprint).
- Wu, Y.-S., Bourbiaux, B. J., Wang, C., Ding, Y. D. and Farah, N. 2014. Numerical Simulation of Low Permeability Unconventional Gas Reservoirs. Paper SPE-167711-MS presented at the SPE/EAGE European Unconventional Resources Conference and Exhibition, Vienna, Austria, 25-27 February. <http://dx.doi.org/10.2118/167711-MS>.
- Xu, T. 2013. Hydraulic Fracture Orientation for Miscible Gas Injection EOR in the Elm Coulee Field, Colorado School of Mines.
- Younglove, B. A. and Ely, J. F. 1987. Thermophysical Properties of Fluids: II. Methane, Ethane, Propane, Isobutane, and Normal Butane. *Journal of Physical and Chemical Reference Data* **16** (4): 577-798. <http://dx.doi.org/10.1063/1.555785>.
- Yu, W. and Sepehrnoori, K. 2014. Simulation of Gas Desorption and Geomechanics Effects for Unconventional Gas Reservoirs. *Fuel* **116**: 455-464. <http://10.1016/j.fuel.2013.08.032>.
- Zeng, Z. and Jiang, A. 2009. Geomechanical Study of Bakken Formation For Improved Oil Recovery. Paper ISRM-SINOROCK-2009-067 presented at the ISRM International Symposium on Rock Mechanics-SINOROCK 2009, The University of Hong Kong, China, 19-22 May.
- Zhang, T., Ellis, G. S., Ruppel, S. C., Milliken, K. and Yang, R. 2012. Effect of Organic-Matter Type and Thermal Maturity on Methane Adsorption in Shale-Gas Systems. *Organic Geochemistry* **47** (June): 120-131. <http://10.1016/j.orggeochem.2012.03.012>.
- Zhou, X. J., Zeng, Z., Belobraydic, M. and Han, Y. 2008. Geomechanical Stability Assessment of Williston Basin Formations for Petroleum Production and CO₂ Sequestration. Paper ARMA-08-211 presented at the The 42nd US Rock Mechanics Symposium (USRMS), San Francisco, California, 29 June-2 Jul.

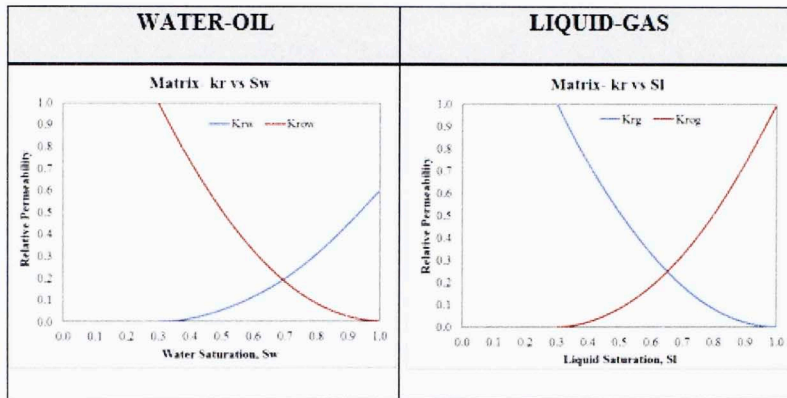
APPENDIX A: BASE MODEL RESERVOIR DESCRIPTION

RESERVOIR PROPERTIES OF MIDDLE BAKKEN					
Parameter	Range		Average	Unit	References
	Min.	Max.			
Reference Depth	9,500	11,500	10,500	ft	Wang et al. (2010)
Initial Reservoir Pressure	4,060	7,325	6,000	psia	Cramer (1986)
Pay Zone Thickness	25	75	40	ft	Cramer (1986)
Total Compressibility	2.0 E-06	8.5 E-06	6.4 E-06	$\frac{1}{psia}$	Dechongkit and Prasad (2011)
Reservoir Temperature	175	260	240	°F	LeFever (2005)
Oil API Gravity	39	45	42	°API	Clark (2009), Breit et al. (1992)
Reservoir Permeability	0.0001	0.02	0.005	mD	Sarg (2012), Simenson (2010)
k_v/k_h	0.001	1	0.1		Pitman et al. (2001)
Reservoir Porosity	2.0	10.0	5.0	%	Sonnenberg (2011)
Initial Water Saturation	0.25	0.45	0.30		Simenson (2010)

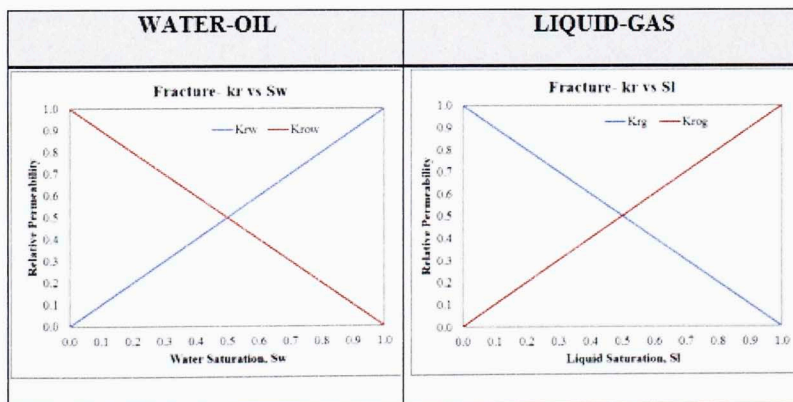
GRID PROPERTIES AND RESERVOIR VOLUME		
Length, L	400	ft
Breadth, B	1,000	ft
Thickness, h	40	ft
Number of Grid Blocks	NX, NY, NZ	28, 25, 10
Grid Dimensions	LX, LY, LZ	(...), 40, 4 X-direction has variable length (local grid refinement)
Bulk Reservoir Volume	1.6 E+07	RES FT ³
Total Pore Volume	8.0 E+05	RES FT ³
Hydrocarbon Pore Volume	5.6 E+05	RES FT ³
Original Oil in Place (OOIP)	6.6 E+04	STB
Original Gas in Place (OGIP)	9.1 E+07	SCF

HYDRAULIC FRACTURE PROPERTIES		
Parameter	Injector Fracture	Producer Fracture
Fracture Width	0.0292 ft	0.0292 ft
Fracture Half length	400 ft	400 ft
Fracture Height	40 ft	40 ft
Fracture Permeability	230 mD	70 mD
Fracture Conductivity	6.7 mD-ft	2.0 mD-ft

Relative Permeability curves for Matrix:



Relative Permeability curves for Fracture:



WELL PROPERTIES

Injection Well	Maximum Rate	1.0	<i>MMSCF/Day</i>
	Injection Bottomhole Pressure	10,000	<i>psia</i>
Producer Well	Maximum Rate	300	<i>STB/day</i>
	Production Bottomhole Pressure	500	<i>psia</i>
Simulation Time		30	<i>years</i>

Where μ and σ are mean and standard deviation of the variable's logarithm.

The cumulative distribution function $C(x)$ is:

$$C(x) = \frac{1}{2} \left[1 + \operatorname{erf} \left(\frac{\ln(x/k) - \mu}{\sigma \sqrt{2}} \right) \right] \quad (A.1)$$

From this distribution, the median permeability is:

$$k' = e^{\mu} \quad (A.2)$$

The above equation can be written as:

$$C(k) = \frac{1}{2} \left[1 + \operatorname{erf} \left(\frac{\ln(k/k')}{\sigma \sqrt{2}} \right) \right] \quad (A.3)$$

$$\text{Derive } \sigma = \frac{\ln(k/k')}{\sigma \sqrt{2}} \quad (A.4)$$

Dykstra-Parsons coefficient is defined as:

$$D_{p} = \frac{k' - k_p}{k'} \quad (A.5)$$

APPENDIX B: PERMEABILITY ESTIMATION FOR EACH GRID

BLOCK FROM DYKSTRA-PARSONS COEFFICIENT

Permeability is usually characterized as log normal distribution in nature. The log-normal distribution has the probability density function (PDF) as follows:

$$f(k, \mu, \sigma) = \frac{e^{-\frac{(\ln k - \mu)^2}{2\sigma^2}}}{k \sigma \sqrt{2\pi}} \quad \dots\dots\dots (B.1)$$

Where μ and σ are mean and standard deviation of the variable's logarithm.

The cumulative distribution function (CDF) is:

$$C(k) = \frac{1}{2} \left[1 - \operatorname{erf} \left(\frac{\ln(k) - \mu}{\sigma \sqrt{2}} \right) \right] \quad \dots\dots\dots (B.2)$$

From this distribution, the median permeability is:

$$k' = e^{\mu} \quad \dots\dots\dots (B.3)$$

So above equation can be written as:

$$C(k) = \frac{1}{2} \left[1 - \operatorname{erf} \left(\frac{\ln(k/k')}{\sigma \sqrt{2}} \right) \right] \quad \dots\dots\dots (B.4)$$

Define $\tau = \frac{\ln(k/k')}{\sigma}$ (B.5)

Dykstra-Parsons coefficient is defined as:

$$V_{DP} = \frac{k' - k_{\sigma}}{k'} \quad \dots\dots\dots (B.6)$$

Where k' is the median of the distribution, and k_σ is the permeability at which 84.1% of the distribution has a great permeability. The permeability, k_σ corresponds to $\tau = -1$. From which we can solve the $k_\sigma = k'e^{-\sigma}$

By substituting Equation (8) into equation (7), an expression can be derived for the relationship between the permeability variation and the standard derivation.

$$V_{DP} = 1 - e^{-\sigma^2} \dots\dots\dots (B.7)$$

Or the standard derivation can be calculated from the Dykstra-Parsons Coefficient,

$$\sigma = -(1 - V_{DP}) \dots\dots\dots (B.8)$$

And the variance of the permeability distribution is:

$$v = \sigma^2 = [\ln(1 - V_{DP})]^2 \dots\dots\dots (B.9)$$

For this study, sgsim (Sequential Gaussian Simulation) modeling in sGEMS software was utilized for generating permeability for each grid block. Defining the number of grid block and their dimensions, sgsim provides random number distribution based on cumulative distribution function (CDF) for each grid block, which is characterized through simple kriging system. Using mean permeability and standard deviation, permeability can be generated for each grid block defining the reservoir.

APPENDIX C: PRODUCTION RATE HISTORY FOR BARTELSON

1-3H

Date	Days	BBL S Oil	MCF Prod	Date	Days	BBLS Oil	MCF Prod
Jun-14	0	0	0	Aug-10	31	3086	2803
May-14	6	396	238	Jul-10	31	3184	2687
Apr-14	30	1714	1011	Jun-10	30	2442	1885
Mar-14	31	1955	1078	May-10	28	3382	2335
Feb-14	24	1648	863	Apr-10	30	3014	1708
Jan-14	0	0	0	Mar-10	29	2544	1836
Dec-13	31	2120	1481	Feb-10	28	3671	2412
Nov-13	24	1952	1182	Jan-10	30	4101	2403
Oct-13	30	2112	1132	Dec-09	18	2332	1342
Sep-13	15	1252	739	Nov-09	28	3413	2367
Aug-13	31	2229	1275	Oct-09	31	4200	2425
Jul-13	31	2248	1205	Sep-09	30	4411	2604
Jun-13	30	2451	1233	Aug-09	31	4939	2447
May-13	31	2708	1300	Jul-09	29	4866	2606
Apr-13	30	2895	1011	Jun-09	22	3833	1792
Mar-13	24	1730	790	May-09	28	4248	2299
Feb-13	28	1970	967	Apr-09	30	5204	2886
Jan-13	31	2694	1293	Mar-09	31	5643	2630
Dec-12	31	2925	1402	Feb-09	28	5276	2355
Nov-12	30	494	305	Jan-09	31	6665	3332
Oct-12	23	285	140	Dec-08	31	7357	3430
Sep-12	30	356	277	Nov-08	30	7602	3371
Aug-12	25	439	571	Oct-08	31	8397	3139
Jul-12	31	2212	2740	Sep-08	28	7499	2616

Jun-12	30	2903	2848	Aug-08	31	8594	3123
May-12	31	2065	1999	Jul-08	31	8966	3204
Apr-12	30	2023	1895	Jun-08	30	8617	3157
Mar-12	31	2029	1923	May-08	30	8750	3169
Feb-12	29	1833	1810	Apr-08	30	10073	3512
Jan-12	31	2106	1914	Mar-08	30	7154	2675
Dec-11	31	2006	1848	Feb-08	29	10661	3746
Nov-11	30	2054	1701	Jan-08	31	12136	4262
Oct-11	31	2104	1765	Dec-07	31	12749	4451
Sep-11	30	2068	1714	Nov-07	30	12627	4425
Aug-11	31	2367	1762	Oct-07	31	12740	4489
Jul-11	31	2276	1820	Sep-07	30	12505	4418
Jun-11	30	2371	1771	Aug-07	29	16460	5810
May-11	31	2613	1852	Jul-07	3	2461	990
Apr-11	29	2593	1757	Jun-07	26	8310	3253
Mar-11	31	3028	1848	May-07	31	11092	4274
Feb-11	28	3153	1723	Apr-07	30	11766	4498
Jan-11	22	2384	1231	Mar-07	28	11302	4346
Dec-10	0	0	0	Feb-07	28	8880	3119
Nov-10	26	598	368	Jan-07	31	11150	3984
Oct-10	28	1570	1492	Dec-06	31	15993	5779
Sep-10	30	2620	2680	Nov-06	14	14202	3777

APPENDIX D: STATISTICAL ANALYSIS FOR PROXY

EQUATION BY RESPONSE SURFACE MODEL

RESPONSE SURFACE MODEL

In order to compare the effect of each parameter, the uncertainty parameter range is normalized between -1 and 1. The resulting tornado chart displays a $(2 \times \text{coefficient})$ of the normalized polynomial regression. With linear effects, the bar length represents the average change due to the parameter change between minimum and maximum value. Non-linear effects are included in the equation with quadratic terms. If modifying 2 parameters simultaneously will strongly effect the objective function higher than the sum of their individual linear or quadratic effects, a cross term $(x \cdot y)$ is utilized to generate a proxy equation.

ANALYSIS OF VARIANCE

Degree of Freedom

Total	Number of samples – 1
Model	Number of coefficients for the response surface
Error	Total - Model

Sum of Squares

Total	Sum of Squared distances of each response from the sample mean
Error	Sum of Squared differences between the fitted (RS) values and the actual simulated values
Model	Total - Error

Mean Square/Variance: It represents an averaged sum of squares.

$$\text{Mean Square} = \frac{\text{Sum of Square}}{\text{Degree of Freedom}}$$

F-Ratio: The ratio tests the hypothesis that all the regression parameters are zero, except the intercept. The significance level also needs to be defined.

$$F \text{ Ratio} = \frac{\text{Model mean square}}{\text{Error mean square}}$$

Prob > F: It is the probability of obtaining a greater F-value by chance alone if the specified model fits no better than the overall response mean. A Significance probability of 0.05 or less are often considered as an evidence that there is at least one significant regression factor in the model.

Source	Degrees of Freedom	Sum of Squares	Mean Square	F Ratio	Prob > F
Model	20	38128.3	1906.41	229.87	<0.00001
Error	81	671.769	8.29345		
Total	101	38800.1			

EFFECT SCREENING USING NORMALIZED PARAMETERS (-1, +1)

Coefficient: Coefficients are the response surface model found by least squares.

Standard Error: It estimates the standard deviation of the deviation of the distribution of the parameter coefficient.

t-Ratio: It is a statistic that tests whether the true parameter (coefficient) is zero.

$$t - \text{Ratio} = \frac{\text{Coefficient}}{\text{Standard Error}}$$

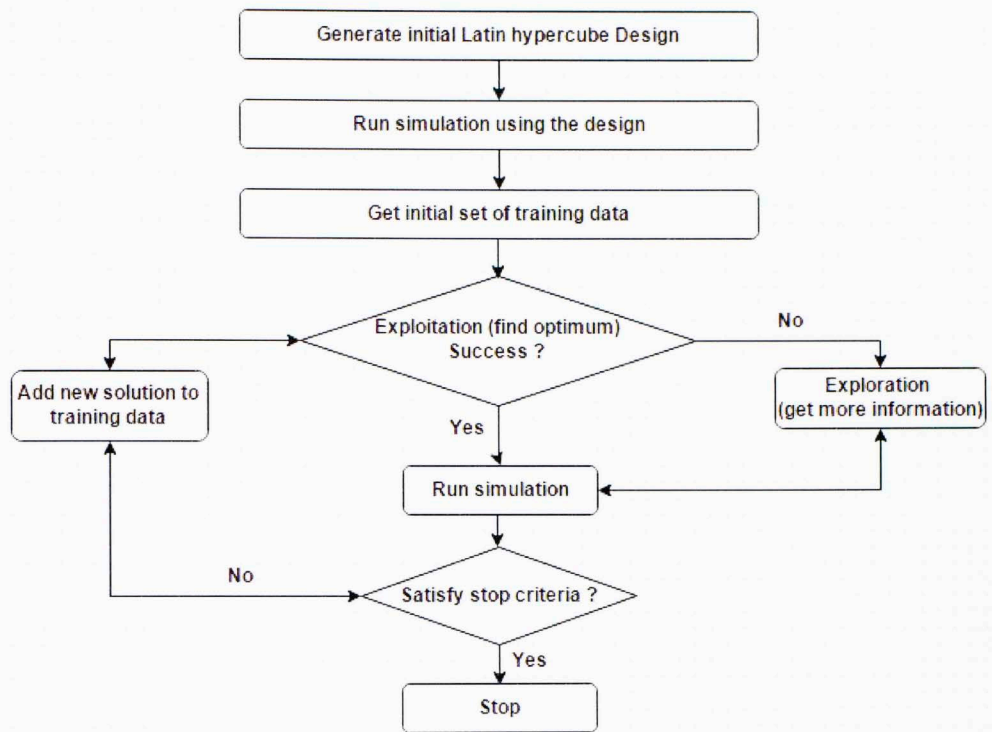
Prob > |t|: It is the probability of getting an even greater t-statistic (absolute value), given the hypothesis that the parameter coefficient is zero. Probability less than 0.05 are

often considered as significant evidence that the parameter coefficient is not zero. This term is used to remove the insignificant terms from the regression model. The parameter values less than the significance probability (α) will be considered significant terms and other terms will be neglected.

Term	Coefficient	Standard Error	t Ratio	Prob > t
Intercept	40.1134	0.769946	52.0989	<0.00001
Inj_HL (5, 15)	0.861217	0.495941	1.73653	0.08627
Prod_HL (10, 20)	-2.97349	0.3125	-9.51517	<0.00001
Inj_BHP (7000, 11000)	14.2871	0.763129	18.7218	<0.00001
K_v / K_H (0.01, 1)	8.56045	0.647173	13.2274	<0.00001
Inj_Perm (70, 400)	0.750078	0.318131	2.35776	0.02080
Prod_Perm (10, 150)	6.68698	0.328089	20.3816	<0.00001
Dist_Wells (17, 77)	-14.975	0.579659	-25.8341	<0.00001
Dist_Frac (20, 50)	-11.282	0.325265	-34.6855	<0.00001
Inj_HL * Inj_BHP	-1.43063	0.472723	-3.02637	0.00332
Inj_HL * Prod_Perm	0.548255	0.311695	1.75895	0.08236
Inj_HL * Dist_Wells	-1.08994	0.320358	-3.40227	0.00104
Prod_HL * Prod_Perm	-1.8227	0.30896	-5.89948	<0.00001
Prod_HL * Dist_Wells	1.26213	0.312453	4.03942	0.00012
Inj_BHP * K_v / K_H	4.44213	0.62134	7.14927	<0.00001
Inj_BHP * Dist_Wells	-2.31334	0.578703	-3.99745	0.00014
K_v / K_H * Dist_Wells	-1.2216	0.33872	-3.60653	0.00054
K_v / K_H * Dist_Frac	-2.53536	0.318854	-7.95147	<0.00001
Prod_Perm * Dist_Wells	-2.43607	0.313342	-7.77449	<0.00001
Prod_Perm * Dist_Frac	-1.32351	0.312155	-4.23991	0.00006
Dist_Wells * Dist_Frac	5.00183	0.322246	15.5218	<0.00001

CMG –DECE HISTROY MATCHING TECHNIQUE

CMOST uses the proprietary model DECE - Designed Exploration and Controlled Evolution, for history matching and optimization process. DECE is an iterative optimization process carried out in two steps. Step 1 is the designed exploration stage with a goal to explore the search space in a designed random manner to attain maximum information possible. Experimental Design models are implemented to multiple simulation dataset with respect to uncertainty parameters. Step 2 is the controlled evolution stage with a goal to statistically analyze all the simulation runs of the dataset obtained through exploration design stage. With statistical analyses, DECE evaluates each simulated value of every uncertainty parameter. To improve solution quality, some candidate values are rejected, reducing the sample space for optimization. The algorithm will remember the rejected values and will not be utilized again in the exploration design stage. To minimize the possibility of being trapped in local minima, the DECE algorithm checks rejected candidate values from time to time to make sure previous rejection decisions are still valid. If the algorithm determines that certain rejection decisions are not valid, the rejection decisions are recalled and corresponding candidate values are used again. The flowchart for DECE optimization and history matching process is elaborated in the figure.



This volume is the property of the University of Oklahoma, but the literary rights of the author are a separate property and must be respected. Passages must not be copied or closely paraphrased without the previous written consent of the author. If the reader obtains any assistance from this volume, he or she must give proper credit in his own work.

I grant the University of Oklahoma Libraries permission to make a copy of my thesis upon the request of individuals or libraries. This permission is granted with the understanding that a copy will be provided for research purposes only, and that requestors will be informed of these restrictions.

NAME _____
DATE _____

A library which borrows this thesis for use by its patrons is expected to secure the signature of each user.

This thesis by Sumeer Kalra has been used by the following persons, whose signatures attest their acceptance of the above restrictions.

NAME AND ADDRESS

DATE